THE OCEAN TIDE AND WAVES BENEATH THE ROSS ICE SHELF, ANTARCTICA

by

Richard T. Williams, II

Dissertation submitted to the Graduate Faculty of the
Virginia Polytechnic Institute and State University
in partial fulfillment of the requirements for the degree of
DOCTOR OF PHILOSOPHY
in
Geophysics

APPROVED:

Edwin S. Robinson, Chairman

Gilbert A. Bollinger

John K. Costain

Robert A. Heller

Lee W. Johnson

J. Arthur Snoke

February, 1979

Blacksburg, Virginia

ACKNOWLEDGEMENTS

The author is indebted to Professor Edwin S. Robinson for his guidance throughout the course of this study. His interest and encouragement were indispensible.

The field parties who gathered the data were ably led by Mr. H. A. C. Neuburg. Messers. R. L. Ayers, K. E. Bubriski, T. M. Kolich, G. Moss, C. S. Rohrer, and B. Whitehurst assisted with the field work. The assistance and cooperation of the staffs of the Ross Ice Shelf Management Office, and Holmes and Narver, Inc. contributed greatly to the successful completion of this project.

This work was supported by research grants GV-40434 and DPP-73--5873 from the National Science Foundation.

This dissertation is dedicated to my wife, Lois, who quite literally traveled to one end of the earth to help me complete my formal education. On my behalf, she endured the rigors of life in Antarctica and spent long hours preparing this manuscript, and her efforts deserve special recognition.

TABLE OF CONTENTS

	Page
INTRODUCTION	1
THE OCEAN TIDE IN THE ROSS SEA	5
Introduction	5
Previous Work	7
Instrumentation	13
RISP Tidal Gravity Measurements	14
The Gravimetric Effect of the Ocean Tide	21
Tidal Harmonic Analysis	23
Uncertainties in the Harmonic Constants	31
Cotidal-Coamplitude Charts	36
Tide Prediction	58
Summary	63
TIDAL CURRENTS BENEATH THE ROSS ICE SHELF	64
Introduction	64
A Theoretical Basis for Tidal Current Calculations	66
Current Meter Data from J9	73
Theoretical J9 Tidal Current	83
Semidiurnal Current Resonance in the Ross Sea	94
Mass Transport by Tidal Currents at J9	97
Summary	98
FLEXURAL WAVES IN THE ROSS ICE SHELF	101
Introduction	101
Flexural Wave Theory	108

Page

Digital Recorders for the Gravimeters 111

Gravimeter Frequency Respone 114

Nontidal Wave Data 119

Speed and Direction of the Nontidal Waves at J9 125

Flexural Wave Power Spectrum 134

Summary 147

RESULTS 150

BIBLIOGRAPHY 153

APPENDIX I 157

APPENDIX II 183

APPENDIX III 203

VITA 204

INTRODUCTION

The quasi-periodic fluctuation in the elevation of the sea surface was one of the earliest observed physical phenomena. The ancient Greeks knew that the time of high tide was somehow related to the positions of the sun and moon, but it was not until the eighteenth century and Newton's formulation of the law of gravity that the tidal forces experienced by the waters on the surface of the earth could be expressed mathematically. The hydrodynamical equations for a column of water on a rigid, rotating earth were first formulated by Laplace in 1775. Since that time, rigorous solutions to these equations for the tide in various tesseral seas have been obtained. Unfortunately, these solutions shed little light on the nature of the ocean tide on the real earth. The irregular shapes of the ocean basins dictate a numerical solution to the problem, and such numerical methods for solving Laplace's tidal equations have become practical only within the past twenty years with the development of the electronic digital computer. In that time the equations have been used to infer the tide in a number of limited areas, and also for the tide in the world ocean. However, there is notable disagreement in the published maps of even the most important components of the global tide, made by different investigators. One area in which serious differences exist is in the southern Pacific Ocean. This uncertainty can be attributed largely to a lack of observational data in the region, particularly in the extreme south, adjacent to the Antarctic

continent. This dissertation represents the conclusion of an extended series of observations of the ocean tide in this region.

The Ross Sea is a marine embayment penetrating more than 1000 km into the Pacific sector of the Antarctic continent (Figure 1). The southern portion of this sea is covered by the Ross Ice Shelf, a tabular mass of floating ice which is almost everywhere between 300 m and 600 m thick. Situated for the most part between 78°S and 85°S latitude, and between 160°E and 210°E longitude, the Ross Ice Shelf compares in areal extent to France, covering about 560,000 sq km. A comprehensive research program, the Ross Ice Shelf Project (RISP), was begun in 1973 to investigate the interdependent glaciologic, oceanographic, geologic, and biologic phenomena pertaining to this region (Zumberge, 1971). A major effort in the project was to drill a hole through the ice shelf to provide direct access for current measurements, water temperature and salinity measurements, and sampling of the bottom sediments and bio-mass beneath the ice shelf.

The tide beneath the Ross Ice Shelf is of interest for several reasons. Knowledge of the variation of the tide in the Ross Sea region contributes to the understanding of the tide in the adjacent southern Pacific Ocean. Knowledge of the ocean currents beneath the ice shelf bears upon the problems of mass wastage by bottom melting of shelf ice, and the transport of marine organisms and sediment. Because of the ice cover, wind driven circulation is minimized, and the tidal current may be the largest component of water movement.

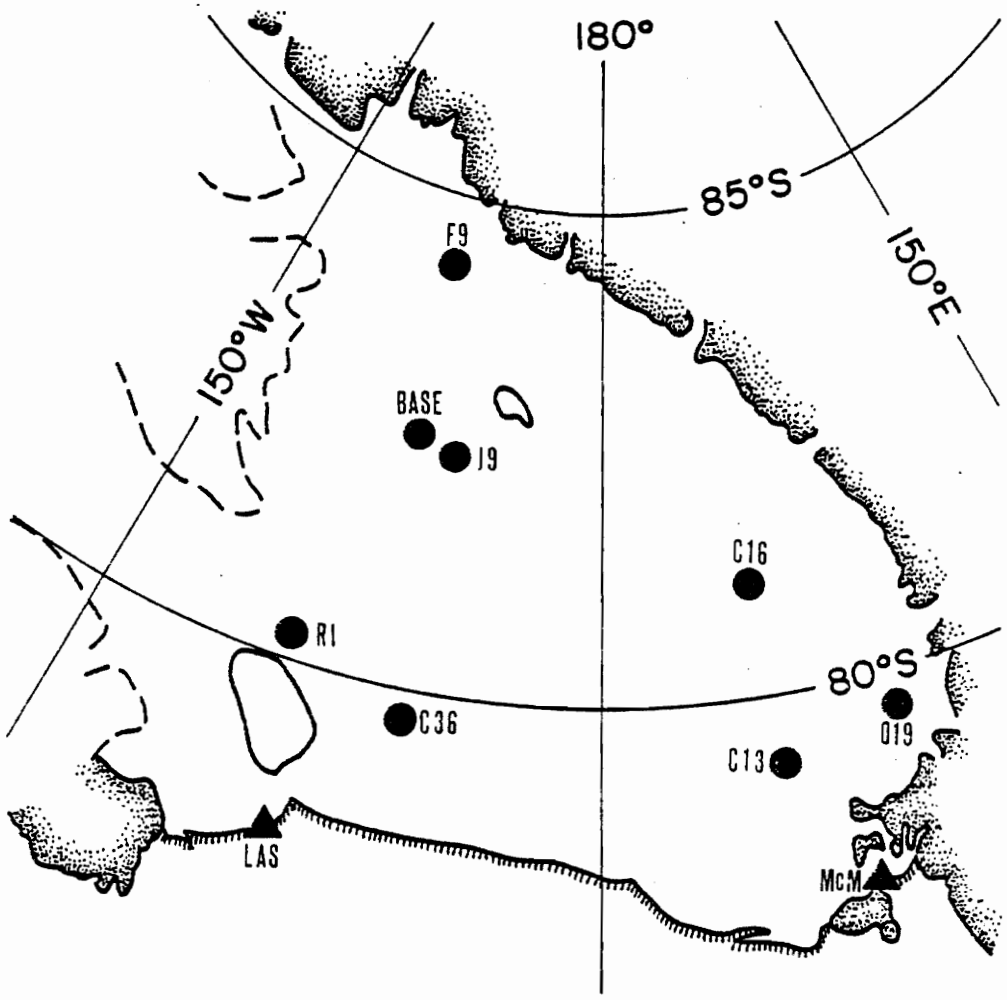

Figure 1. The Ross Sea area of Antarctica. Circles denote observation sites occupied in connection with RISP: triangles denote locations where observations of the ocean tide were made prior to RISP.

The interpretation of short-term current measurements made through boreholes in the ice shelf is facilitated if the tidal variation in the current is known.

The author has participated in research activities related to RISP since the summer of 1974, and traveled to Antarctica to participate in the field program during the 1974-75 and 1977-78 austral summers. Oceanographic data collected by the author and others, working in Antarctica in connection with RISP during four austral summers between 1973 and 1978, are the principal subject of this dissertation. The primary goal of this research program has been the determination of the spatial and temporal variation of the elevation of the ice shelf, due to the ocean tide in the underlying water-layer. Other topics investigated are the tidal currents in the water-layer, and some observed waves in the ice shelf with periods in the 1 min to 15 min range.

THE OCEAN TIDE IN THE ROSS SEA

Introduction

Measurements of the tide beneath the ice shelf cannot easily be made by conventional methods, which require access to the water. While instruments can be adapted for use in an access hole (Jacobs and others, 1978), the cost of drilling a series of access holes for tide measurements is prohibitive. In this study, the tidal elevation change at the surface of the ice due to the tide in the underlying water was inferred from measured tidal gravity variations. The increase in elevation of the floating ice shelf at high tide causes a change in the gravity at the surface which is detectable by a gravimeter. Gravity records were obtained by RISP personnel at eight locations (Figure 1, Table 1) distributed over the Ross Ice Shelf, using Geodynamics model TRG-1 tidal recording gravimeters.

RISP field operations usually commenced about 1 November and terminated before 1 February to take advantage of the relatively good weather of the austral summer. In the field, the gravimeters were installed in 5 m square Jamesway prefabricated buildings. For a stable foundation, the gravimeters were set on platforms mounted on 4 in square wooden posts extending approximately 3 m into the firn through a hole in the Jamesway floor. Electrical power was obtained from Onan 6 kw diesel generators. An attendant at each site was responsible for maintenance of the generator and heating stove, verifying that the gravimeter was operating normally, and placing calibration and hourly time signals on the record.

Table 1. Locations of stations cited in this study.

Designation	Latitude	Longitude
Base	82.53°S	166.00°W
Cape Adare	71.28°S	189.77°W
Cape Evans	77.63°S	193.60°W
Cape Royds	77.55°S	193.85°W
C13	79.25°S	189.67°W
C16	81.19°S	189.50°W
C36	79.75°S	169.05°W
F9	84.25°S	171.33°W
Hut Point	77.85°S	193.37°W
J9	82.37°S	168.63°W
Little America V (LAS)	78.20°S	162.27°W
McMurdo Base (McM)	77.85°S	193.34°W
McMurdo Sound	77.50°S	195.00°W
O19	79.53°S	196.64°W
Roosevelt Island Camp (RI)	80.19°S	161.56°W

Previous Work

The early Antarctic expeditions traveled by ship, and naturally made observations of the ocean tide. Near the turn of the century, four British expeditions made tidal observations in the Ross Sea at (Table 1) Cape Adare (Bernacchi, 1901), Hut Point (Darwin, 1908), Cape Royds (Shackelton, 1909) and Cape Evans (Doodson, 1924). These measurements were not useful for the purpose of this study. The Cape Adare observations were made for one day only, and thus cannot be analyzed for tidal content. The remaining three locations are all on McMurdo Sound (near McM in Figure 1), near the site of major United States and New Zealand base camps and lengthy, higher quality records of the tide have been made there since 1957.

Beginning in the International Geophysical Year (IGY), 1957, ocean tide records have been made at several sites in the Ross Sea. In McMurdo Sound, near the northern extremity of the Ross Ice Shelf, sea level recordings have been reported for two locations near the site of McMurdo Station (McM, Figure 1) by MacDonald and Burrows (1959) and Heath (1971). The results of the analysis of these data have been summarized by Heath, and by Gilmour and others (1962). For the purpose of this dissertation, these two locations are so close together that they will be considered to be one station. At Little America V (LAS, Figure 1), on the eastern side of the ice front, gravity readings were made at one- or two-hour intervals from 11 June through 12 July, 1957, using a Frost gravimeter (Thiel and others, 1960). The observed change in gravity, shown in Figure 2, was shown to be

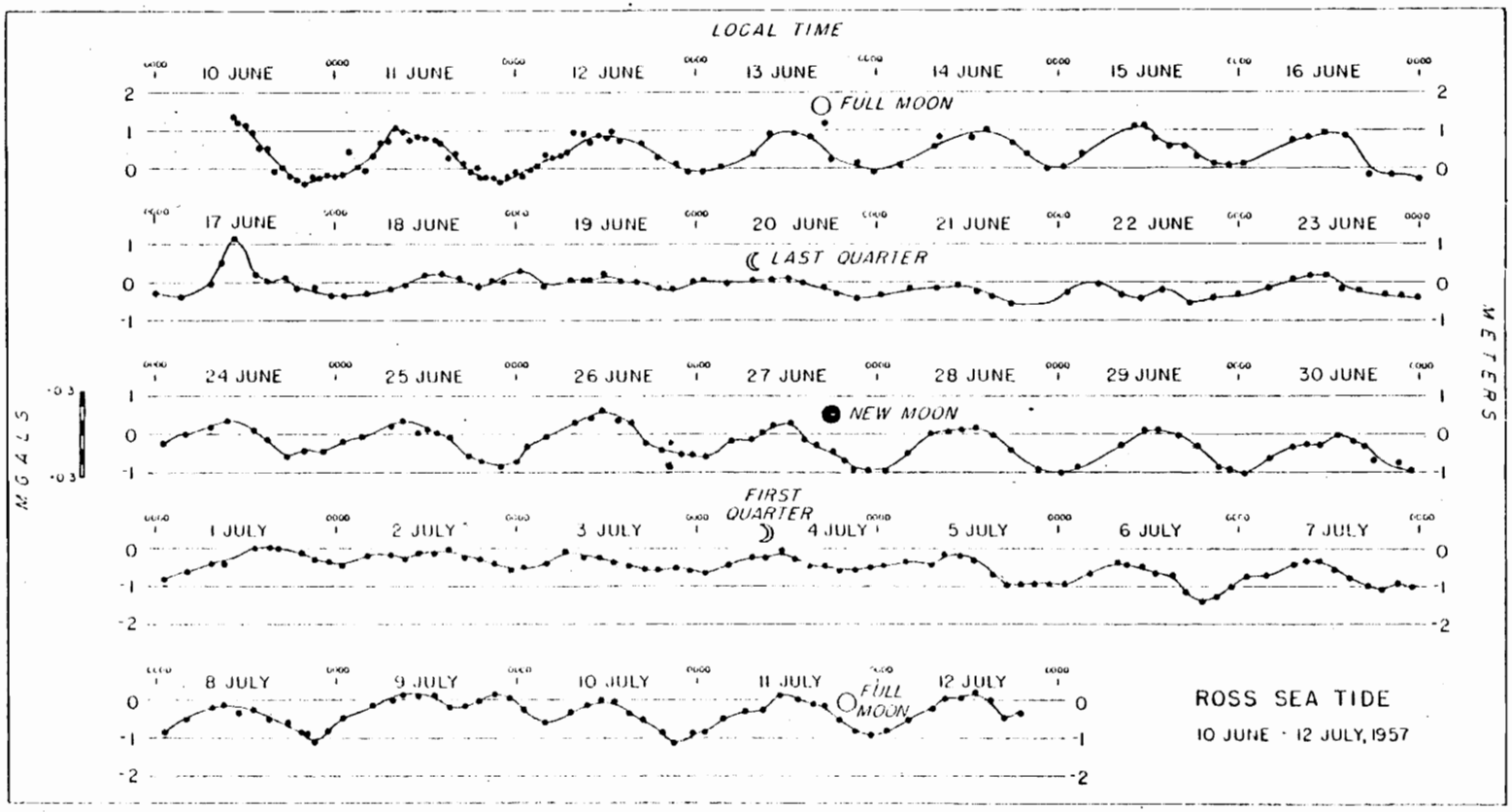

Figure 2. Gravimetric observations at Little America V, after Thiel and others (1960).

caused by the elevation of the station changing in response to the ocean tide beneath the ice shelf. McMurdo Sound and Little America V are the only places in the Ross Sea at which lengthy measurements of the height of the ocean tide were made prior to the present study.

The McMurdo and Little America records were made at the northern edge of the Ross Ice Shelf. There was also evidence developed for the existence of a tide extending beneath the southern extremity of the shelf, about 850 km distant from the ice front. At LAS current measurements made simultaneously with gravimetric surface elevation measurements demonstrated in a crude way that the volume of water flowing from beneath the shelf, per meter of section in a given time interval, was consistent with the flow required if the tide were the same everywhere beneath the shelf. More direct evidence came from gravimeter readings made during the Ross Ice Shelf Traverse (1957-58; Bennett, 1964). A Frost gravimeter was read at irregular intervals at several observation sites (Figure 3), which were occupied for periods of 12 to 48 hours. The gravimeter readings are reproduced in Figure 4, with dashed lines to illustrate that a diurnal fluctuation in gravity can account for the observed variation in the meter readings. A three-day-long study in November 1959 (Thiel, 1960) established the existence of a tide beneath the shelf at a point about 300 km south of the ice front. A graph of the meter readings (Figure 5) shows a diurnal gravity fluctuation, but the record was too short for meaningful analysis.

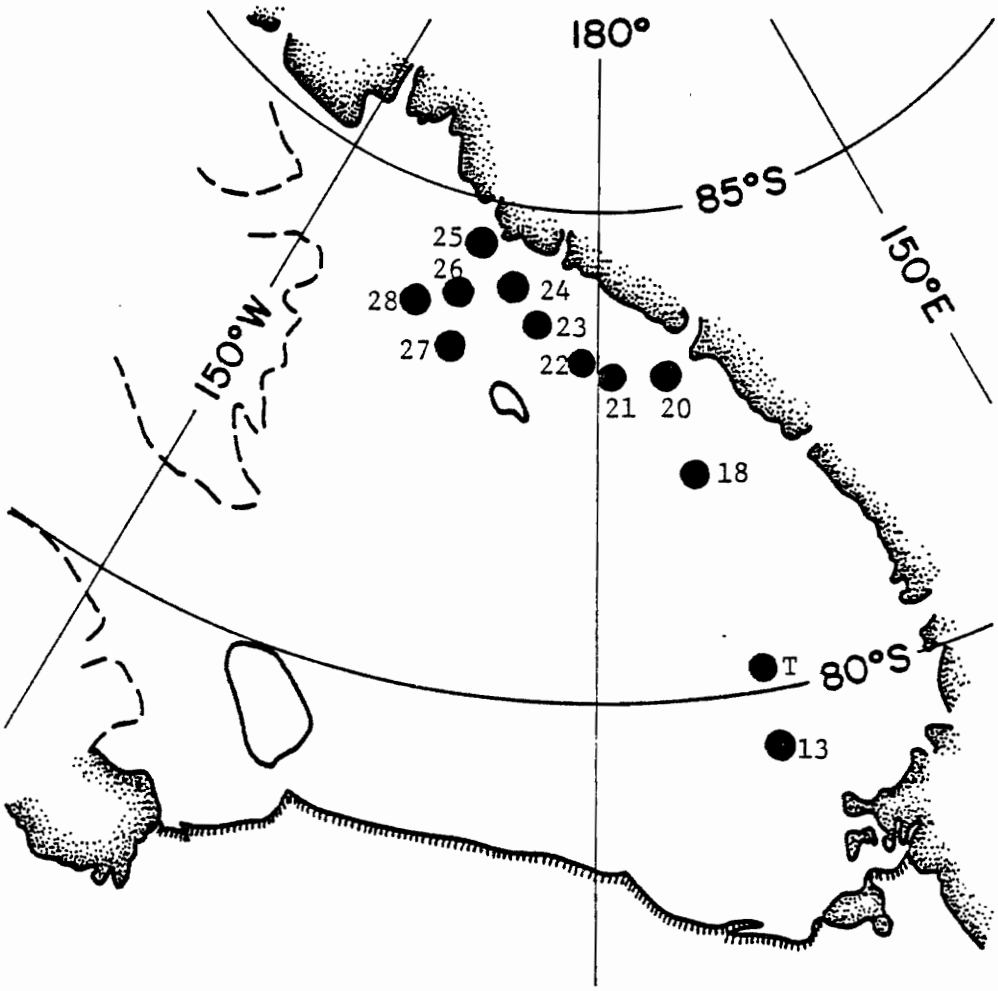

Figure 3. Sites of short term tidal gravity observations on the Ross Ice Shelf. Numbered stations were occupied during the 1957-58 Ross Ice Shelf Traverse (Bennett, 1964). Observations reported by Thiel (1960) were made at site labeled T.

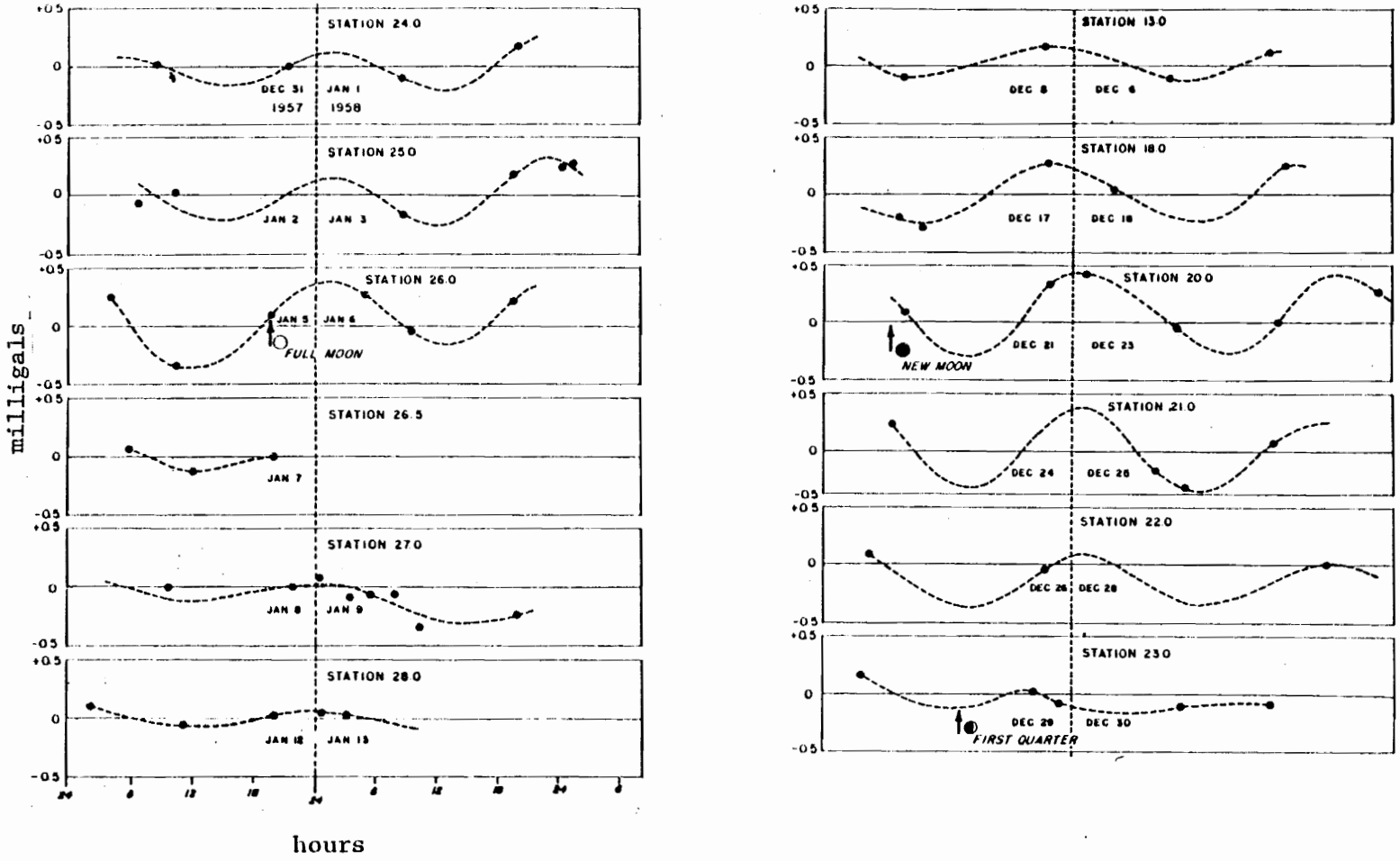

Figure 4. Tidal fluctuations in the southern Ross Ice Shelf as indicated by observed gravity, after Bennett (1964).

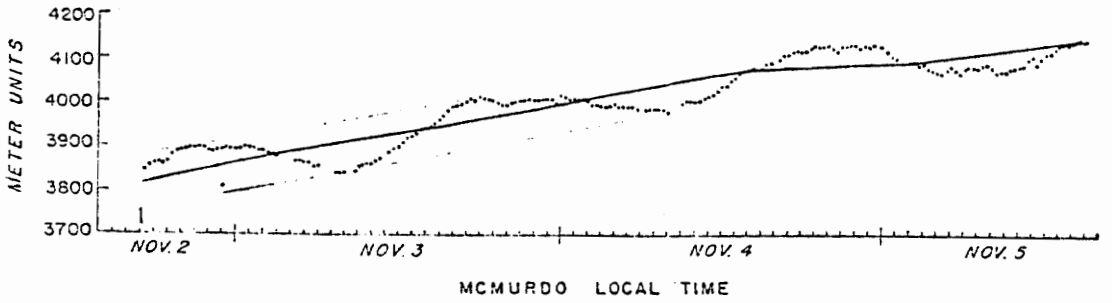

Figure 5. Gravimetric recording of the ocean tide, reported by Thiel (1960), at a site on the Ross Ice Shelf.

Instrumentation

The gravity data obtained during RISP were recorded using three different Geodynamics model TRG-1 gravimeters. The basic unit is a North American exploration-type gravimeter that was modified by Geodynamics, Inc. for continuous and stable long-term recording of tidal gravity variations. The basic design of the gravimeter consists of a mass hinged on quartz wires, and supported by a zero-length spring (LaCoste, 1935). The gravimeter is mounted inside an air-tight container, which is in turn enclosed in a well-insulated wooden case. The manufacturer specifies that the temperature of the instrument, in the inner-most container, is controlled to within 0.005 C degrees of a manufacturer-determined optimum near 36°C. Changes in the gravitational force on the mass in the gravimeter are sensed by monitoring the position of the mass by means of a differential-capacitor transducer. A continuous record of the variations in gravity is obtained by recording a voltage, derived from the transducer, which is proportional to the mass position.

Instrument calibration is possible by means of an electrostatic force generated by applying a precise voltage to a fixed (capacitor) plate mounted over the gravimeter mass. The gravity-change equivalent of the electrostatic force is constant, and can be used to relate observed displacements of the mass to the gravity change. Calibration of the instrument to within about 3% was achieved by using earth-tide recordings made at Blacksburg, Virginia. The equivalent microgal shift in the mass position introduced by activation of the

calibration system was determined for each instrument by comparing the calibration pulse height with the amplitudes of the lunar diurnal (O_1) and lunar semidiurnal (M_2) constituents of the earth tide (Table 2). These amplitudes were assigned the assumed standard values of 34.7 μgals and 56.5 μgals, respectively. Each of these values is the product of the theoretical amplitude at 37.23° latitude on the surface of a rigid earth (Melchoir, 1966; Schureman, 1941), and a tidal gravimetric factor which accounts for elastic yielding of the earth. The following gravimetric factors for Blacksburg were used (Robinson, 1974; Jachens, 1971): $\delta_{O_1} = 1.16$, $\delta_{M_2} = 1.19$.

RISP Tidal Gravity Measurements

Eight tidal gravity stations (Figure 1, Table 1) were established on the Ross Ice Shelf during four austral summers between 1973 and 1978. The station positions were chosen, consistent with available logistical support, so as to cover the study area uniformly. In a given year, generally, two camps were established, one coordinated with other RISP programs and one self-sufficient. During the 1976-77 field season no RISP field program was conducted. At two stations, C13 and O19, two instruments were operated simultaneously. One station, C16, was reoccupied, so that two records from successive years were obtained there. A total of 11 records were obtained from eight RISP camps, and these are shown in Figure 6. The starting time and length of each record is shown in Table 3.

Table 2. Gravimeter calibration pulse gravity-change equivalents.

Instrument	Calibration Pulse Equivalent
826	82.2 μgals
735	133.0 μgals
VPI-17	126.0 μgals

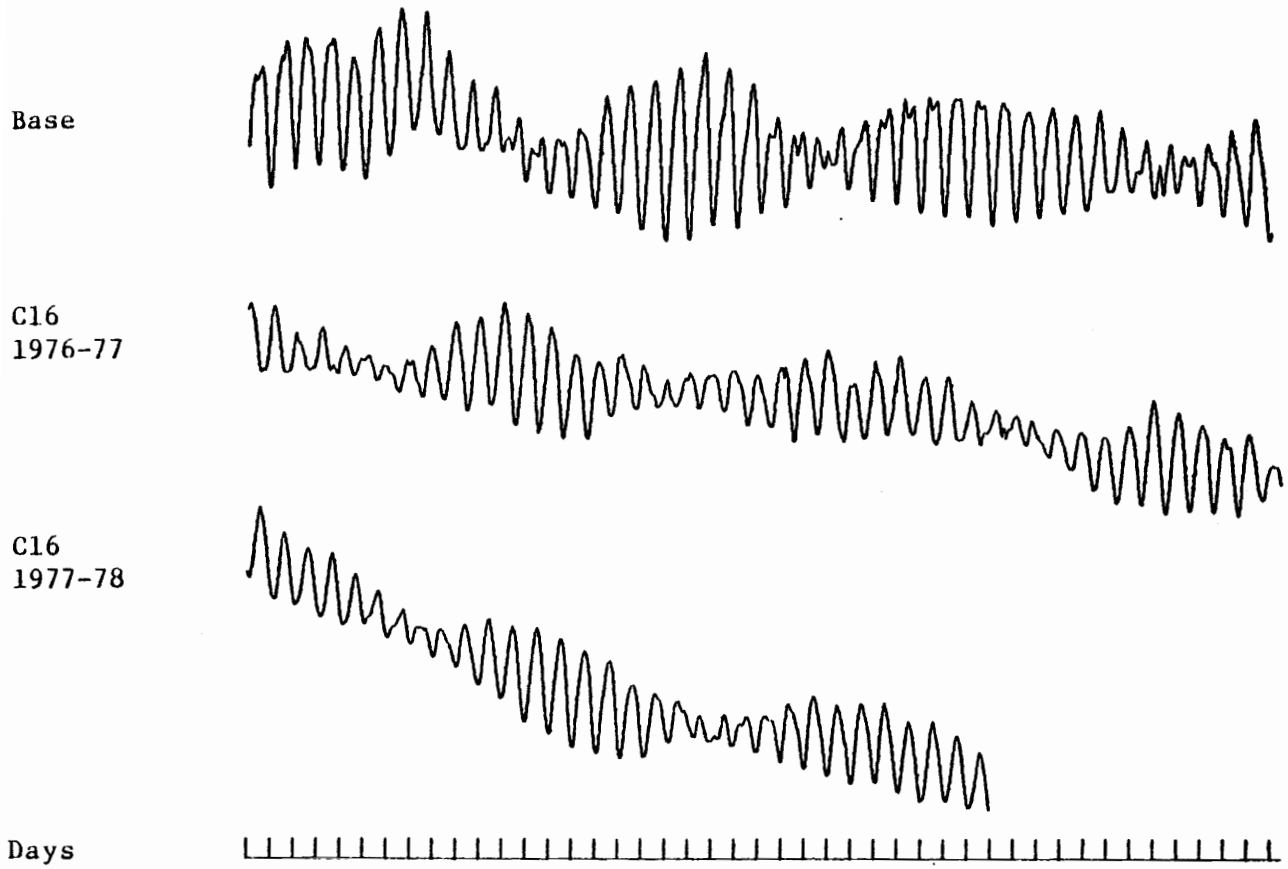

Figure 6a. Tidal gravity records from RISP camps. Station positions are given in Figure 1 and Table 1. Record starting times are given in Table 3.

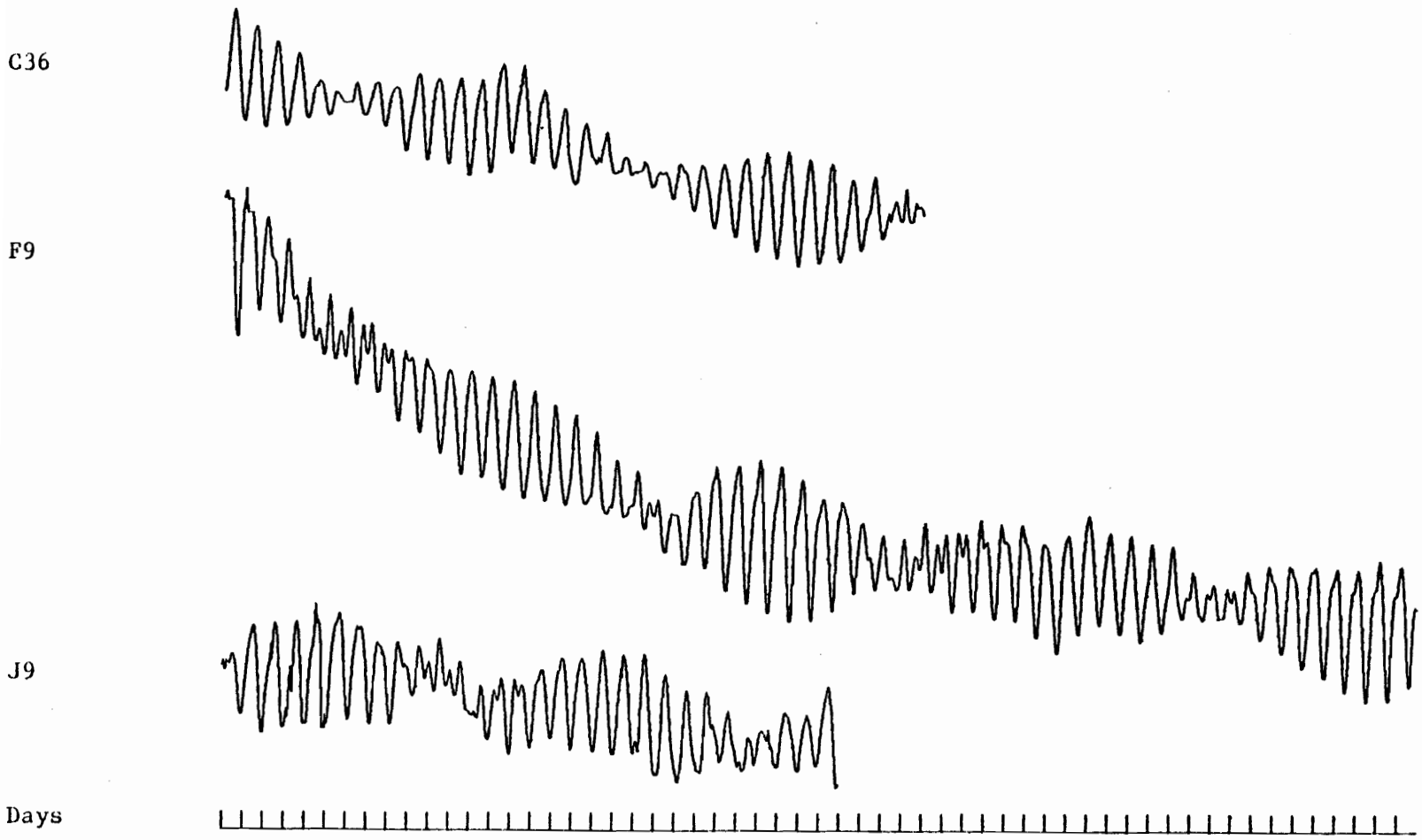

Figure 6b. Tidal gravity records from RISP camps. Station positions are given in Figure 1 and Table 1. Record starting times are given in Table 3.

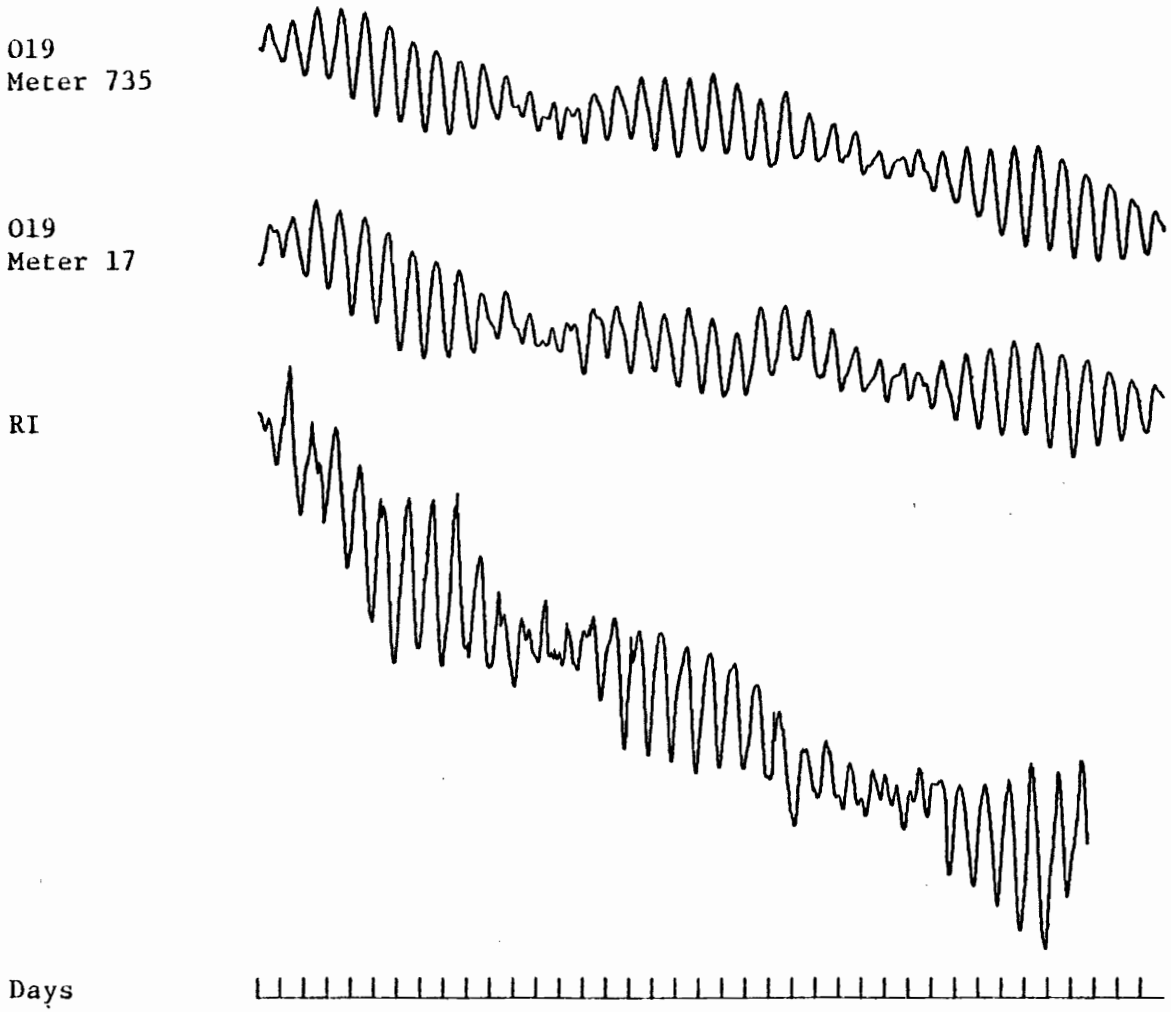

Figure 6c. Tidal gravity records from RISP camps. Station positions are given in Figure 1 and Table 1. Record starting times are given in Table 3.

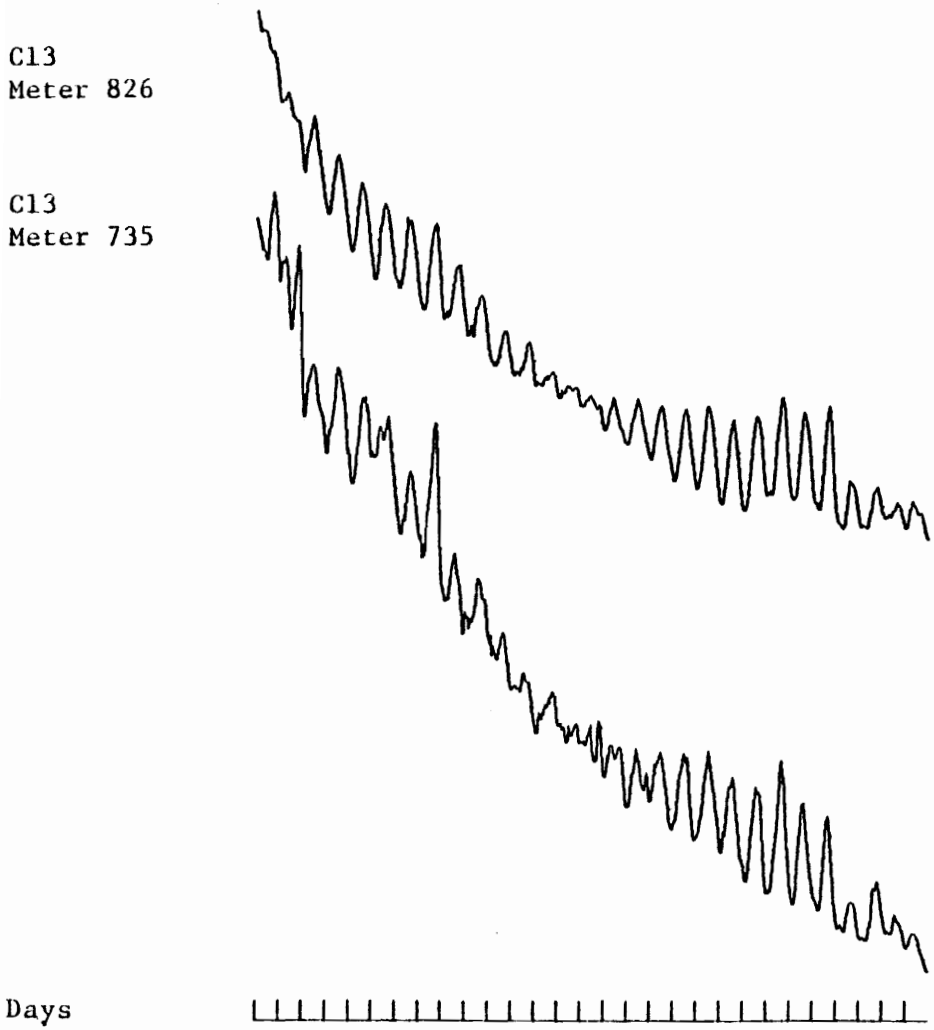

Figure 6d. Tidal gravity records from RISP camps. Station positions are given in Figure 1 and Table 1. Record starting times are given in Table 3.

Table 3. RISP tidal gravity record lengths and starting times.

Station	Instrument	Length (Hours)	Starting Time
Base	826	1056	20 Dec 73 0000 GMT
C13	735, 826	696	10 Nov 74 0000 GMT
C16	735	1068	9 Dec 76 1200 GMT
	826	768	26 Dec 77 0000 GMT
C36	826	816	29 Dec 74 0000 GMT
F9	826	1392	24 Nov 76 1200 GMT
J9	17	720	19 Nov 76 0000 GMT
O19	17, 735	936	6 Dec 77 0000 GMT
RI	17	858	23 Dec 74 0000 GMT

The Gravimetric Effect of the Ocean Tide

The diurnal variation of gravity was generally 300 μgals to 400 μgals at the time of tropic (diurnal spring) tide. This fluctuation is interpreted as resulting principally from changes in elevation and water-mass underlying the recording site associated with the ocean tide. Smaller contributions are due to the direct attraction of the moon and sun on the gravimeter, and from the vertical acceleration associated with elevation changes of the instrument. The ocean tide was discussed by Thiel and others (1960), and a portion of their development is presented here.

During high tide an additional mass of ocean water exists over a local region. The increase in elevation, Δh, of the floating shelf related to the introduction of this mass causes a decrease in the gravity field, Δg_{FA}, detected by a gravimeter on its surface according to the free air effect:

$$\Delta g_{FA} \text{ (mgals)} = - 0.3086 \, \Delta h \text{ (meters)} \qquad (1)$$

At the same time an increase in gravity can be expected from the attraction of the additional water mass, which can be adequately approximated by an infinite plate. Viewing this as similar to a Bouger correction, the gravity change, Δg_B, associated with an increased plate thickness, Δh, is given approximately by:

$$\Delta g_B \text{ (mgals)} = 0.04185 \, \rho \, \Delta h \text{ (meters)} \qquad (2)$$

where ρ is the plate (sea water) density in gm/cm^3. Combining these

two effects, and assuming a water density of 1.028 gm/cm^3, Thiel and others found the relationship between water-layer thickness change and gravity change to be:

$$\Delta h \text{ (meters)} = - 3.7653 \, \Delta g \text{ (mgals)} \qquad (3)$$

A density of 1.030 gm/cm^3 to 1.032 gm/cm^3 would be more appropriate for the sea water beneath the Ross Ice Shelf (Arnold Gordon, personal communication). However these values would change the constant in equation (3) by less than 0.1%, and the difference is not important in this study.

The direct luni-solar gravity can be subtracted from the recorded gravity variations (Robinson and others, 1977). Well known formulas for the gravity tide on a rigid earth have been summarized by Longman (1959), and Broucke and others (1972). However, since the earth is not perfectly rigid, an allowance must be made for its elastic yielding. The effect of the elasticity is to increase the earth tide amplitude by about 16%, and to time-shift the maximum tide by a small amount, probably less than 20 min (Jachens, 1971). The amplitude of the earth tide is about one-fifth as large as the ocean tide effect at LAS, and decreases, due to increasing latitude, to about one-twentieth at F9. Because the earth tide is small compared to the ocean tide effect, the error in the tidal gravity, corrected for the luni-solar effect by assuming a 16% amplitude increase and no time-shift, is probably less than 2% for the amplitude and 5 min in the time-shift of the peaks near LAS. These

errors are smaller at more southern stations, and are acceptable in that they are smaller than the uncertainty in our instrument calibration.

The accelerations resulting directly from the vertical displacements are small, and need not be accounted for. An upper limit on these accelerations can be established based on a 1000 μgal tidal gravity change, which is larger than any observed. This gravity change corresponds to an elevation change (equation 3) of 377 cm. The gravity variation is diurnal, so the acceleration, a_D, is approximately:

$$\begin{aligned} a_D &= 377 \times (2\pi/86400)^2 \times 10^6 \ \mu\text{gal} \\ &= 2 \ \mu\text{gal} \end{aligned} \tag{4}$$

or 0.2% of the gravity change due to the elevation change. This is much less than the uncertainty in the instrument calibration.

Tidal Harmonic Analysis

The tide generating force experienced by the water masses on the earth results primarily from the gravitational attraction of the moon and sun, and the earth's rotation. The height of the tide at a particular place may be represented harmonically by the formula (Schureman, 1941):

$$h = \Sigma f H \cos (at + \phi - \kappa) \tag{5}$$

where

h = height of the tide at time t

H = mean amplitude of the tide constituent

f = factor for correcting the mean amplitude H to the year of t, always near unity

a = constituent frequency

ϕ = phase of the corresponding term in the tide generating force when t = 0

κ = phase lag of the constituent with respect to the generating force

Although the tide-generating force contains a large number of constituents of the form indicated in equation (5), the tidal water level change at a given location can usually be represented accurately by a small number of constituents which have large amplitude. For each constituent in the sum, two quantities, the amplitude H and the phase κ, must be determined from observational data. These quantities are time-independent and are called the harmonic constants.

The tidal gravity records obtained during RISP were analyzed for the harmonic constants of the tide by the standard method of the National Ocean Survey (Schureman, 1941). In addition, the LAS record in Figure 2 was digitized at one-hour intervals and subjected to the same analysis. The results of the analysis are presented in Table 4. Also in the table are the harmonic constants of the tide at McMurdo (Gilmour, 1963). The analysis indicated that the height of the ocean

Table 4. Tidal harmonic constituents in the southern Ross Sea.

Site	K_1		P_1		O_1		M_2		S_2		N_2	
	A[a]	P[b]	A	P	A	P	A	P	A	P	A	P
Base	43	186	14	186	35	174	8	213	10	112	9	94
C13	30	200	10	200	34	190	3	300	4	130	5	160
C16	31	200	10	200	27	190	3	310	2	160	4	147
C36	37	160	12	160	32	153	3	75	6	25	4	44
F9	41	206	14	206	40	190	8	258	11	142	8	138
J9	37	191	12	191	37	172	7	205	8	106	7	78
LAS	34	154	11	154	25	141	3	35	5	342	5	344
McM	26	196	9	196	26	186	4	6	2	268	3	234
019	31	208	10	208	29	196	4	340	2	190	3	185
RI	44	160	15	160	38	140	5	130	10	26	9	5

[a] Amplitude in cm

[b] Phase angle in degrees relative to the Greenwich Meridian

tide in the southern Ross Sea can be represented by six harmonic constituents. The three largest of these are diurnal, and account for the diurnal character of the observed gravity tide (Figure 6). These seven constituents comprise the four largest diurnal constituents, and the three largest semidiurnal constituents in the tide-producing force. Table 4 shows the frequency, maximum amplitude, and amplitude at 78°S latitude of the luni-solar gravity for each of the 9 greatest constituents of the tide-producing force. The results (Table 4) for LAS are about 20% larger than reported by Thiel and others (1960). The difference is due to the luni-solar effect, for which they made no correction.

Calculations required in the analysis were performed using a FORTRAN computer program (Dennis and Long, 1971) developed by the National Oceanic and Atmospheric Administration (NOAA). This particular program was used because it was designed for 29-day data series. The 29-day length is approximately a multiple of the synodic periods of the more important constituents of the tide-producing force. It is considered the minimum length necessary for a satisfactory determination of the most important constituents (Schureman, 1941, p. 51, 52), and it is appropriate for the lengths of the RISP tidal gravity records.

The use of 29-day data windows limits the frequency domain resolution of the analysis. The 29-day boxcar (rectangular) window used adequately separates all the important constituents (Table 5) except P_1 from K_1. Figure 7 shows the amplitude of the boxcar window in

Table 5. Rigid-earth tidal gravity amplitudes.

Constituent	Frequency (°/hr)	Amplitude	
		Maximum (μgals)	At 78°S Latitude (μgals)
Q_1	13.3986609	6	2.4
O_1	13.9430356	31	12.6
P_1	14.9589314	14	5.7
K_1	15.0410686	44	17.9
N_2	28.4397295	14	0.6
ν_2	28.5125831	3	0.1
M_2	28.9841042	75	3.2
S_2	30.0	35	1.5
K_2	30.0821373	9	0.4

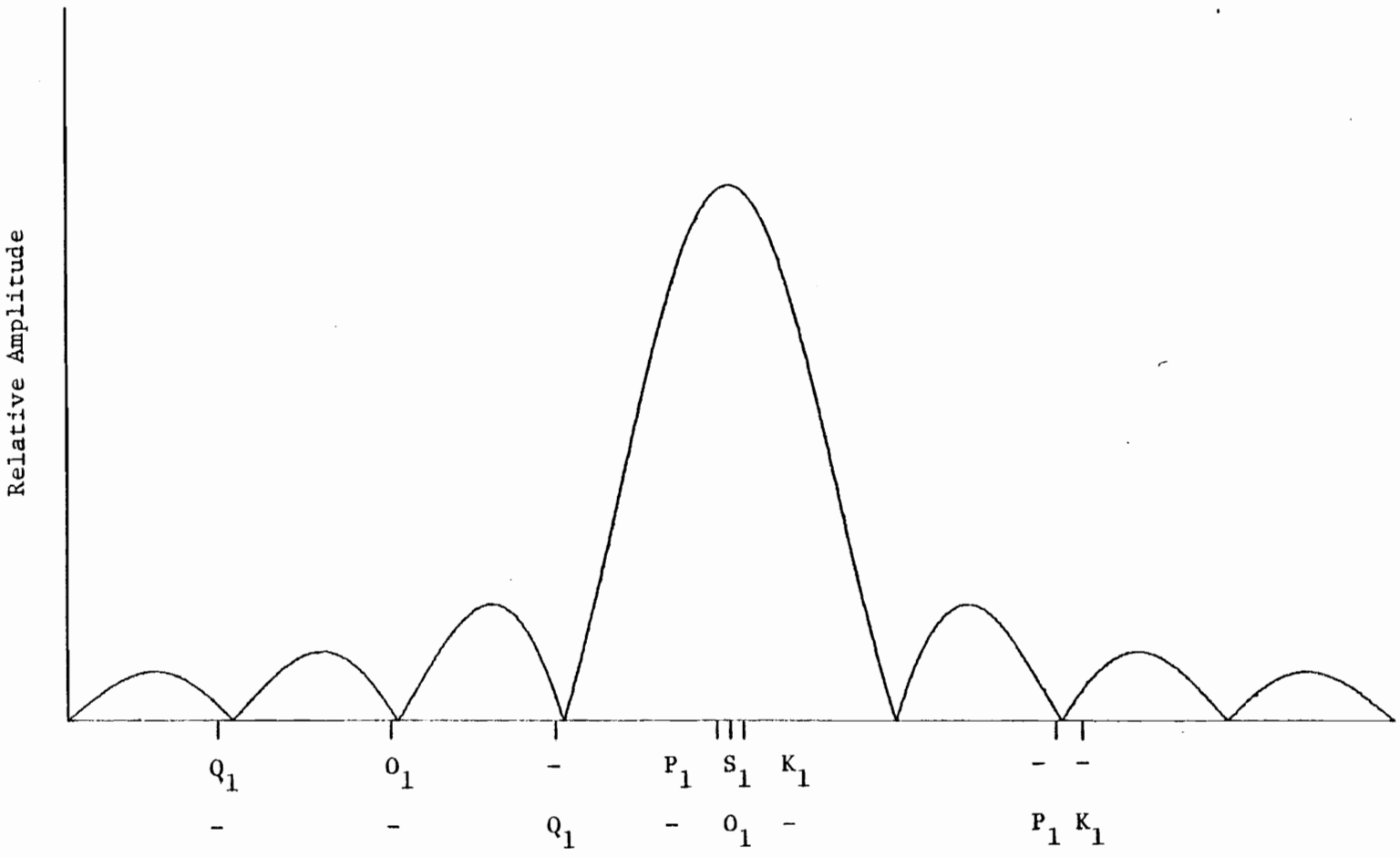

Figure 7a. Relative positions of the diurnal tide constituents in the frequency-domain window associated with a 29-day rectangular time-domain window. Constituent frequencies are given in Table 5.

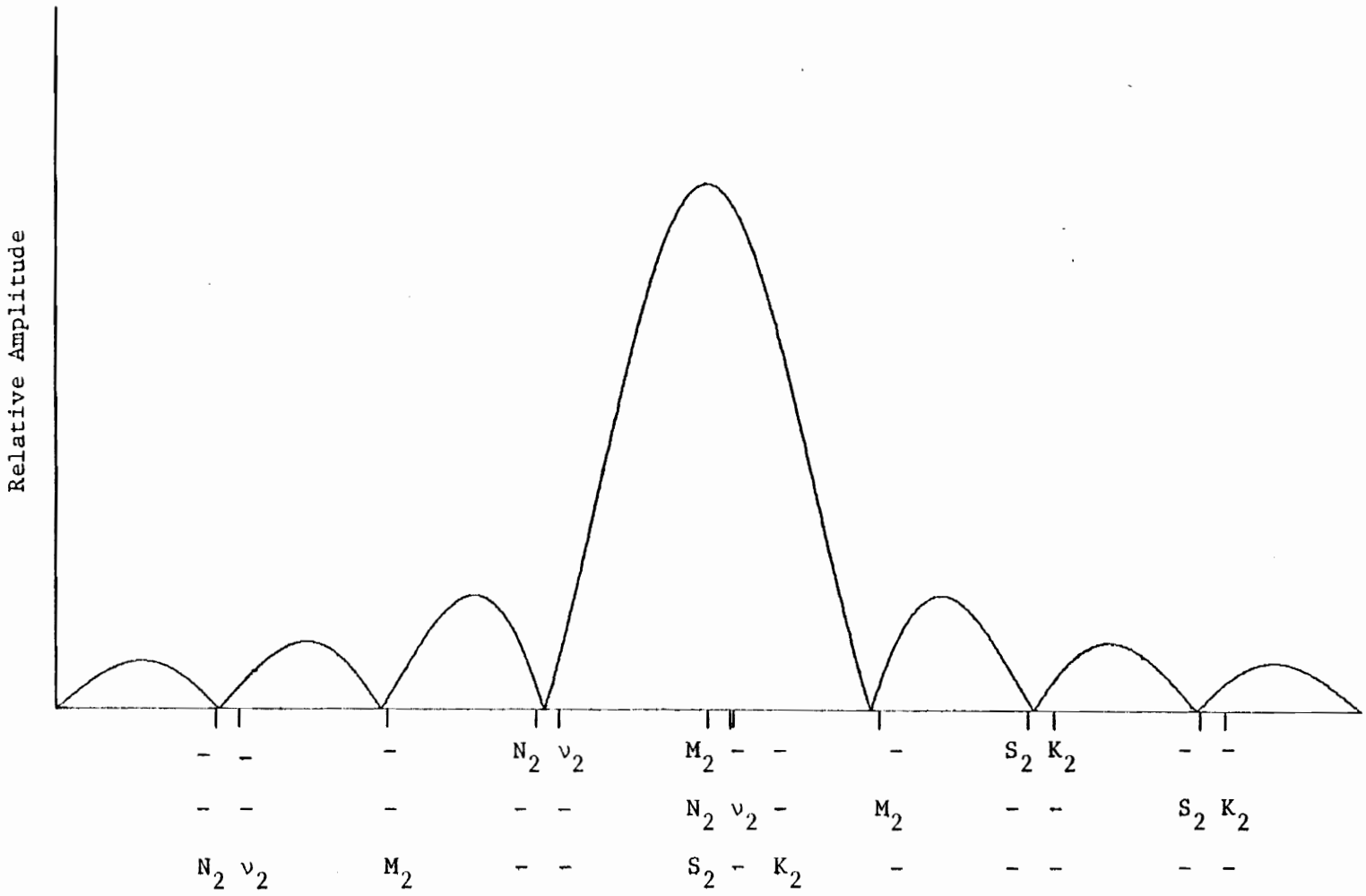

Figure 7b. Relative positions of the semidiurnal tide constituents in the frequency-domain window associated with a 29-day rectangular time-domain window. Constituent frequencies are given in Table 5.

the frequency domain, and the relative positions of the more important constituents. The NOAA analysis separates P_1 and K_1 by assuming that the relationship between the constituents in the observations is the same as in the tide-generating force. The validity of this assumption on a world-wide basis is indicated by a test reported by Schureman (1941, p. 79). In that test 60 stations in different parts of the world where the harmonic constants had been determined from observations were selected, and a comparison was made between the constants obtained by inference and from observations. The following results were obtained: maximum difference 8.2 cm, 49°; average difference 0.9 cm, 8°; differences less than 1.5 cm, 85%; differences less than 3.0 cm, 92%; differences less than 10°, 76%; differences less than 20°, 92%. In most parts of the world, then, P_1 can be adequately separated from K_1 by inference. In the Ross Sea the validity of the inference technique can be tested using the data from two RISP camps, F9 and C16, and from McMurdo. Gilmour and others (1962) reported the analysis of records obtained at McMurdo Sound during the 29-day periods whose central days were 17 December 1957, 16 January 1958, 16 June 1958, and 16 July 1958. It is seen that the records occur in two pairs separated by one-half year. For the constituent P_1, the amplitude average from the four sets was 8.8 cm with the largest deviation from the mean being 0.3 cm or 3.4%. The largest deviation from the mean phase was 5°. At RISP camp F9, 58-days of data were obtained during the 1976-77 field season, which were analyzed as independent 29-day segments. The means of the

P_1 harmonic constants were 13.8 cm and 205°, with deviations of 0.3 cm (2.2%) and 2°. At C16, records obtained during the 1976-77 and 1977-78 field seasons provide independent 29-day sets for analysis. The means of the P_1 constants in this case were 10.6 cm and 199° with deviations of 0.4 cm (3.8%) and 0°. The evidence that P_1 and K_1 can be separated reliably by inference based on the relationship of their driving forces is compelling.

Uncertainties in the Harmonic Constants

The uncertainties in the harmonic constants of the Ross Sea tide determined in this study (Table 4) can be estimated in two ways: (1) examination of Fourier amplitude spectra, and (2) comparison of the values obtained for independent 29-day records at C16 and F9.

Fourier amplitude spectra calculated from a representative 29-day data segment from each of the eight RISP camps are presented in Figure 8. Each of these spectra clearly shows peaks at the diurnal tidal frequencies, the largest peak being due to the combined effect of constituents P_1 and K_1. All of the spectra except C13 also contain peaks at the semidiurnal tidal frequencies. The noise level on the spectra is generally near 5 μgals, except on the C13 record, which corresponds to a 2 cm uncertainty in the amplitudes in Table 3. Viewing the pair of harmonic constants as a vector, the uncertainty in the phase can be estimated by taking the noise to be a second vector of 2 cm amplitude oriented normal to the first. For the diurnal constituents the amplitudes are typically greater than

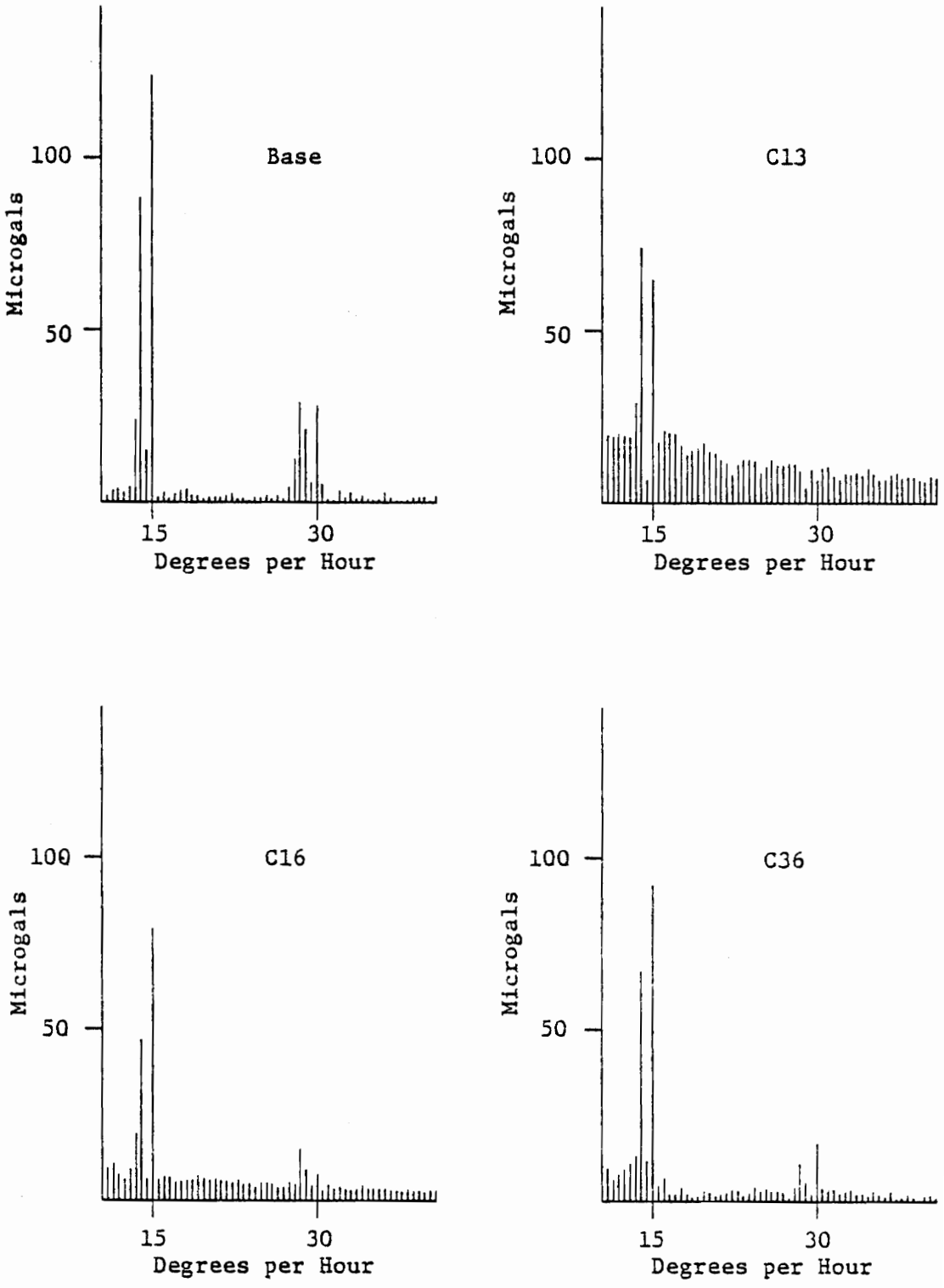

Figure 8a. Fourier amplitude spectra of the last 29 days of the RISP gravity records (Figure 6). The lines near frequency 15°/hr are due to the diurnal constituents. The semidiurnal constituents are near 30°/hr.

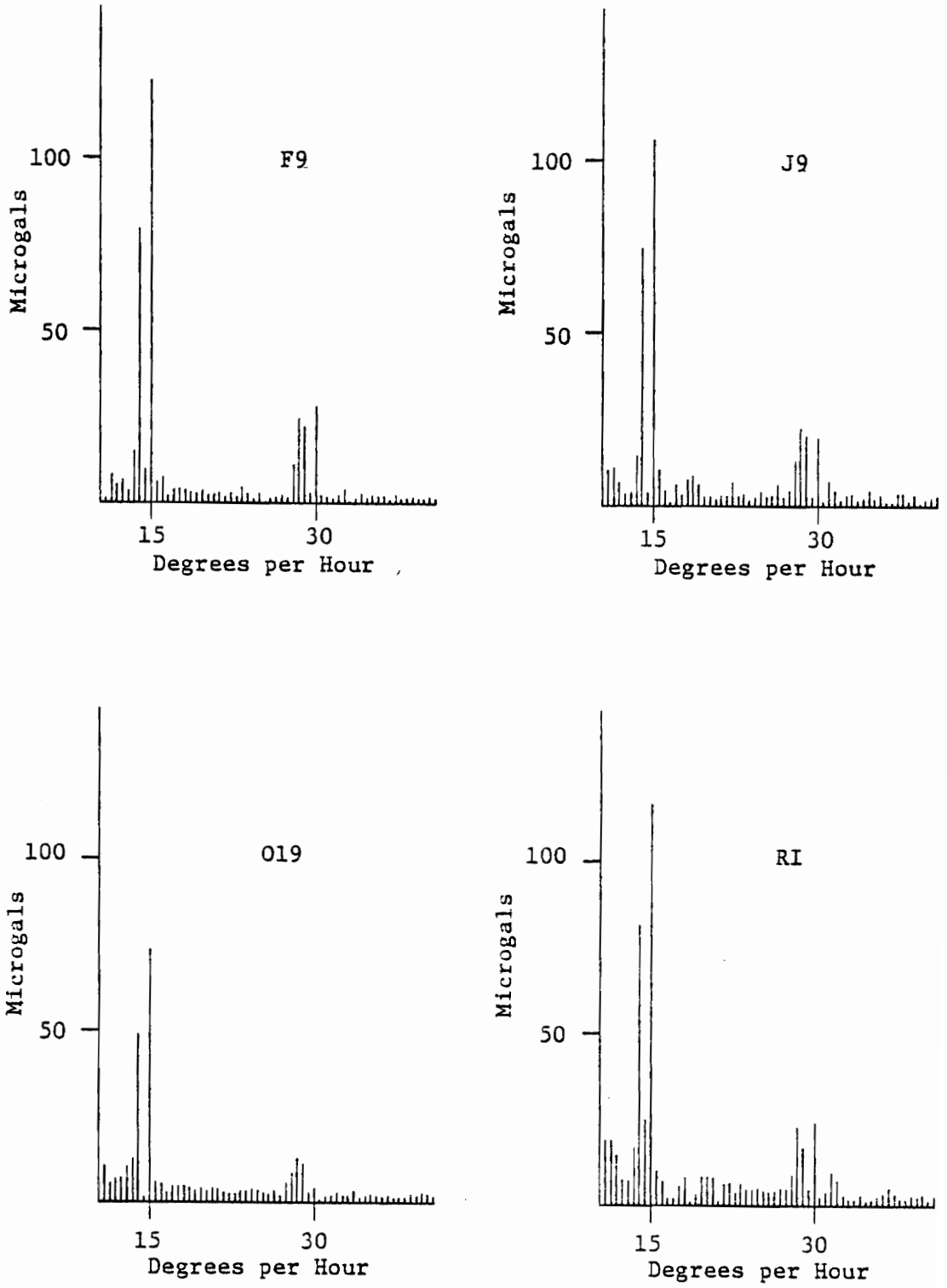

Figure 8b. Fourier amplitude spectra of the last 29 days of the RISP gravity records (Figure 6). The lines near frequency 15°/hr are due to the diurnal constituents. The semidiurnal constituents are near 30°/hr.

30 cm (P_1 and K_1 may be taken together). The maximum effect on the diurnal phase by the 2 cm noise level is approximately 4°, or 16 min uncertainty in the time of the constituent extrema. For the semidiurnal constituents the southeastern stations, Base, J9, and F9, have amplitudes near 8 cm, indicating a phase uncertainty of approximately 14°, or 30 min in the time domain. For the remaining stations, except C13, the semidiurnal amplitudes are near 4 cm, indicating a phase uncertainty of approximately 27°, or about 1 hour in the time domain. No estimates are made for the uncertainties in the harmonic constants at C13, although the results of the analysis are given in Table 4. It is noted that in spite of the apparently high noise level there, the values are consistent with those from other locations on the western side of the shelf (McM, O19, and C16).

Inferences of the uncertainties at F9 and C16 based on independent record segments are summarized in Table 6. The deviation from the mean values for constituents P_1 and K_1 have already been discussed in connection with the validity of the theoretical separation of these two constituents. In general, the deviation of the amplitudes from the mean of the two segments is less than 1 cm, the exception being the F9 O_1 amplitudes where the deviation is 2 cm. The deviations of the diurnal phases are 5° or less. The semidiurnal phase deviations are 4° or less at F9 where the semidiurnal amplitudes are near 10 cm, and are 25° or less at C16 where the amplitudes are near 3 cm. These values are consistent with the error estimates based on the amplitude spectra.

Table 6. Differences in the harmonic constants determined from independent record segments from C16 and F9.

Constituent	F9		C16	
	Mean	Deviation	Mean	Deviation
K_1	41 cm	0.8 cm	31 cm	0.6 cm
	206°	2°	200°	2°
O_1	40 cm	2.1 cm	27 cm	1.0 cm
	190°	2°	190°	5°
M_2	8 cm	0.5 cm	3 cm	0.5 cm
	258°	3°	310°	16°
S_2	11 cm	0.1 cm	2 cm	0.2 cm
	142°	4°	160°	25°
N_2	8 cm	0.6 cm	4 cm	0.5 cm
	138°	4°	147°	14°

Cotidal-Coamplitude Charts

The primary goal of this effort was to determine the spatial variation of the height of the ocean tide beneath the Ross Ice Shelf. Within the previously discussed uncertainties this has been successfully accomplished, and maps showing the spatial variation of the amplitude and phase of the principal constituents of the tide have been prepared. Contours of constituent amplitude (coamplitude lines), and of constituent phase (cotidal lines) for K_1, O_1, M_2, N_2, and S_2 are presented in Figures 9-13 respectively. No separate map was drawn for P_1. The P_1 map is the same as that for K_1, with the amplitudes scaled by one-third. The cotidal lines can be viewed as the position at different times of the crest of a ficticious wave that would exist if only that particular constituent were disturbing the sea surface. The height of the wave crest above mean sea-level is not necessarily constant along the crest. If the cotidal lines are nearly parallel, then the tide propagates as a progressive wave, and the speed of the tidal wave is approximately that of a shallow-water gravity wave, given by

$$C_w = \sqrt{gh}$$

where g is the gravitational acceleration (9.8 m/sec^2), and h is the water depth.

The diurnal cotidal lines (Figures 9, 10) display a simple, nearly parallel pattern. The spacing between 10° lines is in the 100 km to 150 km range, which is appropriate for the 150 m to 400 m

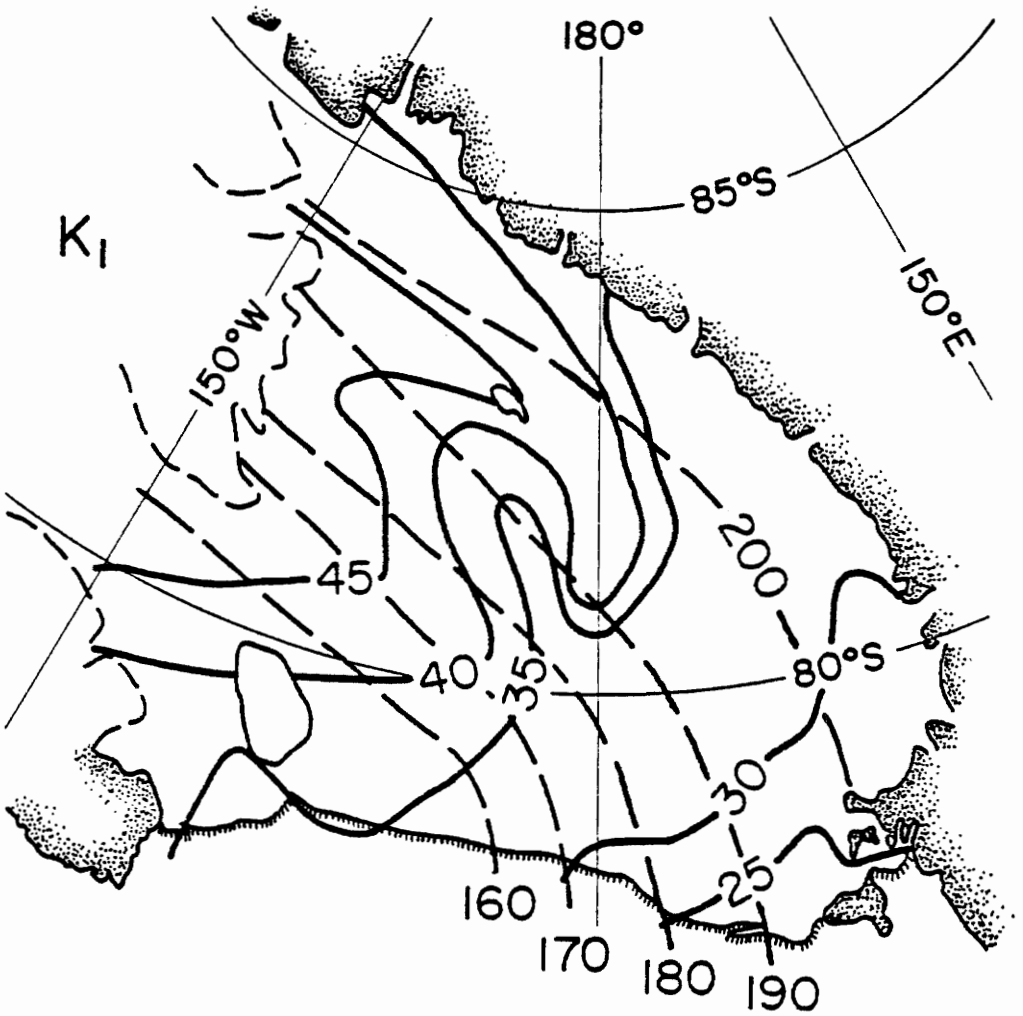

Figure 9. Cotidal (dashed) and coamplitude (solid) lines for the constituent K_1. Cotidal lines are labeled in degrees relative to Greenwich: coamplitude labels are in centimeters. The lines are the same for the constituent P_1 except that the amplitudes are scaled by one-third.

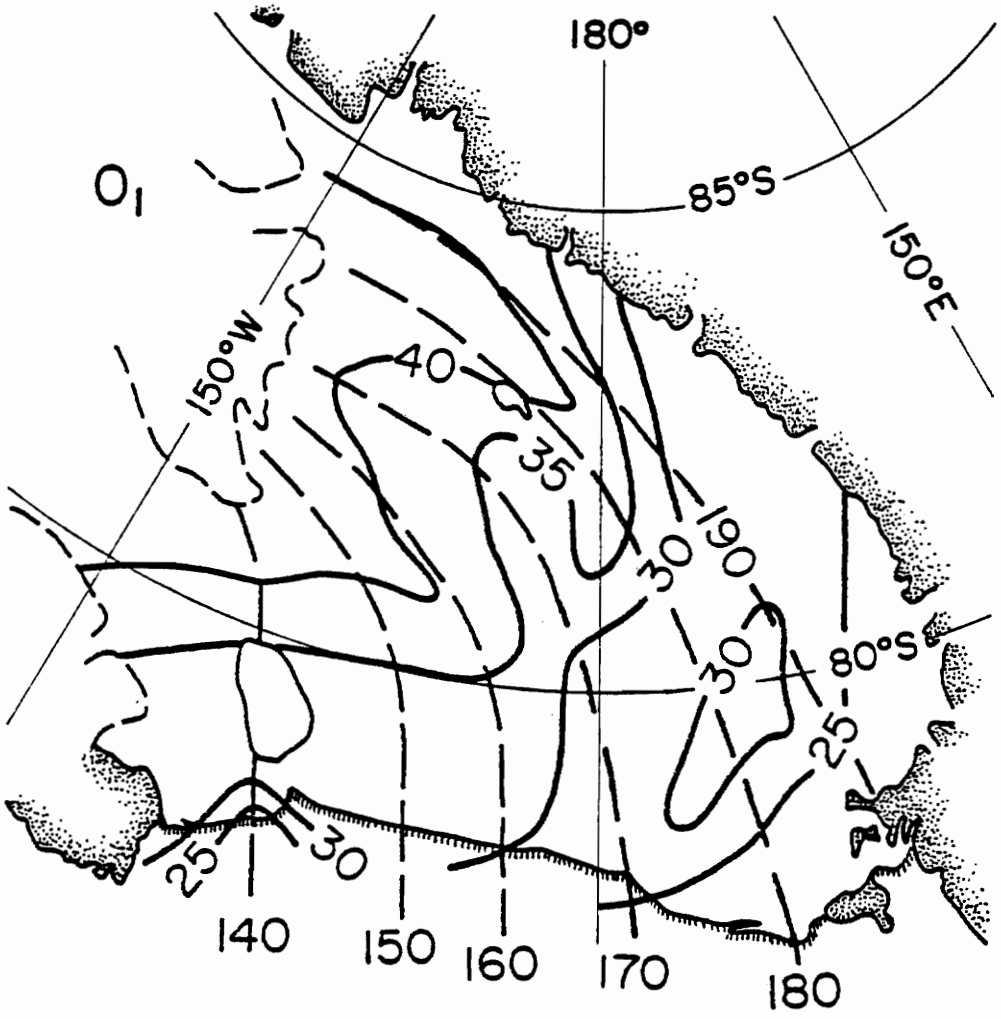

Figure 10. Cotidal (dashed) and coamplitude (solid) lines for the constituent O_1. Cotidal lines are labeled in degrees relative to Greenwich: coamplitude labels are in centimeters.

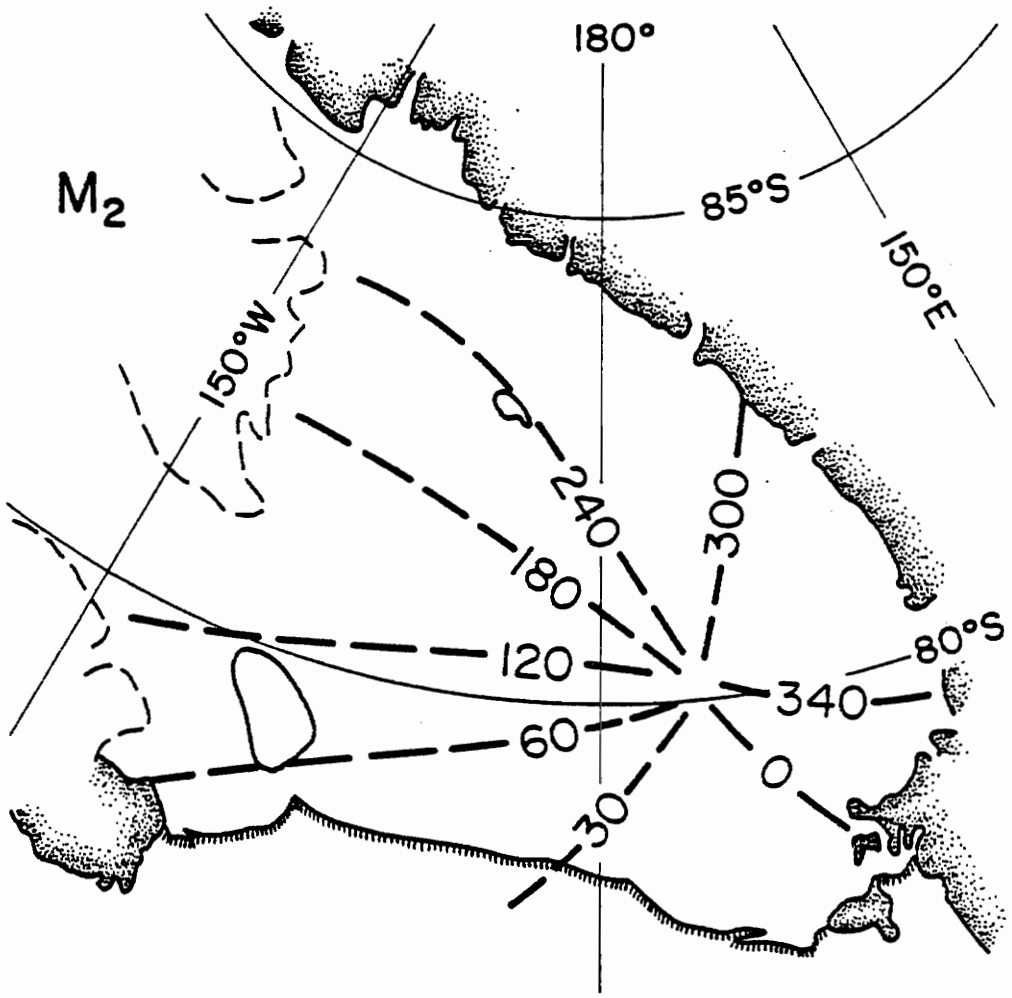

Figure 11. Cotidal lines for M_2 showing an amphidromic region near RISP camp C13. Lines are labeled in degrees relative to Greenwich.

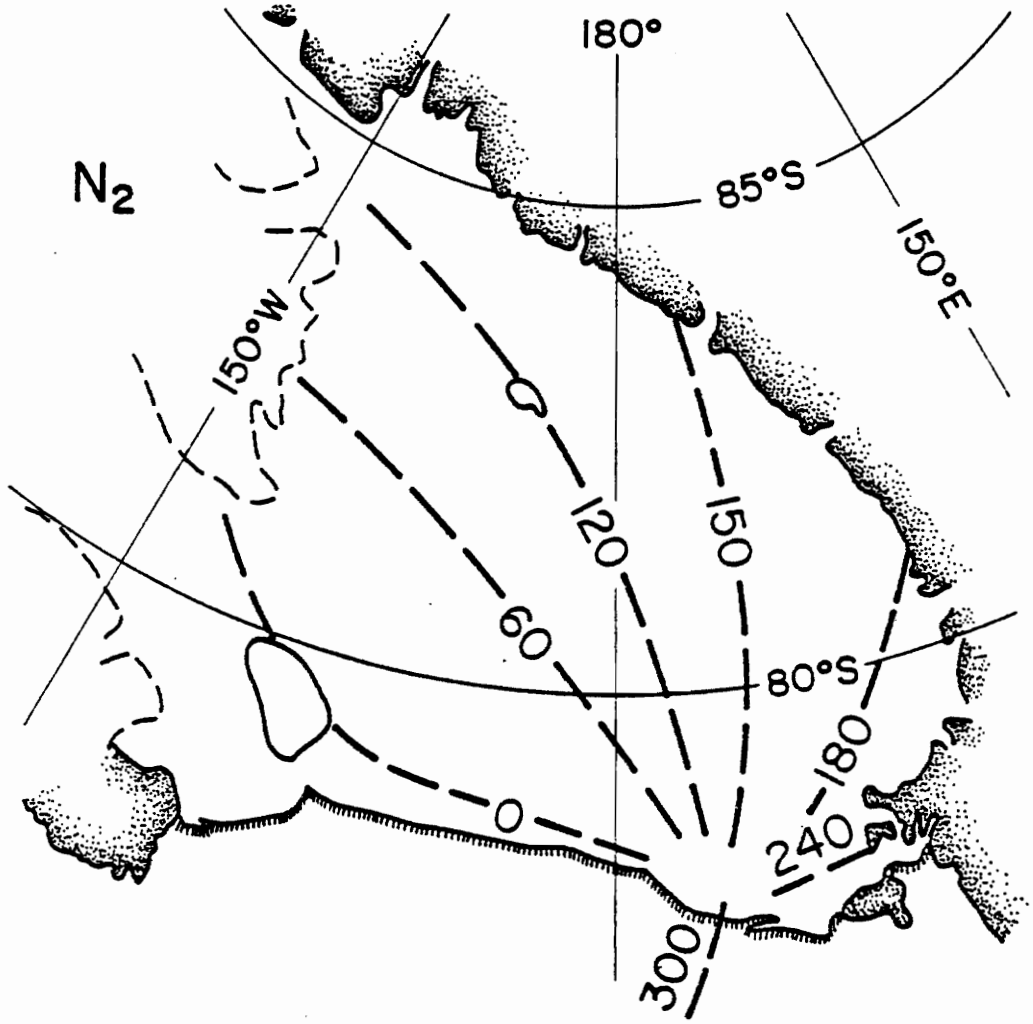

Figure 12. Cotidal lines for N_2 showing an amphidromic region near RISP camp C13. Lines are labeled in degrees relative to Greenwich.

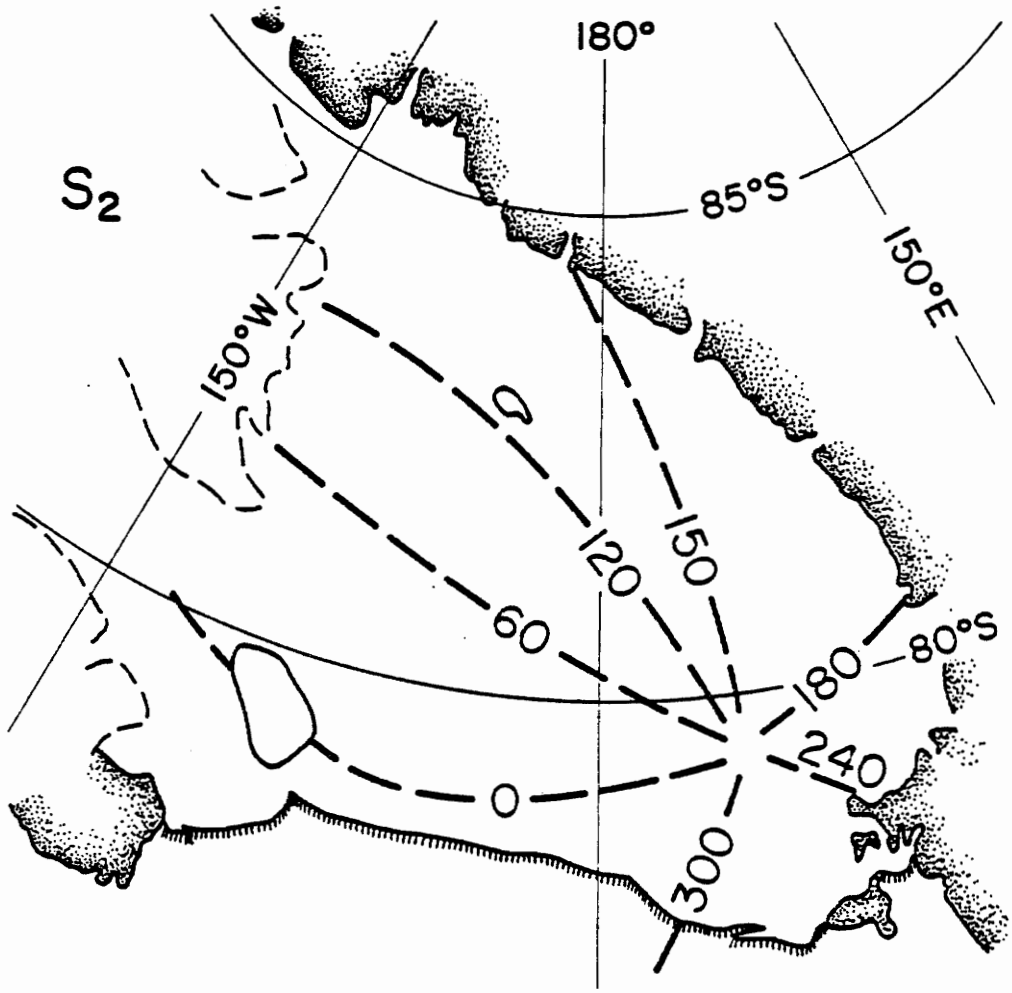

Figure 13. Cotidal lines for S_2 showing an amphidromic region near RISP camp C13. Lines are labeled in degrees relative to Greenwich.

thickness of the water-layer beneath the ice shelf. The diurnal coamplitude lines shown are more complex than could have been drawn by simple interpolation between points where measurements were made. The location of these contours was based on an observed relationship between the constituent amplitude and the thickness of the water-layer beneath the station, together with a map of the thickness of the water-layer beneath the ice (Greishar and Bentley, 1978; Figure 14). This relationship is illustrated in Figure 15, where curves have been fitted to the data on the assumption that the relationship is similar to that between the wave height and ocean depth for a wave in a shallow canal of slowly varying depth. In such a canal the wave amplitude is inversely proportional to the fourth root of the depth (Lamb, 1941). Curves of this form are intuitively attractive since the wave trajectories are nearly constant and parallel. For the constituents K_1 and O_1, proportionality constants of 144 and 129, respectively, for amplitude in centimeters and depth in meters, were found by minimizing the root-mean-square (RMS) error with respect to the constant. The minimum RMS errors were found to be 1.0 cm (K_1) and 2.4 cm (O_1). These values are about the same as the estimated uncertainty in the constituent amplitudes. Only data from the RISP camps were used to fit the curves in Figure 15, and the C13 data were excluded because of the greater uncertainty in those values. However, the C13 data are not inconsistent with the relationship, although the deviations are larger, as can be seen in Figure 15. The LAS data were not used because the station was at the ice front,

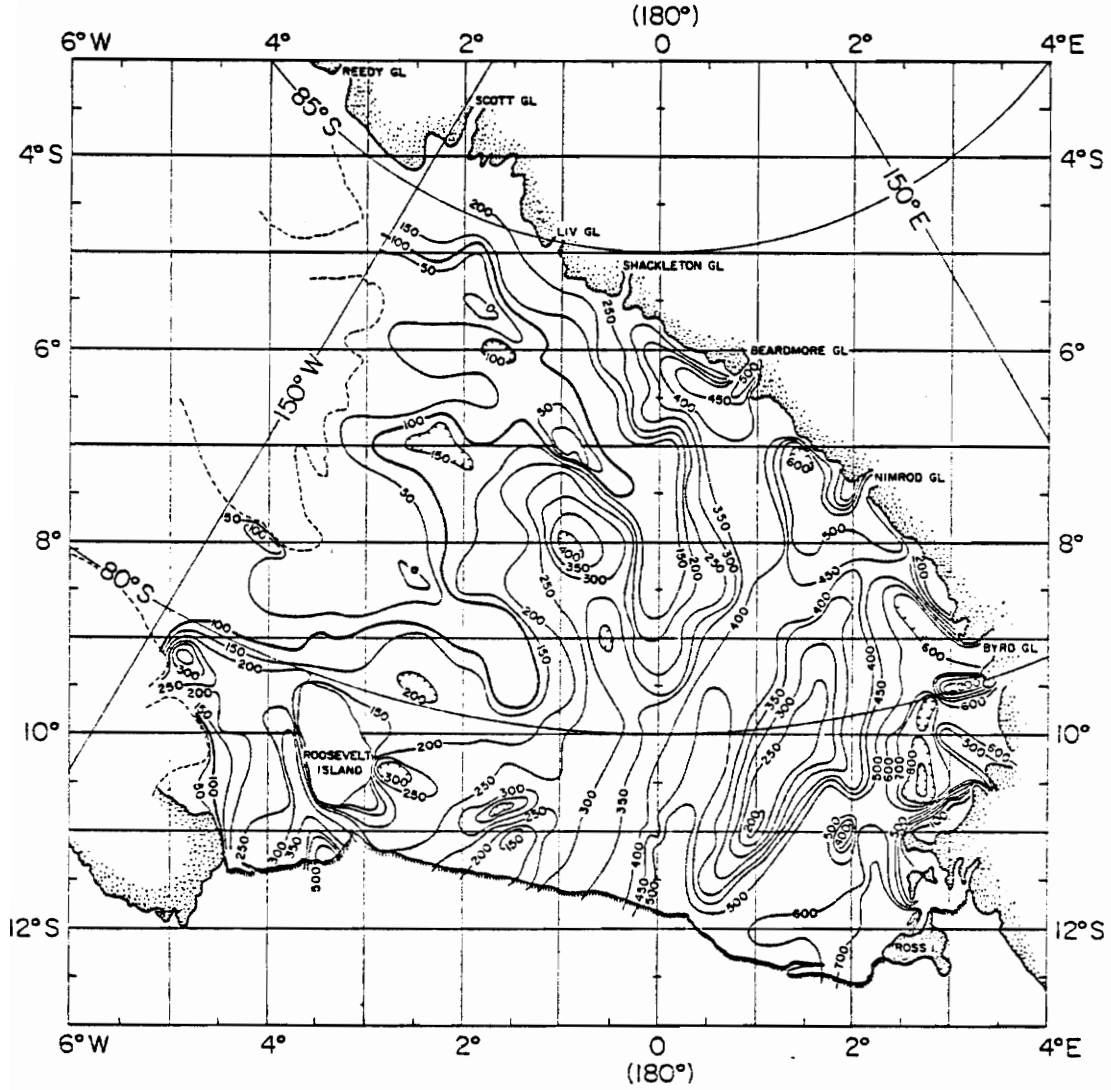

Figure 14. Contours of water-layer thickness beneath the floating ice shelf in meters (Greischar and Bentley, 1978).

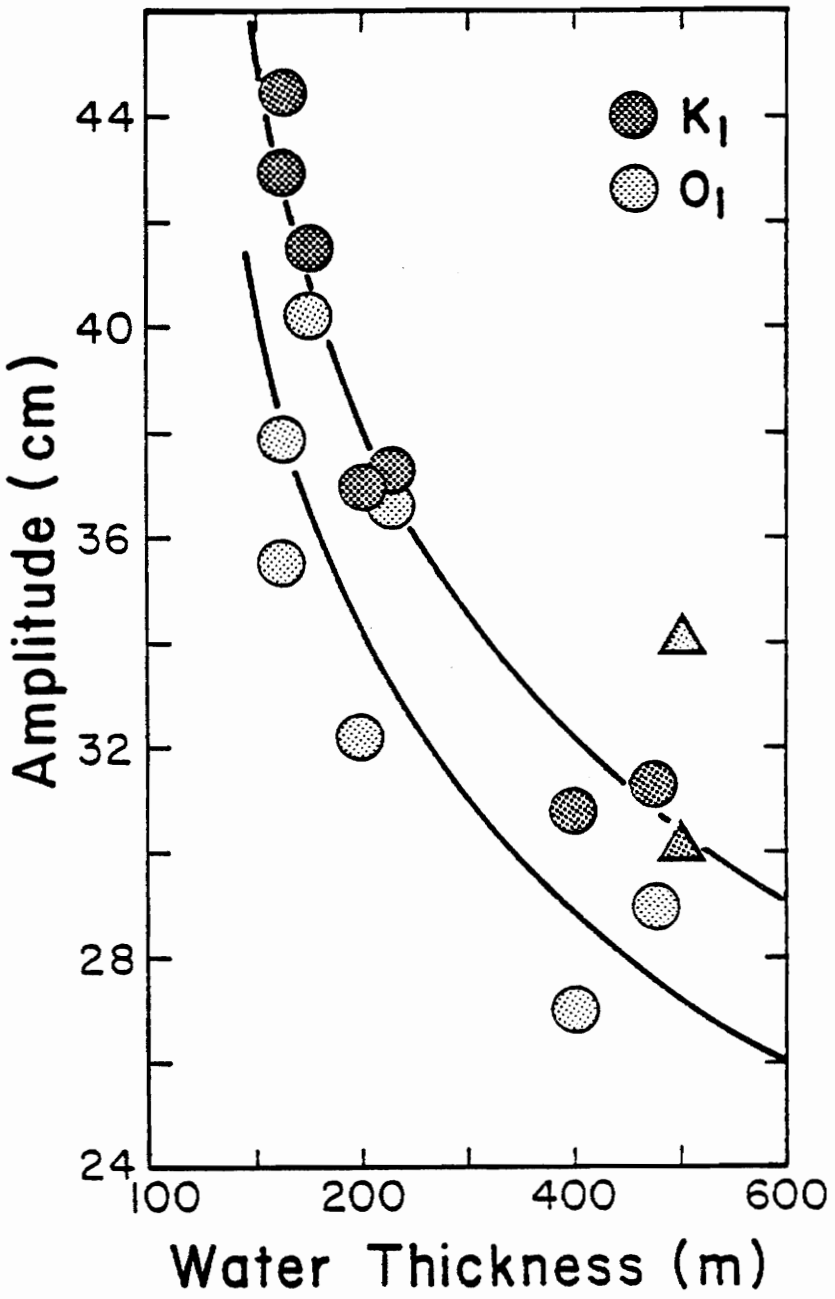

Figure 15. K_1 and O_1 constituent amplitudes plotted versus water-layer thickness for the RISP camps. Curves of the form $A = Ch^{-1/4}$ were fitted to the data on the assumption that the relationship is analogous to that for a wave in a shallow canal. The proportionality constants are 144 and 129 (amplitude in centimeters and water thickness in meters) for K_1 and O_1, respectively.

and the water depth there changes rapidly from 580 m to 360 m. This rapid change is inconsistent with the assumption that the water-layer thickness is slowly changing. Similarly, the data from McMurdo Sound were recorded near shore, and the complex topography of the sound is inconsistent with the required assumption.

The ocean tide in the Ross Sea must merge with the tide in the southern Pacific Ocean along the common boundary. The cotidal and coamplitude contours for the diurnal constituents shown in Figures 9 and 10 are reasonably continuous with corresponding contours for the same constituents shown on global ocean tide maps. For reference, global ocean tide maps by Estes (1977) and Tiron and others (1967) for the constituent K_1 are shown in Figures 16 and 17, respectively. A K_1 map for the Pacific Ocean only by Bogdanov (1973) is shown in Figure 18. Maps by the same authors for the constituent O_1 are shown in Figures 19, 20, and 21. For both K_1 and O_1, the map by Estes shows the phase to be about 30°, or 2 hr, behind the observed phase: Tiron's map shows the phase to be about 15°, or 1 hr, ahead of the observation. Bogdanov's maps appear to agree with the observed phases within about 15°, although his maps only extend to 66°S latitude, about 1300 km north of the Ross Ice Shelf. This agreement is quite good considering the dearth of observational values in the Ross Sea available at the time the global maps were made.

The spatial variation of the semidiurnal constituents is more complex. Because of the relatively greater uncertainties no coamplitude contours have been drawn: it is expected that the more

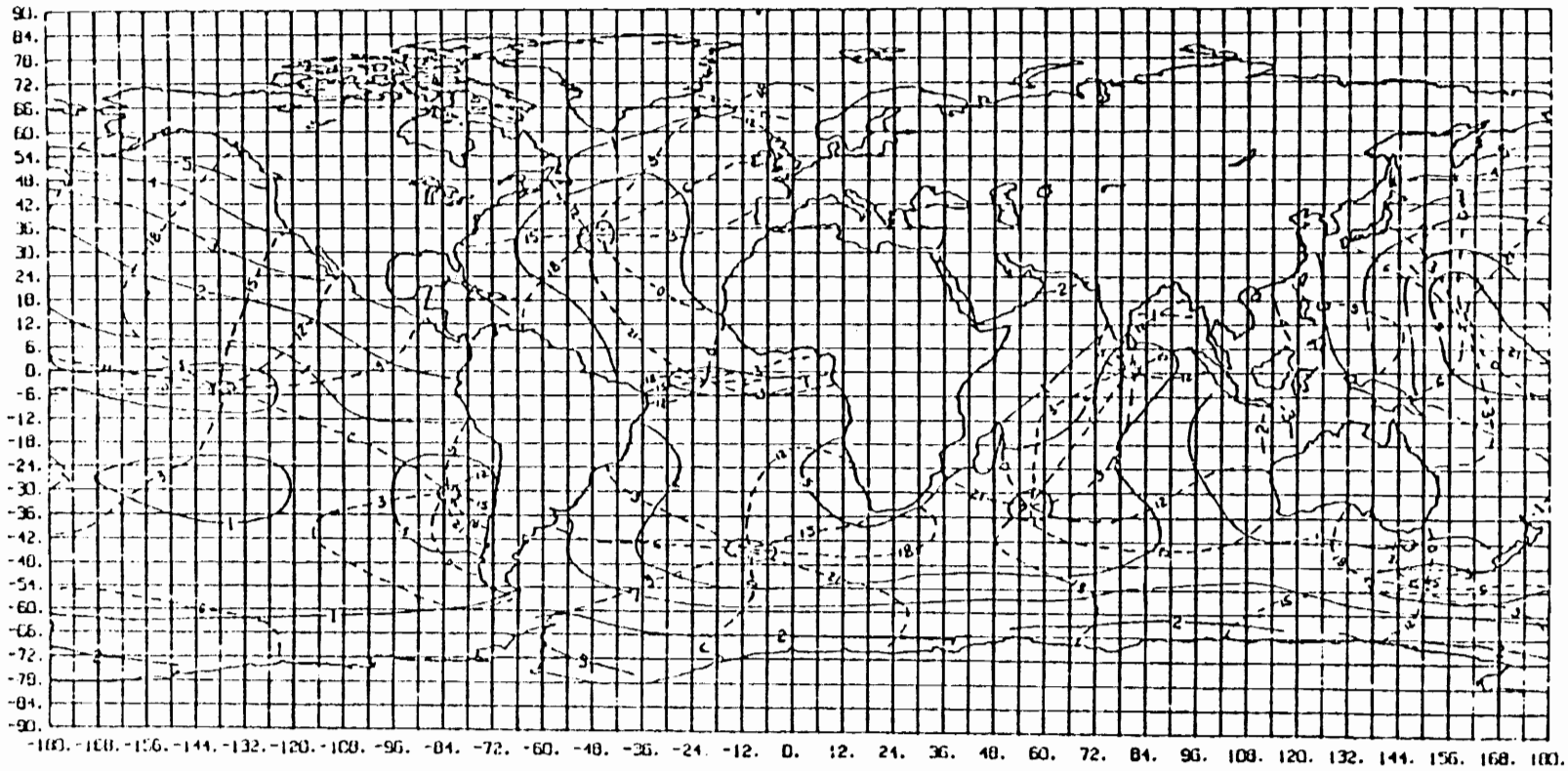

Figure 16. Global K_1 cotidal (dashed) and coamplitude (solid) lines from Estes (1977). Cotidal lines are labeled in solar hours (15°/hr) relative to Greenwich. Amplitudes are shown in decimeters.

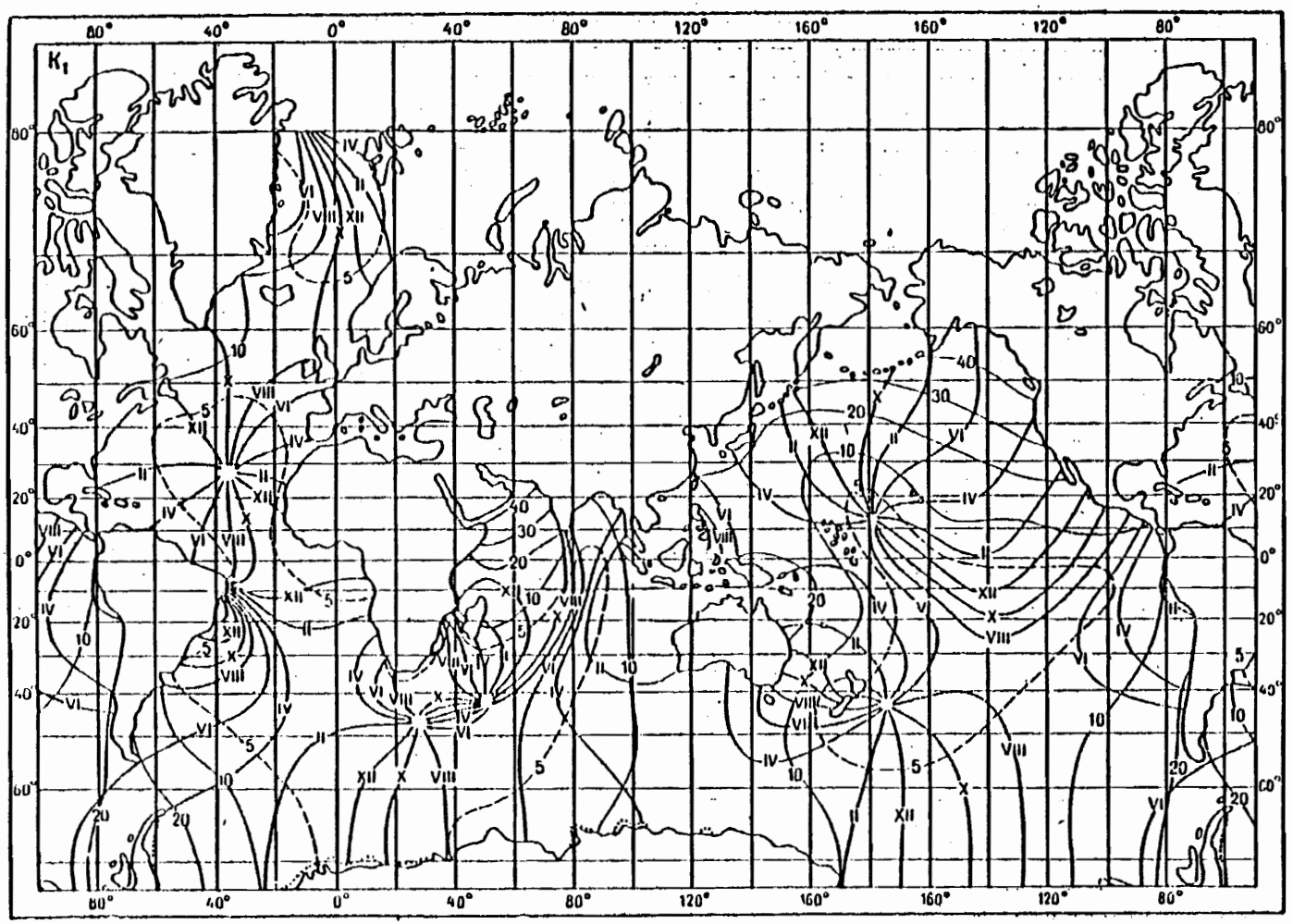

Figure 17. Global K_1 cotidal (Roman numerals) and coamplitude (Arabic numerals) lines from Tiron and others (1967). Cotidal lines are labeled in constituent hours (Table 5) relative to Greenwich. Amplitudes are in centimeters.

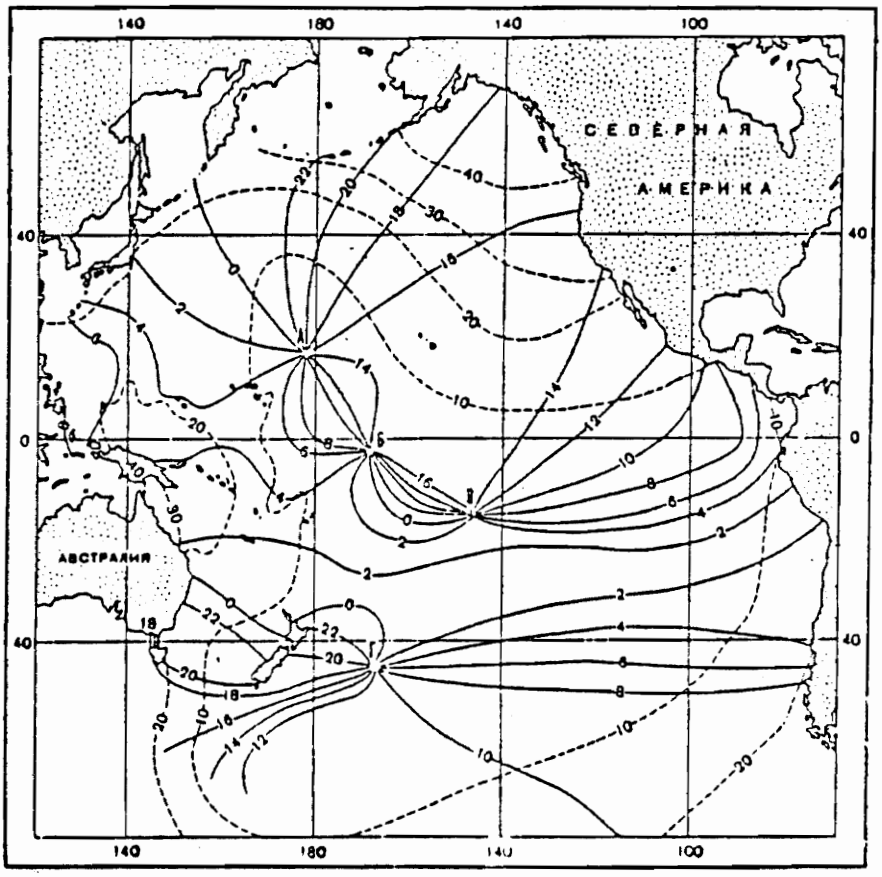

Figure 18. Pacific Ocean K_1 cotidal (solid) and coamplitude (dashed) lines from Bogdanov (1973). Cotidal lines are labeled in constituent hours (Table 5) relative to Greenwich. Amplitudes are in centimeters.

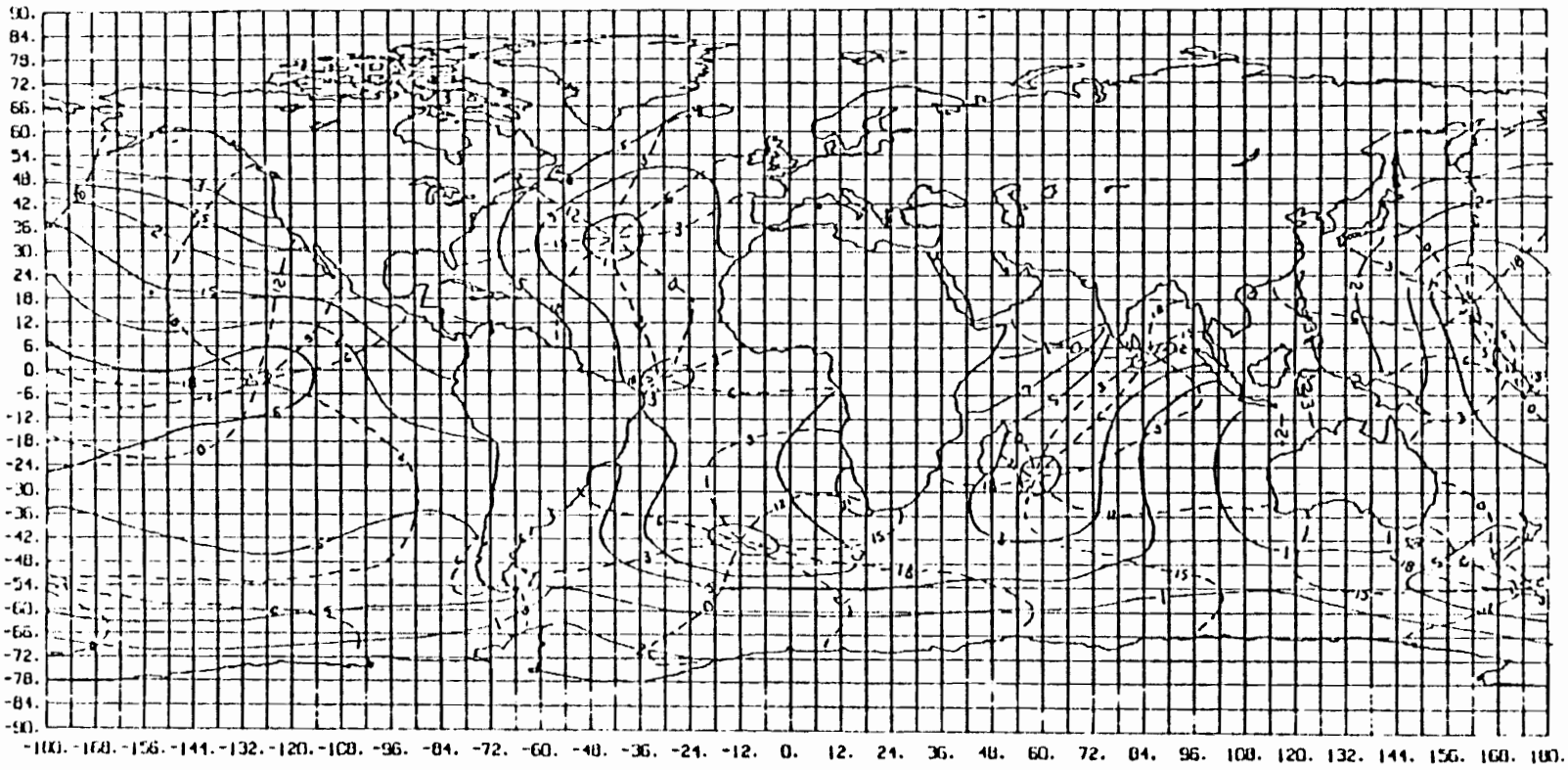

Figure 19. Global O_1 cotidal (dashed) and coamplitude (solid) lines from Estes (1977). Cotidal lines are labeled in solar hours (15°/hr) relative to Greenwich. Amplitudes are shown in decimeters.

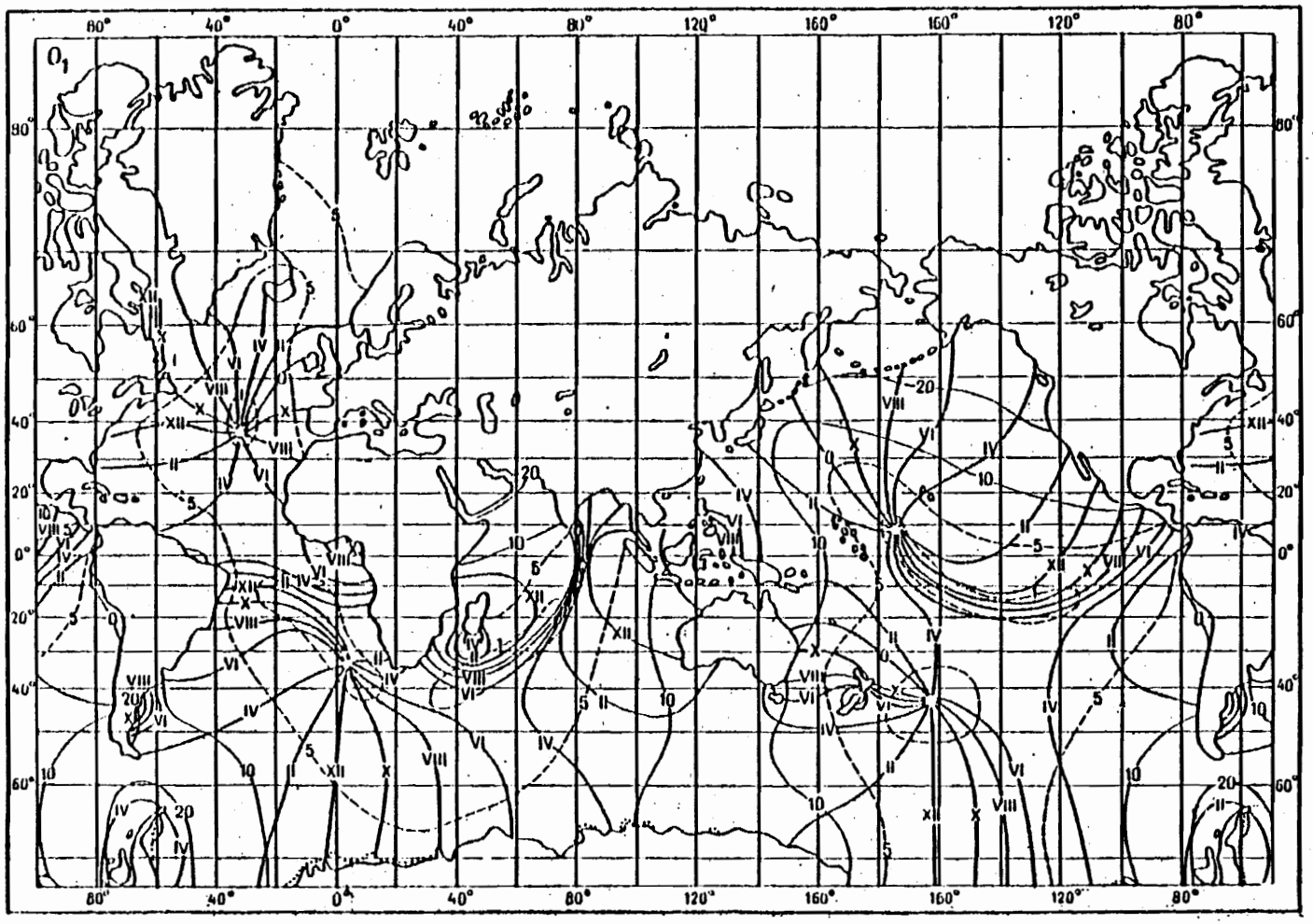

Figure 20. Global O_1 cotidal (Roman numerals) and coamplitude (Arabic numerals) lines from Tiron and others (1967). Cotidal lines are labeled in constituent hours (Table 5) relative to Greenwich. Amplitudes are in centimeters.

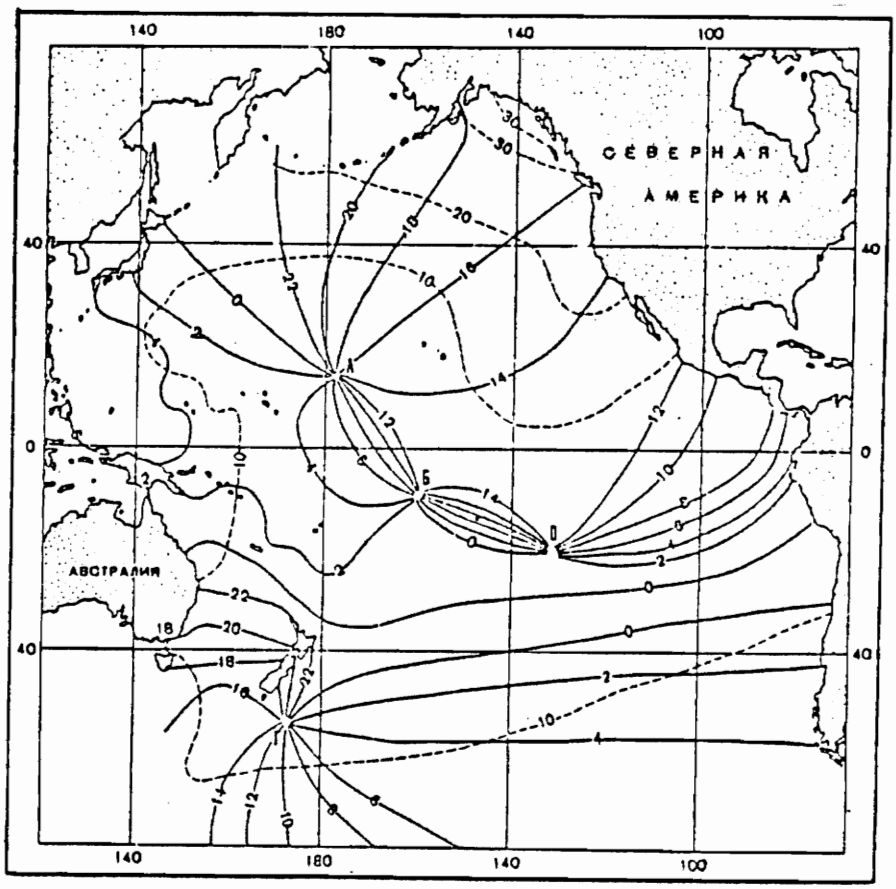

Figure 21. Pacific Ocean O_1 cotidal (solid) and coamplitude (dashed) lines from Bogdanov (1973). Cotidal ines are labeled in constituent hours (Table 5) relative to Greenwich. Amplitudes are in centimeters.

complex configuration of the cotidal contours would preclude a canal-type amplitude-depth dependence, such as that observed for the diurnal constituents. There is a similar phase variation in each of the three semidiurnal constituents having amplitude sufficiently great as to be measurable in this study (Figures 11-13). The small amplitudes in the northwestern portion of the region, and the regular increase in the constituent phase clockwise around the shelf indicate the existence of an amphidromic region (an area surrounding a notide point from which the radiating cotidal lines progress through all hours of the tidal cycle (Schureman, 1949)) near C13.

The semidiurnal constituent maps should merge with corresponding maps for the global ocean tide in the southern Pacific Ocean region. Recent maps of M_2 have been made by Zahel (1977), Estes (1977), Bogdanov (1973), Henderschott and Munk (1970), and Tiron and others (1967). These are shown in Figures 22-26, respectively. These maps can be divided into two classes according to the direction of increasing phase at the northern extremity of the Ross Ice Shelf, i.e., from LAS to McMurdo. This study indicates that the M_2 phase is about 35° at LAS and approximately 0° at McMurdo, and the cotidal-coamplitude map (Figure 11) reflects these values. In Figure 11 the phase is shown decreasing progressively from LAS to McMurdo, from 35° to 0°. The global maps by Estes, Bogdanov, and Tiron are consistent with this direction of decreasing phase. Estes' map indicates a decrease from about 130° at LAS to about 90° at McMurdo. Tiron's map shows

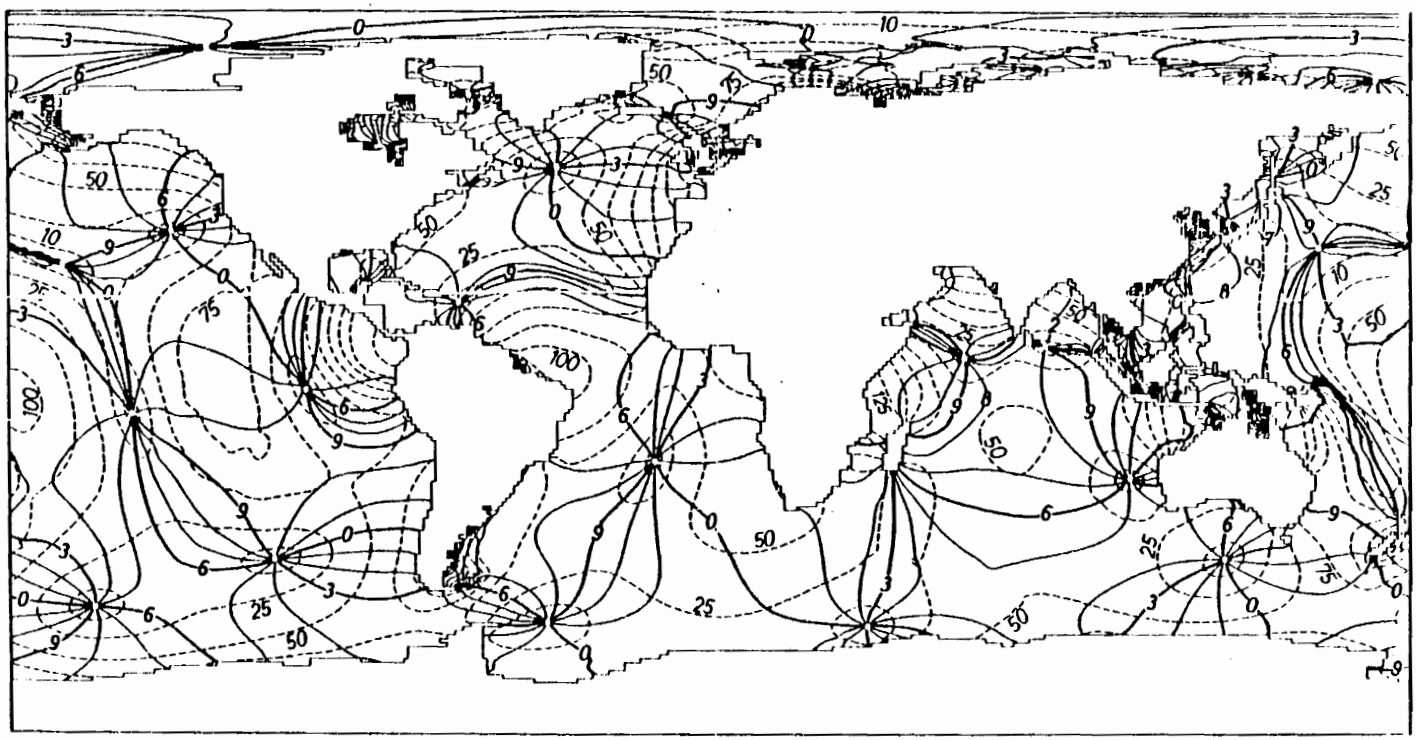

Figure 22. Global M_2 cotidal (solid) and coamplitude (dashed) lines from Zahel (1977). Cotidal lines are labeled in constituent hours (Table 5) relative to Greenwich. Amplitudes are in centimeters.

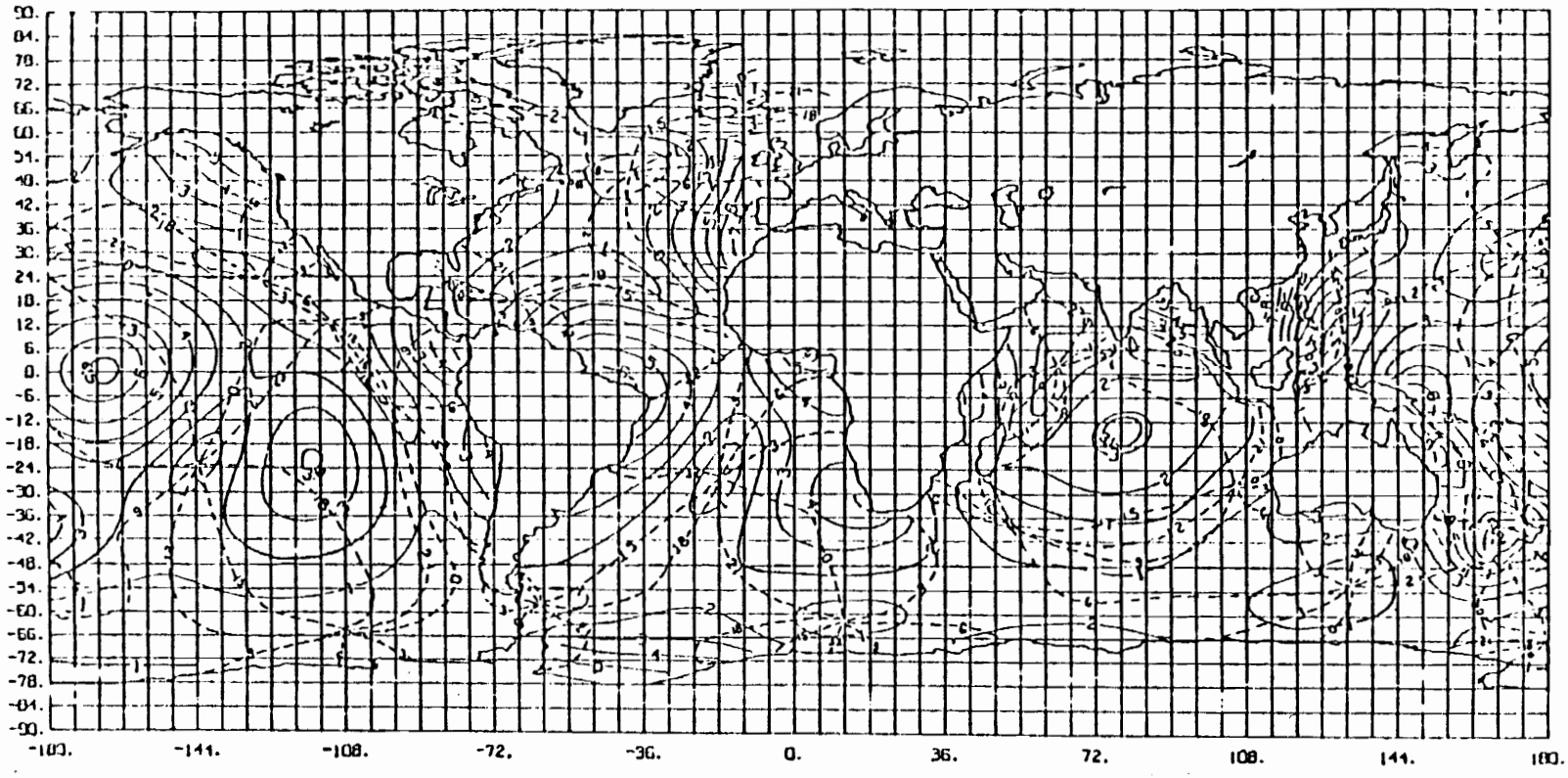

Figure 23. Global M_2 cotidal (dashed) and coamplitude (solid) lines from Estes (1977). Cotidal lines are labeled in solar hours (15°/hr) relative to Greenwich. Amplitudes are shown in decimeters.

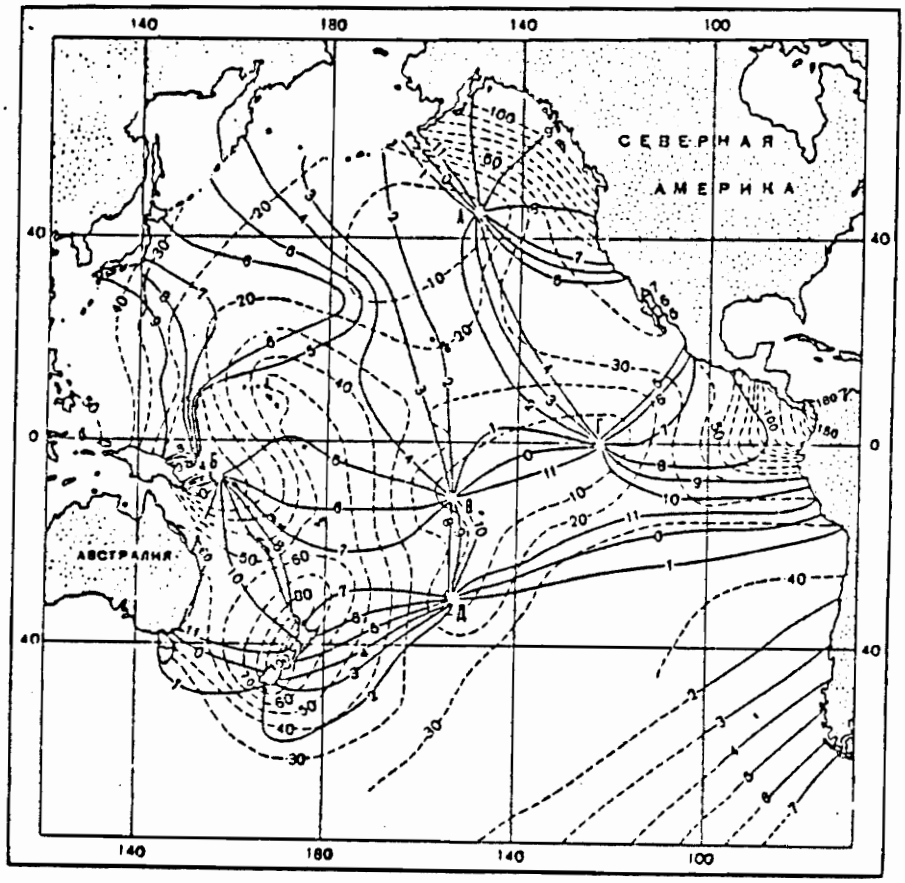

Figure 24. Pacific Ocean M_2 cotidal (solid) and coamplitude (dashed) lines from Bogdanov (1973). Cotidal lines are labeled in constituent hours (Table 5) relative to Greenwich. Amplitudes are in centimeters.

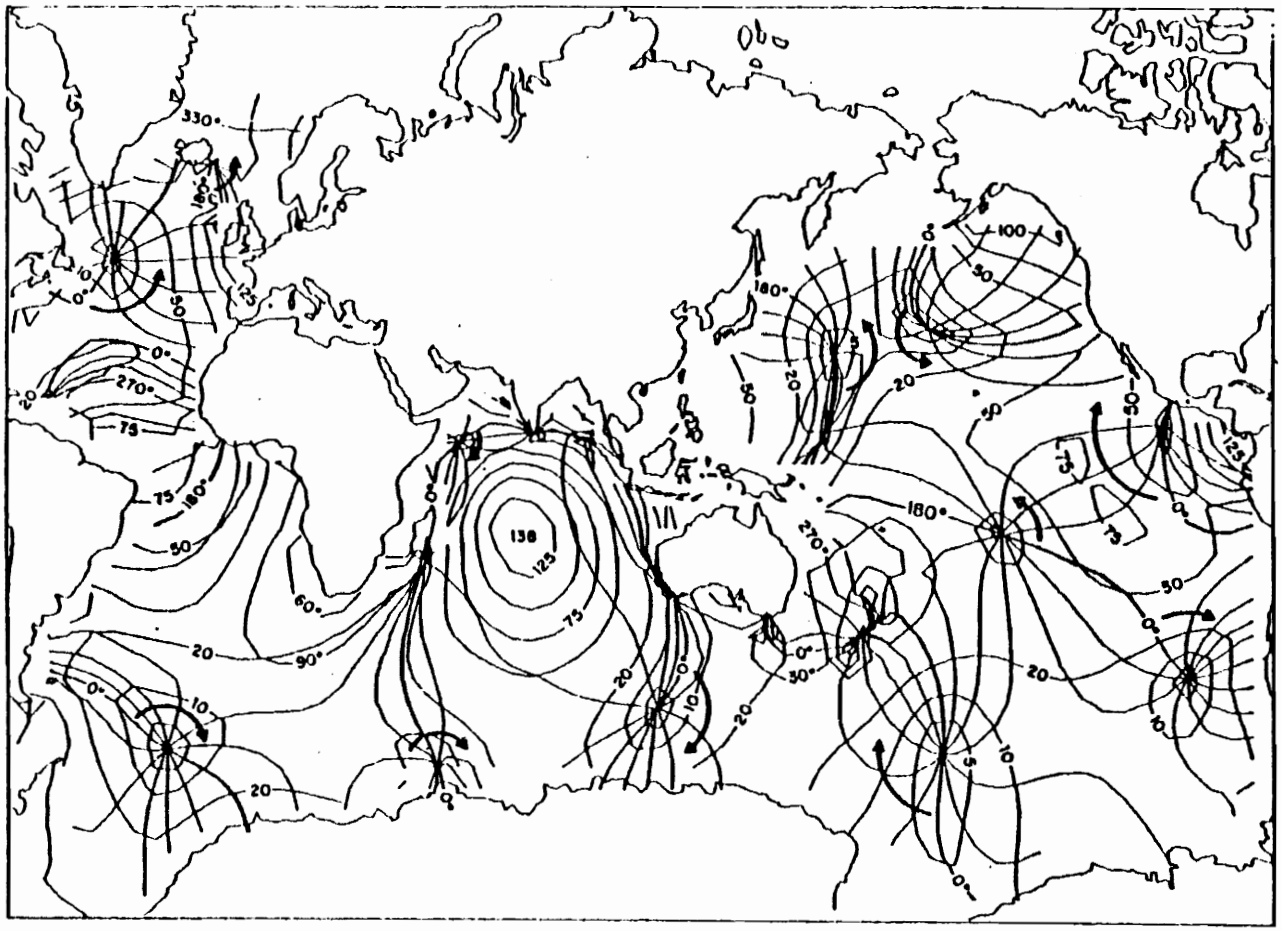

Figure 25. Global M_2 cotidal and coamplitude lines from Henderschott and Munk (1970). Cotidal lines are labeled in degrees relative to Greenwich. Amplitudes are in centimeters.

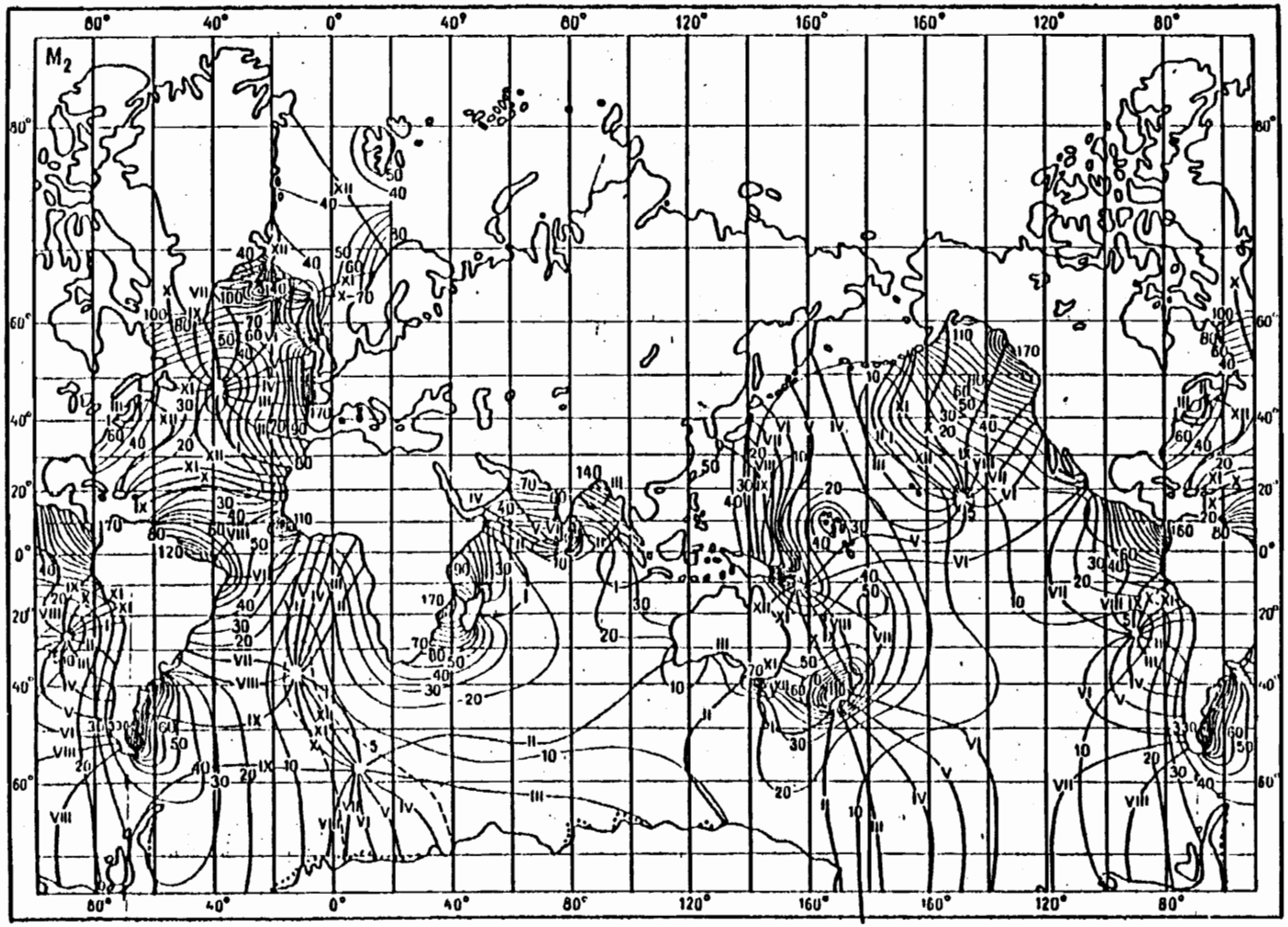

Figure 26. Global M_2 cotidal (Roman numerals) and coamplitude (Arabic numerals) lines from Tiron and others (1967). Cotidal lines are labeled in constituent hours (Table 5) relative to Greenwich. Amplitudes are in centimeters.

a decrease from 120° at LAS to 60° at McMurdo. Bogdanov's map is consistent with these two, but does not extend sufficiently far south for detailed comparison. The global maps by Zahel, and Henderschott and Munk show increasing constituent phase from LAS to McMurdo, and are thus inconsistent with the map presented in Figure 11. Zahel shows the phase to increase from 237° at 160°W longitude (near LAS) to 265° at 190°W longitude (near McMurdo). The map by Henderschott and Munk shows the phase increasing from about 0° at LAS to about 30° at McMurdo. An interpretation of the data which is consistent with Zahel's global M_2 map requires a complex variation in the LAS-C36-Roosevelt Island area. Such an interpretation is presented in Figure 27.

Tide Prediction

The maps of Figures 9-11 describe the spatial and temporal variation of the six most significant harmonic constituents of the ocean tide in the southern Ross Sea, within the uncertainties previously considered. These maps can be used to predict the tide at any point on the ice shelf, for any time interval. To do this, values of amplitude and phase read from the maps are used to solve equation (5). To illustrate the accuracy with which these six harmonic constituents represent the elevation changes of the ice shelf, the record for Base has been reconstructed from the harmonic constants determined from the record. For convenient comparison, the observed and reconstructed records are presented together in Figure 28. To illustrate the time-invarient nature of the harmonic constants, and the accuracy to which

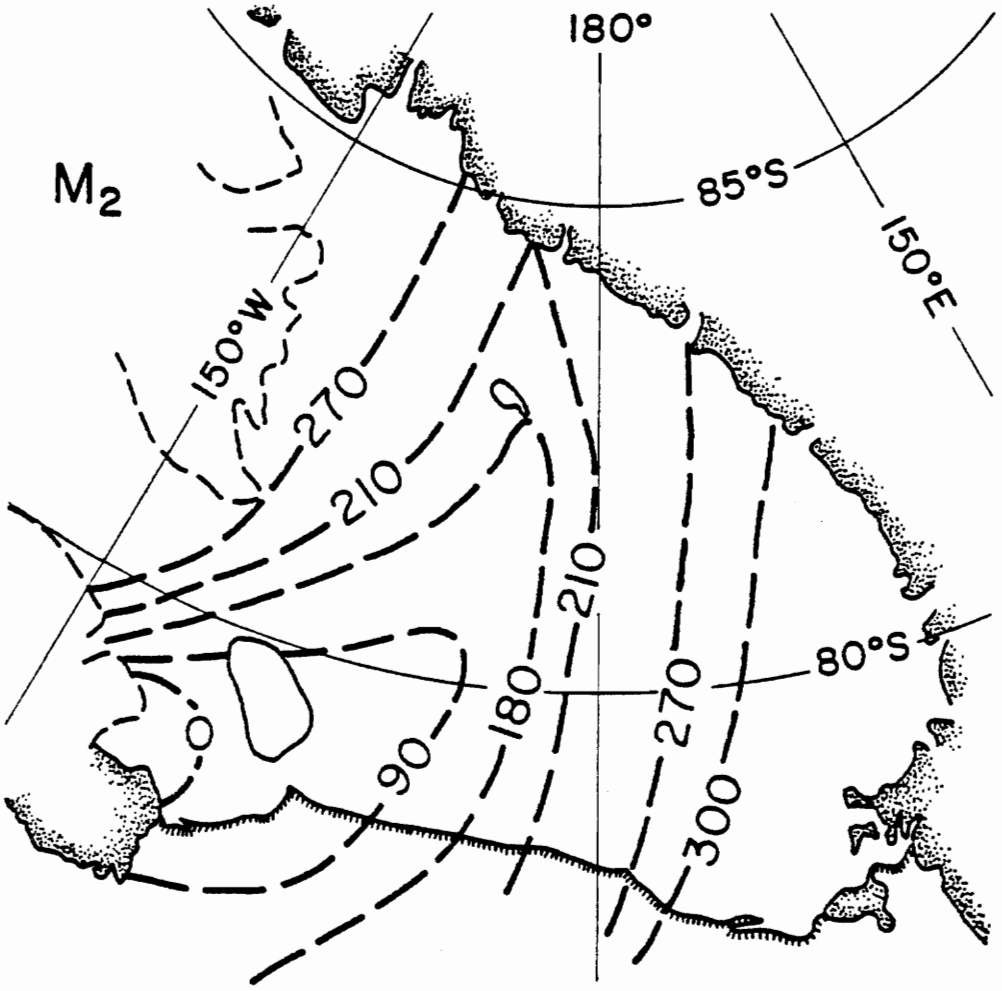

Figure 27. Ross Sea M_2 cotidal lines consistent with both the RISP data and Zahel's global M_2 in the southern Pacific Ocean (Figure 22).

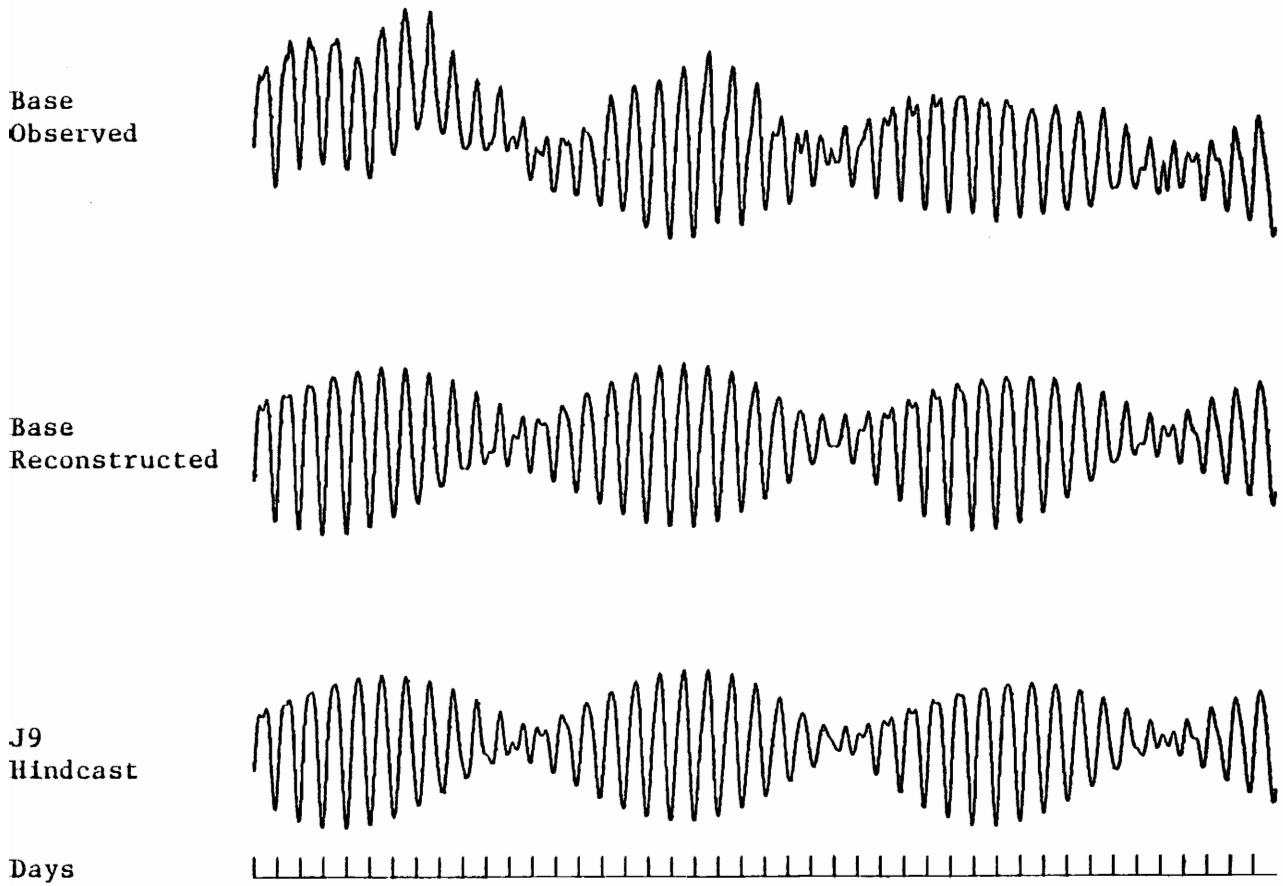

Figure 28. Comparison of observed Base tidal gravity record with the Base tidal gravity synthesized from the six largest constituents of the tide, and the record for nearby (Figure 1) J9 hindcast from data obtained three years later.

the tide can be predicted for past or future times, the J9 tide has been hindcast for the time interval of the Base record. This record is also presented in Figure 28. The quantities required in equation (5) for the prediction are summarized in Table 7.

The reconstructed Base record correctly reproduces the principal features of the observed Base record, including the days of tropic and equatorial tide, and the time of day of high and low water. However, there are differences between the two records which can be attributed to several factors. The most notable difference is caused by instrument drift, which the reconstructed record does not reproduce. Differences in the tidal variations result from the uncertainties in the harmonic constants, and from the failure to include more than six of the tide-constituents in the reconstructed record. There are certainly more than six constituents with nonzero amplitude present in the Ross Sea: all of the constituents in Table 5, and others, are likely to be present. This is indicated by the number of spikes (more than 5) in the diurnal and semidiurnal frequency ranges of the Fourier spectra of the records (Figure 8). Although the amplitudes of these lesser constituents are too small to permit the accurate determination of their harmonic constants from the records obtained in this study, their aggregate effect can be observable.

The success of the prediction technique is evidenced by the striking similarity of the reconstructed Base and hindcast J9 records. Since these two stations are near to each other (Figure 1), it may be

Table 7. Parameters used to hindcast the J9 record to 20 Dec 1973 starting time.[a]

Constituent	f	ϕ
P_1	1.0	1.6°
K_1	1.010	6.9°
O_1	1.016	107.1°
M_2	1.002	117.8°
N_2	1.002	11.4°
S_2	1.0	0.0°

[a] Values from Schureman (1941).

anticipated that the tide will be similar, but not identical, at the two locations.

Summary

The elevation of the Ross Ice Shelf varies in response to the ocean tide in the subjacent water-layer. The motion can be represented accurately by a sum of six harmonic constituents. Maps of the amplitude and phase of each of these were produced from measurements of tidal variations of gravity. The tide is principally diurnal; the diurnal constituent amplitudes are approximately three times larger than the semidiurnal amplitudes. At tropic (diurnal spring) tide the diurnal elevation fluctuation is in the 1 m to 2 m range.

The diurnal tide constituents (Figures 9 and 10) enter the Ross Ice Shelf region as a wave progressing towards the southwest. The height of the wave generally increases from near 10 cm in the southern Pacific Ocean to approximately 30 cm in the southern Ross Sea. This increase can be attributed to constructive interference between the wave and its reflection from the southwestern coast of the Ross Sea. Within the Ross Ice Shelf region, the height of the tide is closely related to the local water-layer thickness. The semidiurnal tidal waves rotate clockwise about an amphidromic point near C13.

TIDAL CURRENTS BENEATH THE ROSS ICE SHELF

Introduction

One of the measurable physical manifestations of the ocean tide is the tidal current. It is essentially the particle motion associated with the tidal wave that propagates in the sea. Like the surface motion, the currents can be decomposed into a quasi-harmonic series, as given in equation (5). For the current associated with a particular tide constituent, the periodic flow does not result in any net transport of the water mass: the water particles move around an ellipse or back and forth along a line.

Currents are important because they transport energy and mass, including heat, solutes, sediments, living organisms and nutrients. In most bodies of water, the tidal currents are only one aspect of the horizontal water movement. Other currents are caused by wind-stress at the surface, and temperature and density gradients in the water mass. Because of the ice cover, wind-driven circulation in the southern Ross Sea is minimized, but other currents are likely to exist. Knowledge of these currents bears upon the interpretation of observational data related to the physical and biological processes taking place in the water-layer beneath the ice shelf. One of the principal objectives of RISP is to determine whether the bottom surface of the Ross Ice Shelf is melting, or accreting mass by freezing sea water. In the larger perspective, this question is related to whether the Antarctic ice cap is growing or melting. Knowledge of the

ocean current beneath the ice shelf is important in determining the source of heat and solutes indicated by water temperature and salinity data from beneath the shelf. Biologically, knowledge of the current is important in determing the range over which nutrients may be transported, and from which biological specimens may be attracted by bait placed in the water.

In addition to the importance of the currents in relationship to other disciplines, the physical environment beneath the Ross Ice Shelf is unique, and the current is interesting in itself. Beneath the Ross Ice Shelf there are two surfaces which resist the flow of the water, and the effect of the upper surface on the current may shed additional light on the mechanism of friction in the global ocean. Also, because of the high latitude, or more accurately, the proximity of the rotational pole, there is a resonance effect which may greatly increase the amplitudes of the semidiurnal currents. The effect of this resonance on the tide in the Ross Sea is interesting, particularly because the tidal elevation changes are principally diurnal.

The objective of this portion of the dissertation is to develop a technique for calculating the currents associated with the ocean tide beneath the ice shelf. The results are then evaluated by comparing the calculated currents to those which have been measured with a current meter that was lowered through a borehole into the sea beneath the J9 camp. In addition, the area over which a particular mass of water moves in the course of a tidal cycle is estimated.

A Theoretical Basis for Tidal Current Calculations

The relationship between the height of the tide and the associated tidal current was first expressed mathematically by Laplace in 1775. These equations (the Laplace Tidal Equations, LTE) can be written (Doodson, 1958) as:

$$\frac{\partial u}{\partial t} - 2\,\Omega \cos\theta\, v = -\frac{g}{a}\frac{\partial}{\partial \theta}(\zeta - \overline{\zeta}) - G \qquad (6a)$$

$$\frac{\partial v}{\partial t} + 2\,\Omega \cos\theta\, u = -\frac{g}{a}\frac{1}{\sin\theta}\frac{\partial}{\partial \chi}(\zeta - \overline{\zeta}) - F \qquad (6b)$$

$$\frac{1}{a \sin\theta}\left[\frac{\partial}{\partial \theta}(hu \sin\theta) + \frac{\partial}{\partial \chi}(hv)\right] = -\frac{\partial \zeta}{\partial t} \qquad (6c)$$

where:

θ is the colatitude,

χ is the east longitude,

Ω is the angular frequency of rotation of the earth,

$\omega = 2\,\Omega \cos\theta$

a is the mean spherical earth radius,

g is the mean gravitational acceleration,

ζ is the height of the tide,

$\overline{\zeta}$ is the height of the fictitious equilibrium tide,

h is the (undisturbed) thickness of the water layer,

u,v are the current speeds south and east, respectively, and

G,F represent the south and east components of the frictional forces (per unit mass)

For the equations in this form, it has been assumed that the current speeds, u and v, are independent of depth, and that the vertical current speed is small compared to the horizontal. Essentially this is the shallow-water wave assumption, which is true for the tide. A criterion that a wave be a shallow-water wave is (Kinsman, 1965, p. 126), for wave period T:

$$T^2 \geqq 200\ h\ \frac{2\pi}{g} \tag{7}$$

Taking 700 meters as representative of the greatest thickness of the water-layer beneath the Ross Ice Shelf, waves having periods longer than 5 minutes can be considered shallow. Tidal periods are far greater than this.

The first two (6a,b) of the LTE relate the currents, and their time derivatives, to the surface elevations. Inasmuch as the most significant constituents of the tidal elevations have been determined, these two equations can be solved simultaneously for the horizontal current components. Setting $\zeta^* = \zeta - \overline{\zeta}$, and rewriting 6a and 6b in vector notation:

$$\frac{\partial}{\partial t}\begin{pmatrix} u \\ v \end{pmatrix} = -\frac{g}{a}\begin{pmatrix} \dfrac{\partial \zeta^*}{\partial \theta} \\ \dfrac{1}{\sin\theta}\dfrac{\partial \zeta^*}{\partial \chi} \end{pmatrix} - \omega\begin{pmatrix} -v \\ u \end{pmatrix} - \begin{pmatrix} G \\ F \end{pmatrix} \tag{8}$$

In this form, the equations may be solved step-wise in time for given initial values of u and v. A FORTRAN program to solve this equation was written, which implements the International Mathematics and

Statistics Library (IMSL, 1977) subroutine DREBS. Subroutine Drebs is based on an algorithm by Bulirsch and Stoer (1966) that is said to have computational advantages over the Runge-Kutta method. The computation time required to solve this equation is long, depending on the number of time-steps desired in the solution. This program, presented in Appendix I, provides the option of treating the friction terms F and G in the different ways that are described in the following discussion.

Thus far the mathematical form of the retarding forces represented by F and G has not been specified. At the time of this writing, the phenomenon of energy dissipation in marine circulation is not well understood. However, important insights have been gained in recent years with expanded research efforts motivated by the need for extensive exploitation of off-shore resources (Nihoul, 1977, p. v). For the water layer beneath the Ross Ice Shelf, there are insufficient observational data upon which to base a detailed model of the retarding effects of the sea floor and lower surface of the ice shelf. For that reason, and consistent with the shallow water nature of the tidal wave, the retarding effects will be treated here as a body force, acting on the entire water column, and increasing as the speed of the current increases. Classically, two forms of the frictional forces have been used when bottom friction has been treated in this fashion, one nonlinear and one linear. The nonlinear form can be traced to Young (1813), and is expressed by the equation:

$$\begin{pmatrix} G \\ F \end{pmatrix} = k_n \sqrt{u^2 + v^2} \begin{pmatrix} u \\ v \end{pmatrix} \tag{9}$$

The value of the proportionality constant, k_n, is determined empirically. Retarding effects of this form have been included as part of the description of friction by a number of investigators, including Estes (1977) and Zahel (1977), in their recent attempts to solve the LTE for the global ocean tide. The linear treatment of the frictional forces is attractive because of its mathematical simplicity, and its application can be traced to Guldberg and Mohn (1876). For G and F linearly dependent on the horizontal current components, the frictional terms can be expressed as:

$$\begin{bmatrix} G \\ F \end{bmatrix} = k_1 \begin{bmatrix} u \\ v \end{bmatrix} \tag{10}$$

As in the nonlinear case (equation 9) the proportionality constant, k_1, is determined empirically.

If it is assumed that the frictional forces are linear, at least to a first approximation, a simpler method can be used to solve equation (8) for the current components. Substituting from equation (10) equation (8) may be written:

$$\frac{\partial}{\partial t} \begin{pmatrix} u \\ v \end{pmatrix} + \begin{bmatrix} k_1 & -\omega \\ \omega & k_1 \end{bmatrix} \begin{pmatrix} u \\ v \end{pmatrix} = -\frac{g}{a} \begin{pmatrix} \frac{\partial \zeta^*}{\partial \theta} \\ \frac{1}{\sin \theta} \frac{\partial \zeta^*}{\partial \chi} \end{pmatrix} \tag{11}$$

Since the equation is linear, the solution for each constituent of the tide will be independent of all the others. So for the constituent having frequency σ, let

$$u = A_u \cos(\sigma t - \phi_u)$$
$$v = A_v \cos(\sigma t - \phi_v)$$
$$\zeta^* = A_\zeta \cos(\sigma t - \phi_\zeta)$$

where A and ϕ are the amplitude and phase, respectively, and apply:

$$A \cos(\sigma t - \phi) = A \cos\phi \cos \sigma t + A \sin \sigma \sin \sigma t$$

Also let

$$c_i = A_i \cos \phi_i$$
$$s_i = A_i \sin \phi_i$$

Then differentiating and substituting into equation (11) yields:

$$\begin{bmatrix} -\sigma \sin \sigma t & \sigma \cos \sigma t & 0 & 0 \\ 0 & 0 & -\sigma \sin \sigma t & \sigma \cos \sigma t \end{bmatrix} \begin{pmatrix} c_u \\ s_u \\ c_v \\ s_v \end{pmatrix}$$

$$+\begin{bmatrix} k_1 & -\omega \\ \omega & k_1 \end{bmatrix}\begin{bmatrix} \cos\sigma t & \sin\sigma t & 0 & 0 \\ 0 & 0 & \cos\sigma t & \sin\sigma t \end{bmatrix}\begin{pmatrix} c_u \\ s_u \\ c_v \\ s_v \end{pmatrix}$$

$$= -\frac{g}{a}\begin{bmatrix} \cos\sigma t & \sin\sigma t & 0 & 0 \\ 0 & 0 & \cos\sigma t & \sin\sigma t \end{bmatrix}\begin{pmatrix} \frac{\partial c_\zeta}{\partial\theta} \\ \frac{\partial s_\zeta}{\partial\theta} \\ \frac{1}{\sin\theta}\frac{\partial c_\zeta}{\partial\chi} \\ \frac{1}{\sin\theta}\frac{\partial s_\zeta}{\partial\chi} \end{pmatrix}$$

Since this equation is true for all times, t, it must be true for $\sigma t = 0°$ and $90°$ in particular. Thus

$$\begin{bmatrix} \sigma & -k_1 & 0 & \omega \\ -k_1 & -\sigma & \omega & 0 \\ 0 & -\omega & \sigma & -k_1 \\ -\omega & 0 & -k_1 & -\sigma \end{bmatrix}\begin{pmatrix} c_u \\ s_u \\ c_v \\ s_v \end{pmatrix} = g/a\begin{pmatrix} \frac{\partial s_\zeta}{\partial\theta} \\ \frac{\partial c_\zeta}{\partial\theta} \\ \frac{1}{\sin\theta}\frac{\partial s_\zeta}{\partial\chi} \\ \frac{1}{\sin\theta}\frac{\partial c_\zeta}{\partial\chi} \end{pmatrix} \tag{12}$$

The harmonic constants of the currents may be obtained directly from the spatial derivatives of the harmonic constants of the elevations using this equation, provided that the frictional forces are specified linearly (equation 10). Two FORTRAN computer programs were written, one of which solves equation (12), while the other reconstructs the current variation with time, for a specific time interval, by substituting the resultant harmonic constants into equation (5). These programs are presented in Appendix II.

In the preceding discussion, two methods for calculating the current associated with a given tidal elevation variation are described. These methods are fundamentally different. The Bulirsch-Stoer method (equation 8) includes both the transient and steady-state parts of the solution, while the other (equation 12) yields only the steady-state part. The transient part of the solution depends on the initial values selected for u and v to start the solution, and should decay with time, so that the two methods produce the same result in the steady-state limit. Thus a comparison of the solutions obtained using both methods to solve the same problem gives a direct measure of the effect of the choice of the initial current on the solution obtained using the Bulirsch-Stoer method. To make an exact comparison, the nonlinear friction calculation in the program using the Bulirsch-Stoer routine (Appendix I) must be replaced by the linear calculation, but this change involves only one statement in the program. It was found that agreement between the two methods was better than 0.1 cm/sec and 1° after the first 6 days

of record, for any initial values of u and v on the order of $\pm$ 10 cm/sec or smaller. This is consistent with Estes (1977) statement that for a time-stepped solution to the complete LTE (equations 6 a, b, c) the steady-state solution is assured in 8 tidal periods.

Theoretical calculations of the tidal current are useful only insofar as they correctly predict the current actually present in the sea. Therefore it is necessary to compare the theoretical results with actual measurements of the current beneath the Ross Ice Shelf. In addition, the theoretical calculations are sensitive to the values of the friction coefficients, k_1 and k_n. The nature of this sensitivity will be explicitly derived in a later section. Because of this sensitivity, it is necessary to use current measurements to guide the selection of the values of the friction coefficient used in the theoretical calculations.

Current Meter Data from J9

Ocean current measurements have been made in the Ross Sea at several locations in open water north of the Ross Ice Shelf (Jacobs and others, 1974), and in McMurdo Sound (Gilmour, 1963; Gilmour and others, 1962). However these locations lie essentially outside the domain of this study. The maps presented here (Figures 9-13, 27), and particularly the semidiurnal ones, cannot be extended north of the ice front. Further, the tide in McMurdo Sound will be greatly influenced by the shape of the sound, and it is not the purpose of this study to produce detailed maps of the tide there. Measurements of the current beneath the ice shelf have been made at one location,

J9 camp. During the austral summer of 1977-78 a hole was bored through the 420 m thick ice shelf to the underlying water. Physical and biological data obtained using that hole were the subject of a RISP symposium at the 1978 Spring Meeting of the American Geophysical Union (AGU). Papers presented at the symposium were abstracted in the AGU bulletin, Eos (June, 1978).

Preliminary results of the current measurements made using the J9 access hole have been published by Jacobs and others (1978). The current records obtained by Jacobs (personal communication) are presented in Table 8 and Figure 29. These records are revisions of the preliminary published data. Briefly, a Geodyne savonius rotor current meter was suspended beneath the ice for periods up to several hours, in the interval from 20 to 27 December 1977. The longest continuous segment of current record obtained spans only six hours, much less than a single cycle of any tide constituent. At the time of this writing, the 1978-79 RISP field program is underway, and additional access holes have been made at J9. However, current records obtained through these holes are not yet available.

Inasmuch as Jacobs' 1977-78 data have been discussed only in a brief and preliminary fashion in the literature, some elaboration on the quality of the data is in order here. The current meter records three parameters: the speed of the current as indicated by the rotation of a horizontal rotor, the direction of the current with respect to the meter case as indicated by a moving vane, and the orientation of the case with respect to magnetic north as indicated by a compass.

Table 8. Current meter data obtained at J9 during December 1977 by Jacobs and others (1978; Stan Jacobs, personal communication).

CM1	20 Dec		CM2	21 Dec		CM3	22-23 Dec		CM4	23 Dec		CM5	27 Dec	
T[a]	S[b]	D[c]	T	S	D	T	S	D	T	S	D	T	S	D
1915	5.6	304	1648	7.7	293	2339	8.4	90	1921	4.5	270	1614	7.3	358
1921	5.3	306	1654	12.8	284	2345	8.8	88	1927	4.5	293	1620	7.2	358
1927	5.5	298	1700	12.6	284	2351	9.4	93	1933	4.6	296	1626	6.8	355
			1706	14.4	284	2357	9.5	99	1939	5.0	304	1632	6.6	355
			1712	14.4	284	0003	9.7	99	1945	4.8	304	1638	6.2	352
			1718	10.1	301	0009	9.7	99	1951	5.8	313	1644	6.2	349
			1724	10.2	290	0015	10.0	102	1957	6.0	307	1650	6.3	349
			1730	10.9	290	0021	10.8	102	2003	6.0	296	1656	6.3	346
			1736	10.1	290	0027	11.0	102	2009	5.7	304	1702	6.2	344
			1742	10.0	284	0033	11.4	104	2015	5.4	296	1708	6.1	341
			1748	10.4	282	0039	12.2	104	2021	6.2	313	1714	5.5	318
			1754	11.4	282	0045	12.2	104	2027	6.0	3.5	1720	5.5	318
			1800	12.3	282	0051	12.9	113	2033	5.1	315	1726	5.6	318

Table 8 (continued)

CM1	20 Dec		CM2	21 Dec		CM3	22-23 Dec		CM4	23 Dec		CM5	27 Dec	
T	S	D	T	S	D	T	S	D	T	S	D	T	S	D
			1806	12.4	282	0057	13.3	116	2039	4.7	310	1732	5.5	315
			1812	11.8	282	0103	14.3	113	2045	4.5	307	1738	5.0	315
			1818	11.7	290	0109	14.4	110	2051	3.6	315	1744	4.9	313
			1824	12.3	290	0115	14.6	113	2057	3.1	318	1750	5.0	313
			1830	12.2	290	0121	14.5	113	2103	2.7	315	1756	4.8	313
			1836	12.3	293	0127	14.4	113	2109	2.7	315	1802	4.7	313
			1842	13.4	293	0133	14.5	113	2115	2.8	324	1808	4.5	310
			1848	18.1	301	0139	14.5	113	2121	2.1	324	1814	4.2	310
			1854	18.1	301	0145	14.5	113	2127	-	324	1820	3.9	287
			1900	17.3	282	0151	14.8	113	2133	-	327	1826	4.0	284
			1906	17.2	293	0157	14.5	119	2139	-	324	1832	3.8	284
			1912	10.9	284	0203	14.5	119	2145	-	324	1838	3.4	284
			1918	10.0	284	0209	14.3	113	2151	-	321	1844	3.4	284
			1924	9.6	284	0215	14.5	110	2157	-	335	1850	3.0	284

Table 8 (continued)

CM1	20 Dec		CM2	21 Dec		CM3	22-23 Dec		CM4	23 Dec		CM5	27 Dec	
T	S	D	T	S	D	T	S	D	T	S	D	T	S	D
			1930	9.4	293	0221	14.5	110	2203	-	344	1856	2.9	282
			1936	9.3	304	0227	14.2	107	2209	-	344	1902	2.7	282
			1942	9.3	304	0233	13.2	110	2215	-	344	1908	2.4	282
			1948	7.4	304	0239	13.3	107	2221	-	014	1914	-	282
			1954	7.0	301	0245	13.1	110	2227	-	034	1920	-	279
			2000	6.1	304	0251	13.0	113	2233	-	068	1926	-	276
			2006	5.2	304	0257	13.1	107	2239	-	071	1932	-	276
			2012	5.2	304	0303	12.9	107	2245	-	082	1938	-	276
			2018	5.4	304	0309	13.3	113	2251	-	082	1944	-	276
			2024	5.2	313	0315	15.9	104	2257	-	090	1950	-	276
			2030	4.5	313	0321	15.0	124	2303	-	093	1956	-	276
			2036	4.0	313	0327	13.7	102	2309	-	093	2002	-	276
			2042	4.0	315	0333	12.9	102	2315	2.0	113	2008	-	270
			2048	3.0	324	0339	12.8	104	2321	5.0	113	2014	-	270

Table 8 (continued)

CM1	20 Dec		CM2	21 Dec		CM3	22-23 Dec		CM4	23 Dec		CM5	27 Dec	
T	S	D	T	S	D	T	S	D	T	S	D	T	S	D
			2054	2.7	315	0345	12.4	119	2327	5.0	113	2020	-	268
						0351	11.0	124	2333	4.6	110	2026	-	268
						0357	9.0	121	2339	5.1	113	2032	-	268
						0403	9.6	124				2038	-	265
						0409	9.1	124				2044	-	265
						0415	8.5	127				2050	-	265
						0421	8.1	133				2056	-	265
						0427	8.0	133				2102	-	265
						0433	8.3	133				2108	-	265
						0439	7.9	133				2114	-	254
						0445	7.5	127				2120	-	254
						0451	6.7	124				2126	-	254
						0457	5.1	121				2132	-	254
						0503	5.1	113				2138	-	251

Table 8 (continued)

CM1	20 Dec		CM2	21 Dec		CM3	22-23 Dec		CM4	23 Dec		CM5	27 Dec	
T	S	D	T	S	D	T	S	D	T	S	D	T	S	D
						0509	3.7	119				2144	-	251
						0515	2.9	121						
						0521	2.4	124						
						0527	2.0	121						

[a]Greenwich Mean Time.

[b]Current speed (cm/sec).

[c]Direction of the current (away from the meter). Measured in degrees north through east.

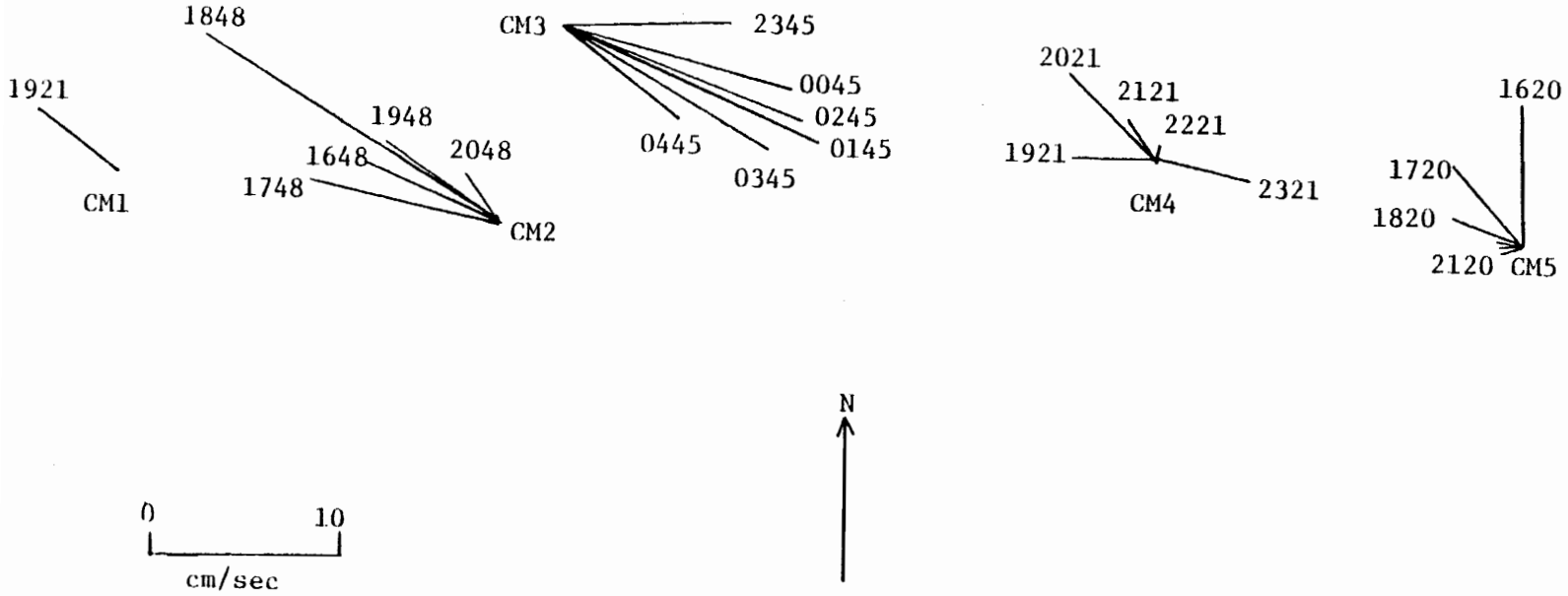

Figure 29. J9 current meter data from Table 8 in vector form at one hour intervals. The current direction is specified away from the observer. For this display, speeds below the instrument threshold, and not given in the table, were taken to be 1 cm/sec.

In operation at J9 the meter was lowered through the access hole on a cable, and suspended in the water column on a cable having length equal to the 420 m thickness of the ice shelf at J9, plus the distance from the meter to the bottom of the ice shelf. The position of the meter in the water column for each of the 5 records (Figure 29) is shown in Figure 30.

There is some indication that the vane measuring the current direction was not working properly on at least one of the records. On record CM5 the vane position remained nearly constant, and the change in current direction on that record is due to rotation of the meter case on the suspending cable. It is possible that on this record, and on others, that the vane was entirely or partially fouled by slushy ice as the meter was lowered through the access hole. The temperature of the water in the column below J9 is shown in Figure 30 by a graph of measurements made by Jacobs. At all points the temperature is below the freezing point of fresh water, and it is slightly colder, 0.3C degree, at the top of the column where CM5 was obtained. If the vane was fouled by ice containing enough salt, it could have been freed by melting while the meter was suspended in the water. Such melting, if it occurred, would have been somewhat slower near the bottom of the ice shelf, where CM5 was recorded.

Although the current directions measured by Jacobs must be accepted with reservation due to the possibility of instrument problems, his are the first measurements of the ocean current beneath the Ross Ice Shelf, and the data presented in Table 8 and Figure 29

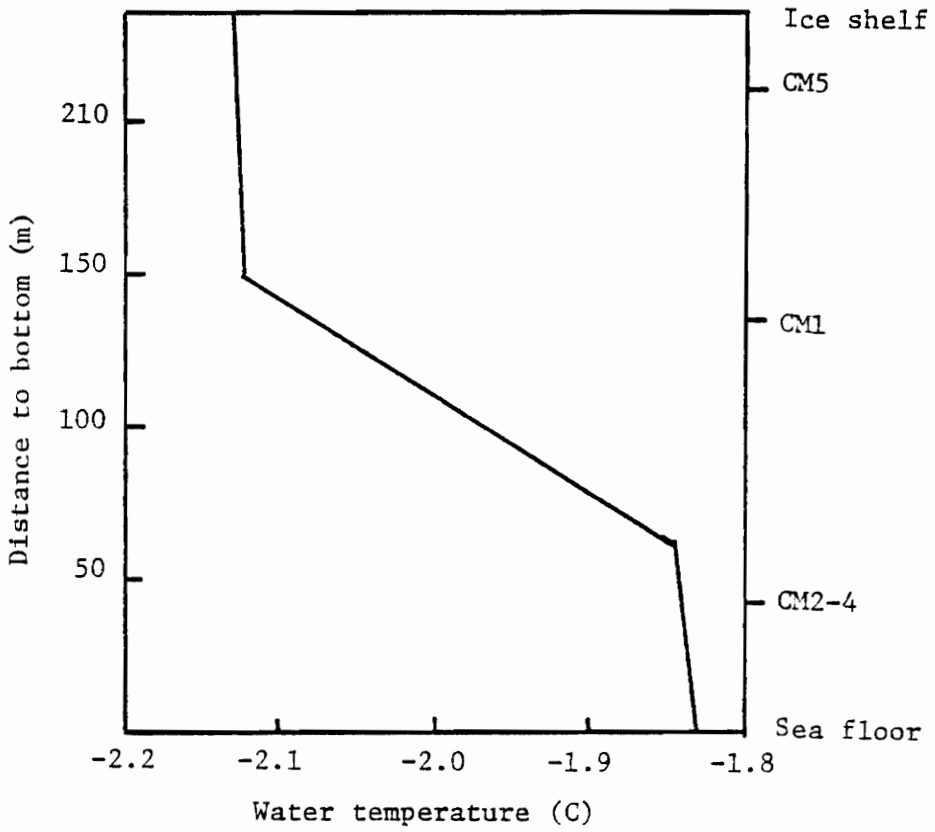

Figure 30. Generalized graph of temperature measurements made by Jacobs in the water column at J9. Also shown are the depths at which current measurements were made.

appear reasonable in the absence of conclusive evidence to the contrary. These measurements appear to confirm the supposition that the current is principally a tidal current. Firstly, the largest current speed observed was near 18 cm/sec, but neither the speed nor the direction of the current was constant. Additionally, the direction changes appear to be tidal, in the 15° to 30° per hour range. On records CM2 and CM4 the azimuth change is clockwise, while CM5 shows a counterclockwise azimuth change. The azimuthal variations of the remaining record, CM3, are irregular. On each record, the current vectors form part of an ellipse having the major axis oriented generally northwest-southeast.

Theoretical J9 Tidal Current

The tidal current at J9 was calculated for the month of December 1977, a time interval that spans the measurements made by Jacobs at that location. The calculations were based on the cotidal-coamplitude maps of Figures 9-13. Both the linear and nonlinear forms of the frictional force, as previously described, were used. The friction coefficients k_1 and k_n were chosen so that the greatest speed of the theoretical current was about the same as the greatest current speed measured by Jacobs (18 cm/sec, Table 8). For the semidiurnal amplitudes, which were not mapped, the values observed at J9 were used. The calculated current is presented in Figure 31. Shown are the southward and eastward components for both treatments of friction. The linear friction calculation yields harmonic constants for the

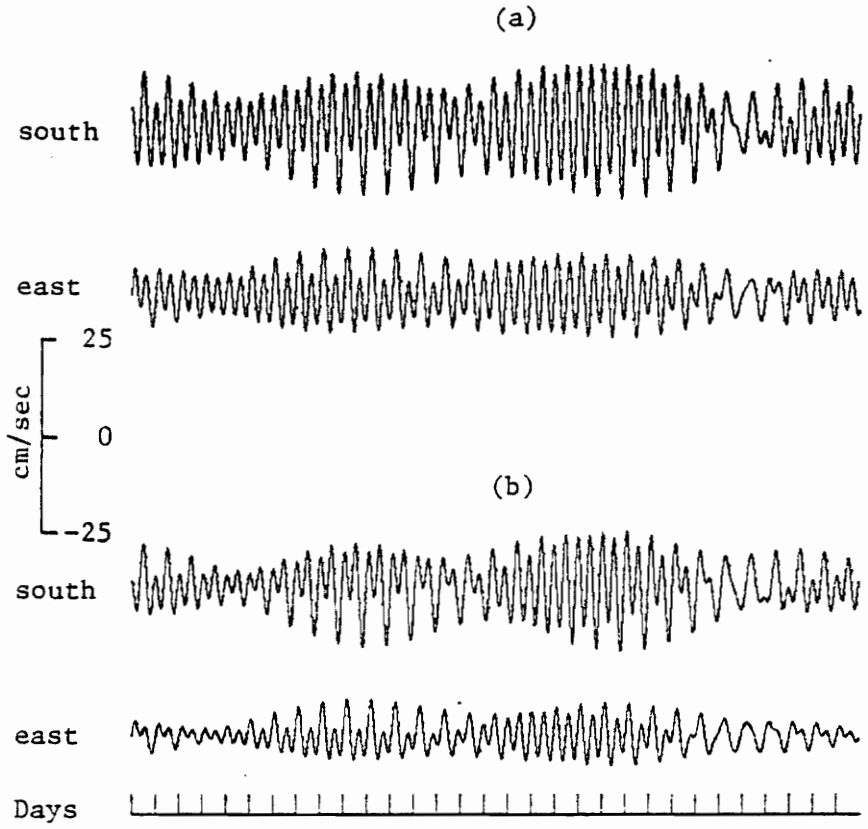

Figure 31. Current components south and east at J9, calculated the month of December 1977. The upper curves (a) are based on the non-linear friction assumption (equation 9) with k_n equal to 3×10^{-6}. The lower curves (b) are based on the linear friction assumption (equation 10) with k_1 equal to 5×10^{-5} sec^{-1}.

tidal current, and these are presented in Table 9 for three values of the friction coefficient k_1.

The values of the friction coefficients required to reduce the theoretical current speeds to the maximum observed during Jacobs' measurements are 5 to 10 times larger than corresponding values which have been deduced or assumed for other parts of the global ocean. For the linear term (equation 10), the value 5×10^{-5} sec^{-1} yielded a maximum current speed of 17 cm/sec. For the nonlinear term (equation 9), k_n equal to 3×10^{-6} yielded a maximum current speed of 19 cm/sec during the month of December, 1977. These values may be compared to corresponding values from the literature. Neumann (1968, pp. 166, 167, 300) summarizes several estimates of the linear coefficient, and concludes that values of k_1 in the range 10^{-6} to 10^{-5} sec^{-1} are appropriate in different areas, the value being higher in shallow seas. For the nonlinear coefficient the value 0.003 cm h^{-1} has been widely used (Estes, 1977; Zahel, 1977; Grijalva, 1964). At J9 where the water layer is 238 m thick, this becomes 1.3×10^{-7}. Since these values of k_1 and k_n have been applied to areas where the seabed is the only surface resisting the current, they may be doubled for comparison with the Ross Sea values because the flow is also opposed by friction due to the bottom of the floating ice shelf.

For comparison of the calculated current with the measurements, hourly values of the theoretical current, at times corresponding to Jacobs' current meter runs, are presented in Table 10, for both linear and nonlinear treatments of the friction. The same data are

Table 9. Harmonic constants of the J9 tidal current, based on a linear friction model, for different coefficients of friction.

Friction Coefficient		10^{-6} sec^{-1}		10^{-5} sec^{-1}		$5x10^{-5}$ sec^{-1}	
		A[a]	P[b]	A	P	A	P
K_1	south	3.0	148	3.2	148	3.4	148
	east	2.7	103	2.6	102	1.9	83
P_1	south	1.0	149	1.1	149	1.1	149
	east	0.9	103	0.8	101	0.6	82
O_1	south	2.6	131	2.7	129	3.0	126
	east	2.9	80	2.7	78	2.2	65
M_2	south	46.3	72	17.2	128	4.4	148
	east	47.1	160	16.0	212	2.7	220
S_2	south	88.6	101	15.2	58	3.9	56
	east	86.5	191	13.1	144	1.9	128
N_2	south	29.5	342	16.8	30	4.8	52
	east	29.0	68	14.7	117	2.5	146

[a] Amplitude in cm/sec

[b] Phase angle in degrees relative to the Greenwich Meridian

Table 10. Theoretical currents for comparisons with observations made by Jacobs.

GMT[a]	Case I[b]		Case II[c]	
	Speed[d]	Direction[e]	Speed	Direction
		CM1 20 Dec 1977		
1900	18.0	2	15.5	2
2000	18.0	350	16.3	351
		CM2 21 Dec 1977		
1600	8.9	143	6.3	150
1700	7.2	84	4.4	75
1800	11.5	34	8.9	25
1900	16.5	12	13.8	9
2000	18.7	359	16.5	359
2100	17.7	349	16.2	351
		CM3 22-23 Dec 1977		
2300	12.0	337	10.8	343
0000	6.6	313	5.1	324
0100	4.7	229	3.0	211
0200	10.2	183	8.3	175
0300	14.6	166	12.4	164
0400	16.1	155	14.0	155
0500	15.0	143	13.2	146
0600	12.1	128	10.5	133

Table 10 (continued)

GMT[a]	Case I[b]		Case II[c]	
	Speed[d]	Direction[e]	Speed	Direction
		CM4 23 Dec 1977		
1600	10.3	190	7.2	199
1700	6.7	166	3.8	186
1800	4.0	98	1.4	46
1900	8.3	34	6.4	13
2000	13.7	14	11.0	6
2100	16.7	3	13.8	1
2200	16.7	355	14.4	357
2300	14.1	347	12.4	352
2400	9.7	337	8.3	347
		CM5 27 Dec 1977		
1500	0.7	268	1.7	239
1600	3.3	312	2.7	295
1700	5.8	3.2	4.4	309
1800	7.3	308	5.6	313
1900	7.9	303	6.2	313
2000	7.6	298	6.2	313
2100	6.5	293	5.5	314

Table 10 (continued)

GMT[a]	Case I[b]		Case II[c]	
	Speed[d]	Direction[e]	Speed	Direction
		CM5 27 Dec 1977		
2200	4.9	291	4.6	318
2300	2.9	297	3.6	331
2400	1.6	343	3.1	354

[a] Greenwich Mean Time

[b] Nonlinear friction (equation 9), $k_1 = 3 \times 10^{-6}$

[c] Linear friction (equation 10), $k_n = 5 \times 10^{-5}$ sec^{-1}

[d] Measured in cm/sec

[e] Measured degrees north through east

presented vectorally in Figure 32. Although the calculated and measured currents do not compare favorably, there are important similarities between the two. Both indicate that the azimuthal variation of the current is sometimes clockwise and sometimes counterclockwise. The theoretical calculations show that this results from the fact that the azimuthal change of the diurnal current constituents is clockwise, while the semidiurnal is counterclockwise. Figure 33 shows the current, in vector form, due to each of the constituents separately. In the figure, the theoretical current constituents given in Table 9, for k_1 equal to 5×10^{-5} sec^{-1}, have been plotted at intervals of one (solar) hour. It is seen that the constituents each form an ellipse having the major axis oriented northwest-southeast, the sense of rotation being clockwise for all the diurnal constituents, and counterclockwise for all the semidiurnal constituents. These characteristics are similar to the observations made earlier about Jacobs' data.

Current calculations based on cotidal charts consistent with Zahel's global map of M_2 (Figure 27) have also been considered. It is emphasized that the author prefers the relatively simple amphidromic M_2 variation of Figure 11, and regards Figure 27 as an unnecessarily complex interpretation of the data. Current calculations based on the M_2 chart in Figure 27, using the linear friction model with k_1 equal to 5×10^{-5} sec^{-1}, yield the following harmonic constants for the M_2 current constituent: southward, 4.2 cm/sec and 39°; eastward, 5.6 cm/sec and 139°. This current is presented

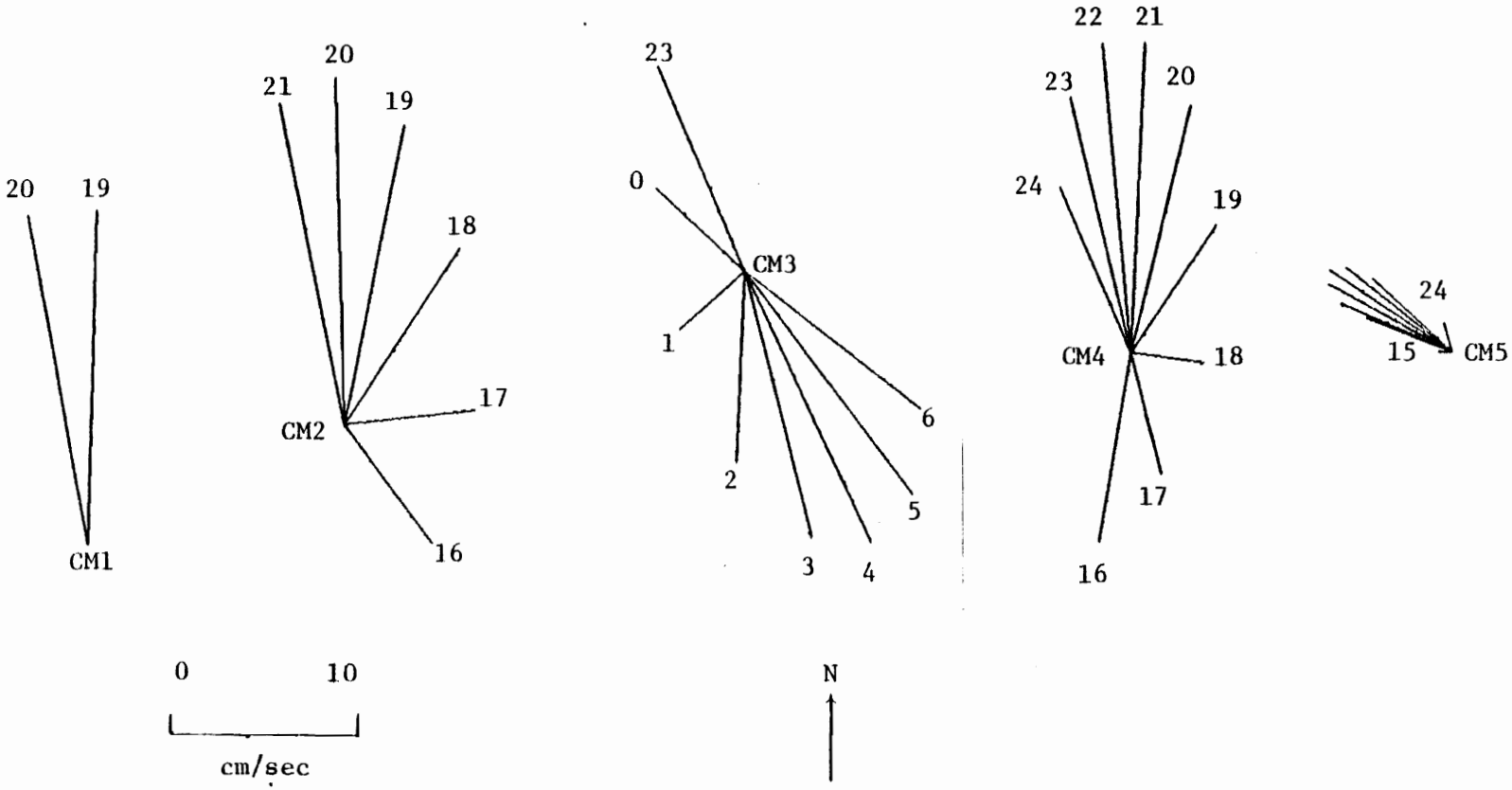

Figure 32a. Theoretical currents from Table 10 in vector form. Numbers are hours Greenwich Mean Time. These are the Case I data, calculated using a nonlinear friction model. These vectors may be compared to the measured current shown in Figure 29.

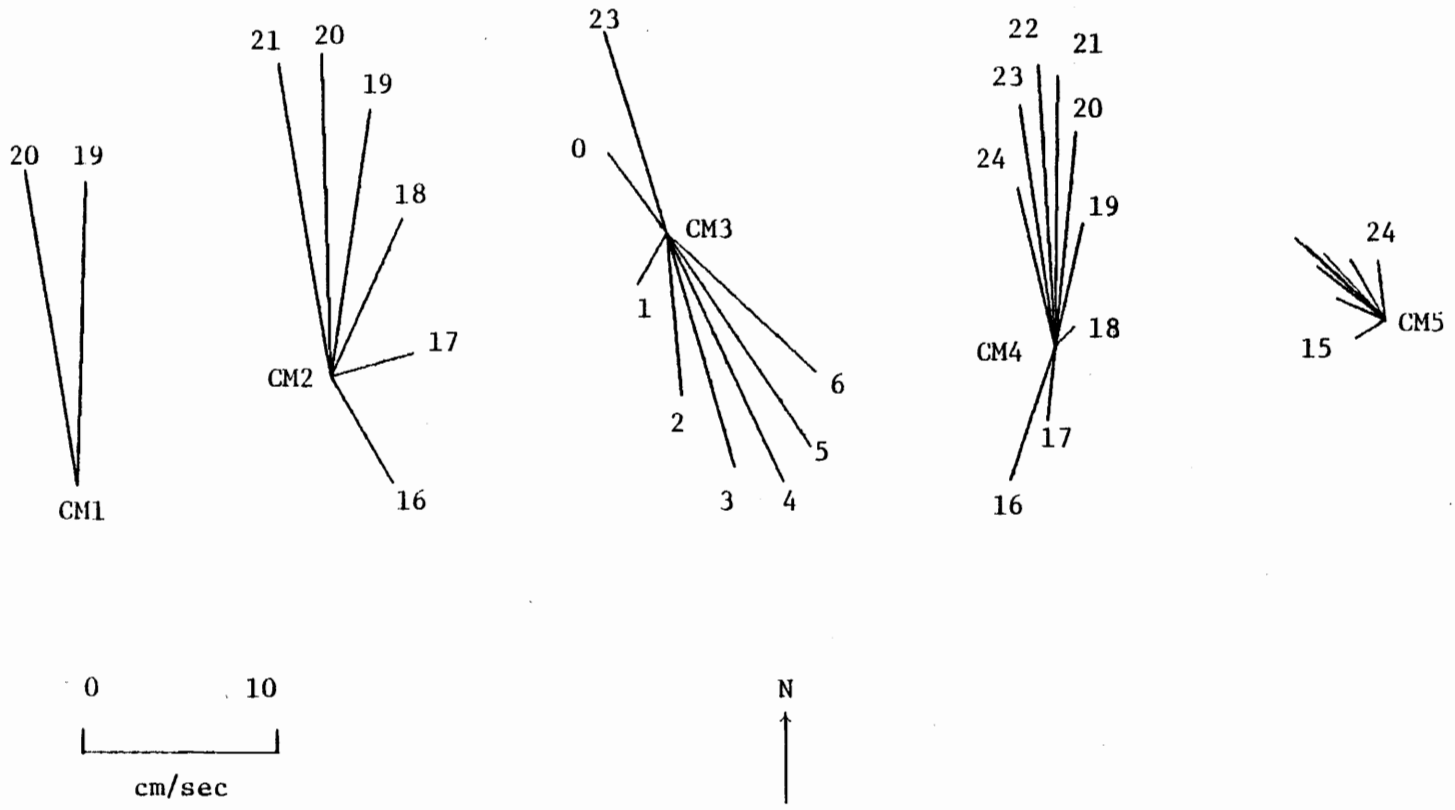

Figure 32b. Same as Figure 32a, except that the Case II data, calculated using a linear friction model, are displayed.

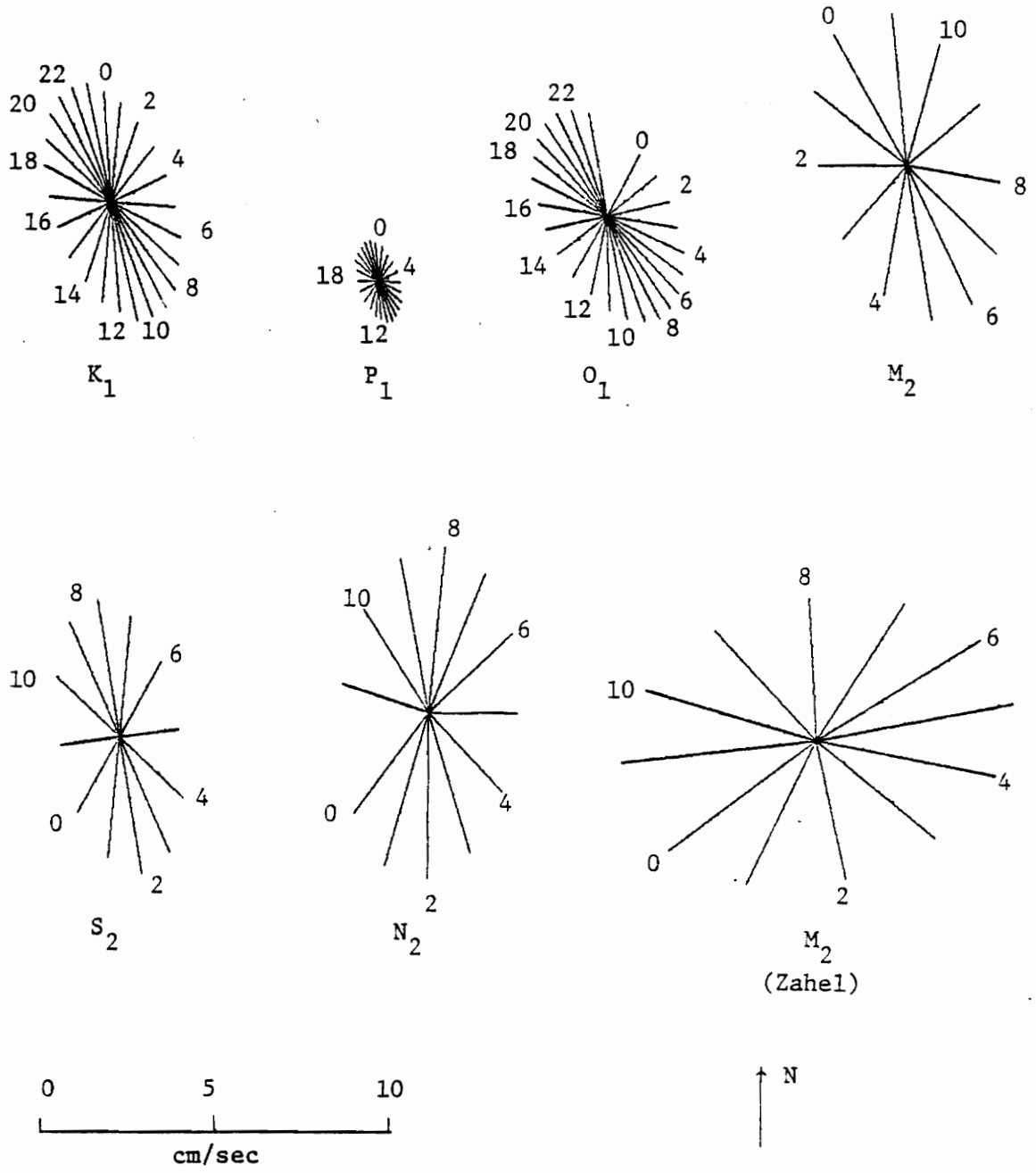

Figure 33. Current due to each constituent of the tide displayed separately in vector form, at hourly intervals. Time 0 is taken, for each constituent, at the passage of the equilibrium constituent over the Greenwich Meridian. Also shown is the current inferred from the M_2 cotidal chart consistent with Zahel's global M_2 (Figure 27).

vectorally in Figure 27 for comparison with the current associated with the amphidromic M_2 chart. These current speeds are somewhat greater than the speeds implied by the amphidromic map (Table 9). For comparison with the observations, the theoretical calculation must include the semidiurnal constituents S_2 and N_2, in addition to M_2. Since it is generally true that the response of the world ocean to the tide generating force is similar for all the semidiurnal constituents, it may be anticipated that if the M_2 variation shown in Figure 27 is correct, then cotidal charts for S_2 and N_2 will be similar to Figure 27, though not identical. Calculations of the J9 tidal current, based on semidiurnal cotidal charts similar to Figure 27 for all three semidiurnal constituents, failed to produce improved agreement with the measured current. However, one significant observation was made: the value of the friction coefficient required to reduce the maximum theoretical current to the 18 cm/sec level was about 50% larger for these charts than for the amphidromic charts of Figures 11-13.

Semidiurnal Current Resonance in the Ross Sea

Calculations of the tidal current at J9 indicate that the semidiurnal components of the current are larger than the diurnal components. This contrasts with the spectrum of the water level fluctuation which is dominated by the diurnal constituents. In addition, it was observed that while larger values of the friction coefficient reduce the amplitude of the semidiurnal current components,

the diurnal components are insensitive to changes in the value of the coefficient (Table 9). The relationship between the linear coefficient of friction and the current can be more clearly seen in the explicit solution to equation (12):

$$\begin{pmatrix} c_u \\ s_u \\ c_v \\ s_v \end{pmatrix} = \frac{g}{aD} \begin{bmatrix} A_1 & A_2 & A_3 & A_4 \\ A_2 & -A_1 & A_4 & -A_3 \\ -A_3 & -A_4 & A_1 & A_2 \\ -A_4 & A_3 & A_2 & -A_1 \end{bmatrix} \begin{pmatrix} \frac{\partial s_\zeta}{\partial \theta} \\ \frac{\partial c_\zeta}{\partial \theta} \\ \frac{1}{\sin\theta}\frac{\partial s_\zeta}{\partial \chi} \\ \frac{1}{\sin\theta}\frac{\partial c_\zeta}{\partial \chi} \end{pmatrix} \tag{13}$$

where

$$A_1 = h^2\sigma\,[h^2\,(\sigma^2 - \omega^2) + k_1^2]$$

$$A_2 = -\,h\,k_1\,[h^2\,(\sigma^2 + \omega^2) + k_1^2]$$

$$A_3 = 2\,h^3\,\sigma\,\omega\,k_1$$

$$A_4 = h^2\,\omega\,[h^2\,(\sigma^2 - \omega^2) - k_1^2]$$

$$D = [h^2\,(\sigma^2 - \omega^2) - k_1^2]^2 + 4h^2\,\sigma^2\,k_1^2$$

At the high latitude of the Ross Sea, ω is semidiurnal, near 29.7°/hr. For the diurnal constituents the quantity $(\sigma^2 - \omega^2)$ in equation (13) is relatively large, and the terms, particularly the divisor D, are not greatly affected by changes in k_1. However, for

the semidiurnal constituents ($\sigma^2 - \omega^2$) is near zero, and the theoretical currents are sensitive to the value of k_1.

The close dependence of the semidiurnal current amplitudes on the magnitude of the frictional force can be viewed as the result of a resonance between the semidiurnal and inertia currents. Inertia currents are a well-known and important component of the current in the global ocean. They arise when there is an imbalance between the inertial, Coriolis, and external forces acting on the water, as for example with the rapid passage of a meteorological front. Assuming that for some unspecified reason the external forces in the LTE (equations 6a,b) go to zero, and neglecting the frictional terms, the currents must satisfy the relationship (Neumann, 1968, p. 150):

$$\frac{\partial u}{\partial t} = \omega v$$

$$\frac{\partial v}{\partial t} = -\omega u$$

which has the solution

$$u = \sin \omega t$$

$$v = \cos \omega t$$

Thus, inertia currents have frequency ω, which in general is intermediate to the diurnal and semidiurnal constituents of the tide, but at the high latitude of the Ross Sea is quite close to the semidiurnal frequencies. An inertial current, once established, may persist for many hours, subject to the frictional effects which reduce its speed.

Mass Transport by Tidal Currents at J9

A tidal current is cyclic in nature, and the net flow averaged over one cycle is zero. However, within a cycle the water mass is transported over a closed path, and as mentioned in the Introduction, the area covered by this motion is of interest. The trajectory of a particular mass of water can be obtained by integrating the speed, as a function of time, of that mass of water. Essentially this requires knowledge of the material description of the motion. In this study the ocean current has been determined at a single point in space, i.e., the spatial description of the motion is known. For the purpose of obtaining an estimate of the area over which water-borne material may be transported by the tide, it is assumed that the tidal current is approximately the same in some region around J9. Under this assumption, the desired trajectory of the water mass is the integral of the current as previously determined.

The precise area traversed by the tidal current will change as the phase relationships between various constituents of the current change. However, what is desired here is an estimate of the greatest size of the area which water-borne material may cover following the tidal current. For the estimate, a diurnal current having a constant speed of 20 cm/sec will be used. For such a current:

$$u = 20 \frac{\text{cm}}{\text{sec}} \cos \frac{15^\circ}{\text{hr}} t$$

$$v = 20 \frac{\text{cm}}{\text{sec}} \sin \frac{15^\circ}{\text{hr}} t$$

The displacements are

$$X_p \simeq 3 \text{ km} \sin \frac{15°}{\text{hr}} t$$

$$Y_p \simeq -3 \text{ km} \cos \frac{15°}{\text{hr}} t$$

which is the equation of a circle having 3 km radius. The area enclosed by this circle is 30 square kilometers. A similar semi-diurnal current would enclose an area about one-fourth this size.

It is concluded that the tidal current at J9 is capable of transporting water-borne material over an area within a 3 km radius of J9. This same estimate applies to transport by inertia currents, provided that the speed of the current during the inertial event does not exceed 40 cm/sec.

Summary

The objective of this part of the dissertation has been to learn what current is associated with the tide beneath the Ross Ice Shelf. In this effort, two FORTRAN computer programs have been developed to calculate the current from a set of cotidal-coamplitude charts, and one which calculates the current for a specified time interval from the harmonic constants of the current. Both of these methods are based on the assumption that the tide can be treated as a shallow-water wave. Within this assumption, one method (equation 8; Appendix I) allows for a general, i.e. nonlinear, treatment of the retarding forces experienced by the tide. The second method

(equation 12; Appendix II) presupposes that each constituent of the tide can be considered independently of the others by using a linear representation of the retarding forces, but is computationally about 100 times faster than the more general treatment.

A number of important results have been obtained from calculations of the tidal current based on the cotidal-coamplitude maps in Figures 9-13 and 27. It has been shown that the semidiurnal current components are quite important, even though the tidal elevation changes are predominately diurnal. It has been demonstrated that the relatively greater semidiurnal currents may be viewed as the result of a near resonance between the semidiurnal tidal components and the inertia currents in the Ross Sea. Because of this resonance effect, the semidiurnal current amplitudes are sensitive to the treatment of the retarding forces which act on the tidal wave, resulting in an opportunity to study the retarding forces more closely than is generally possible. The calculations of this section indicate that to treat friction as it has been elsewhere in the global ocean results in tidal currents which are unreasonably large. To reduce the theoretical current to the level of the observations requires that the frictional force be increased by a factor of 5 to 10 over previous treatments. This is not necessarily unreasonable, but it does point out the need to investigate other possible mathematical formulations of the retarding forces. It is possible that alternate treatments of friction would require that the shallow-water wave

assumption be abandoned, a step that would literally add a new dimension to the complexity of solving the Laplace Tidal Equations.

The characteristics of the current observed at J9 during December 1977 are consistent with the theoretical calculations of this section. However, agreement between the particular current observed and the calculations was not obtained. It is not clear at this time whether the differences are due to the theoretical calculations, particularly the treatment of friction, or to the previously discussed problems of ice jamming the current meter at J9. This question will be answered in the next year or two when the results of more recent current measurements at J9 become available. Other related questions involve the effect of the lesser semidiurnal constituents (Table 5). The aggregate effect of these constituents on the current may be important, especially since they too will be amplified by near resonance with the inertial currents.

The estimate of tidal transport of material beneath the ice shelf indicates that over several tidal cycles a given mass of water may traverse an area of some 30 square kilometers. This implies that in the absence of other strong currents, waterborne material would stay within about 3 km of J9 over a period of several days. Given tidal currents of similar amplitude elsewhere, this estimate may be applied to the entire Ross Ice Shelf region.

FLEXURAL WAVES IN THE ROSS ICE SHELF

Introduction

The principal subject of the research program described in this dissertation has been the ocean tide in the Ross Ice Shelf region of Antarctica. However, the signals recorded during the field program by the gravimeters were of two types. In addition to the tidal gravity changes associated with variations in the elevation of the ice shelf, the RISP gravimeters recorded a continuous motion containing periods shorter than 20 minutes. The nature of these waves is illustrated in Figure 34, which shows segments of the record widely separated points on the ice shelf. Referring to the figure, and to the station positions in Figure 1, it is seen that these oscillations appear to have smaller amplitudes and longer periods at stations farther from the ice front. In addition these oscillations have greater amplitude during bad weather. This is illustrated in Figure 35, which shows record segments from C13. Camp C13 was occupied early in the 1974-75 field season, mostly during the month of November, and the weather at that time was stormy. The segments shown were obtained during a storm on 20 November 1974, and during calmer weather on 6 December. For the study of the tide, these waves were removed from the record by manually drawing a smooth curve on the field records, corresponding to the apparent beam positions in the absence of the oscillations. Thus the oscillations do not appear on RISP tidal gravity records presented in Figure 6.

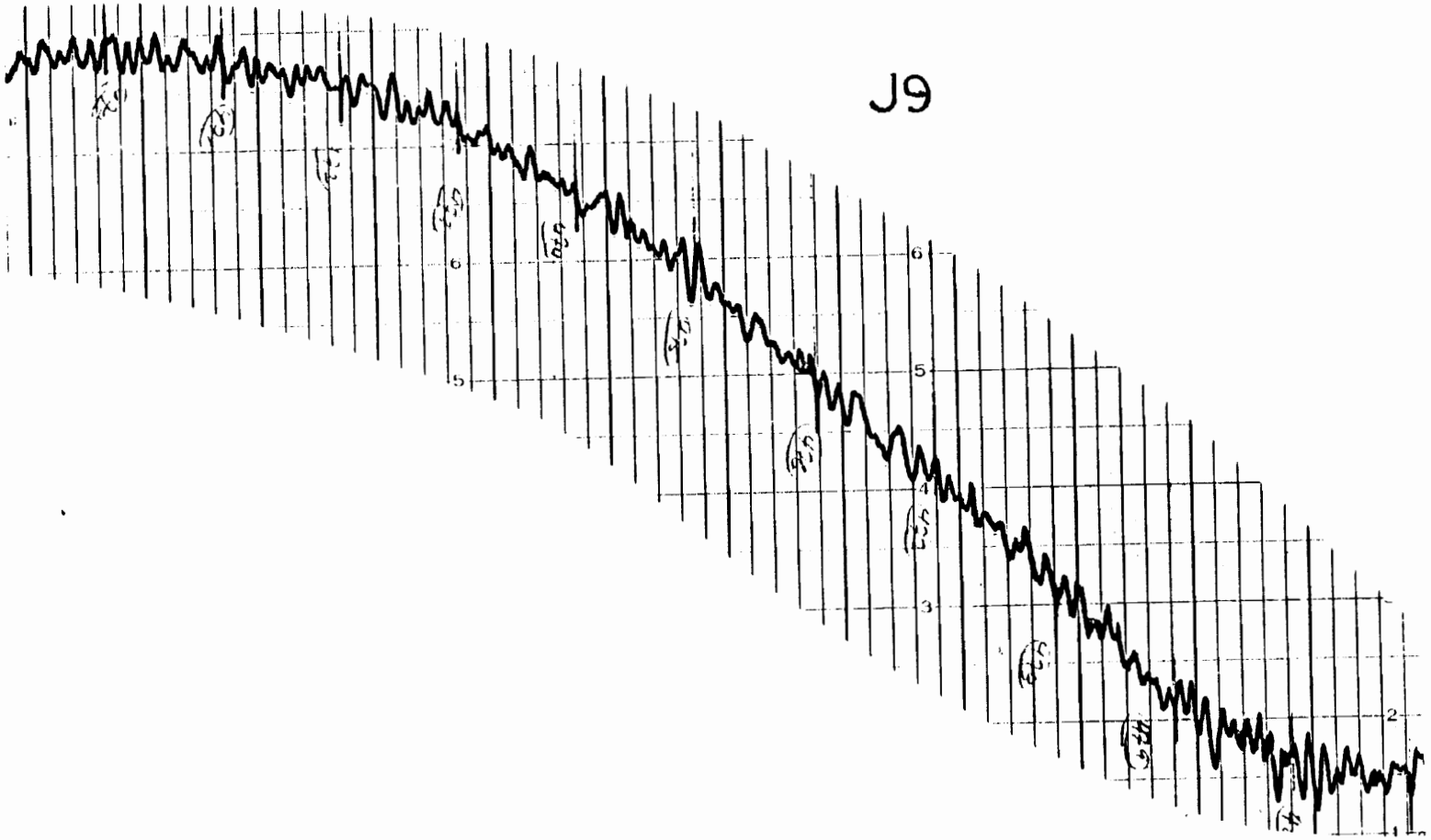

Figure 34a. Twelve-hour long segments of the field record from seven of the RISP tidal gravity camps (Figure 1) show the character of the short period motion of the ice shelf superposed on the tidal cycle. The time scale is slightly different on each record due to differing chart recorder speeds. The record segments from J9, C16 and F9 are simultaneous, beginning at 1200 GMT 12 Dec 1976. The Base segment begins at 1200 GMT 14 Jan 1974. The C36 and Roosevelt Island camp records are simultaneous, and begin at 1200 GMT 9 Jan 1975. The O19 segment begins at 1200 GMT 3 Jan 1978.

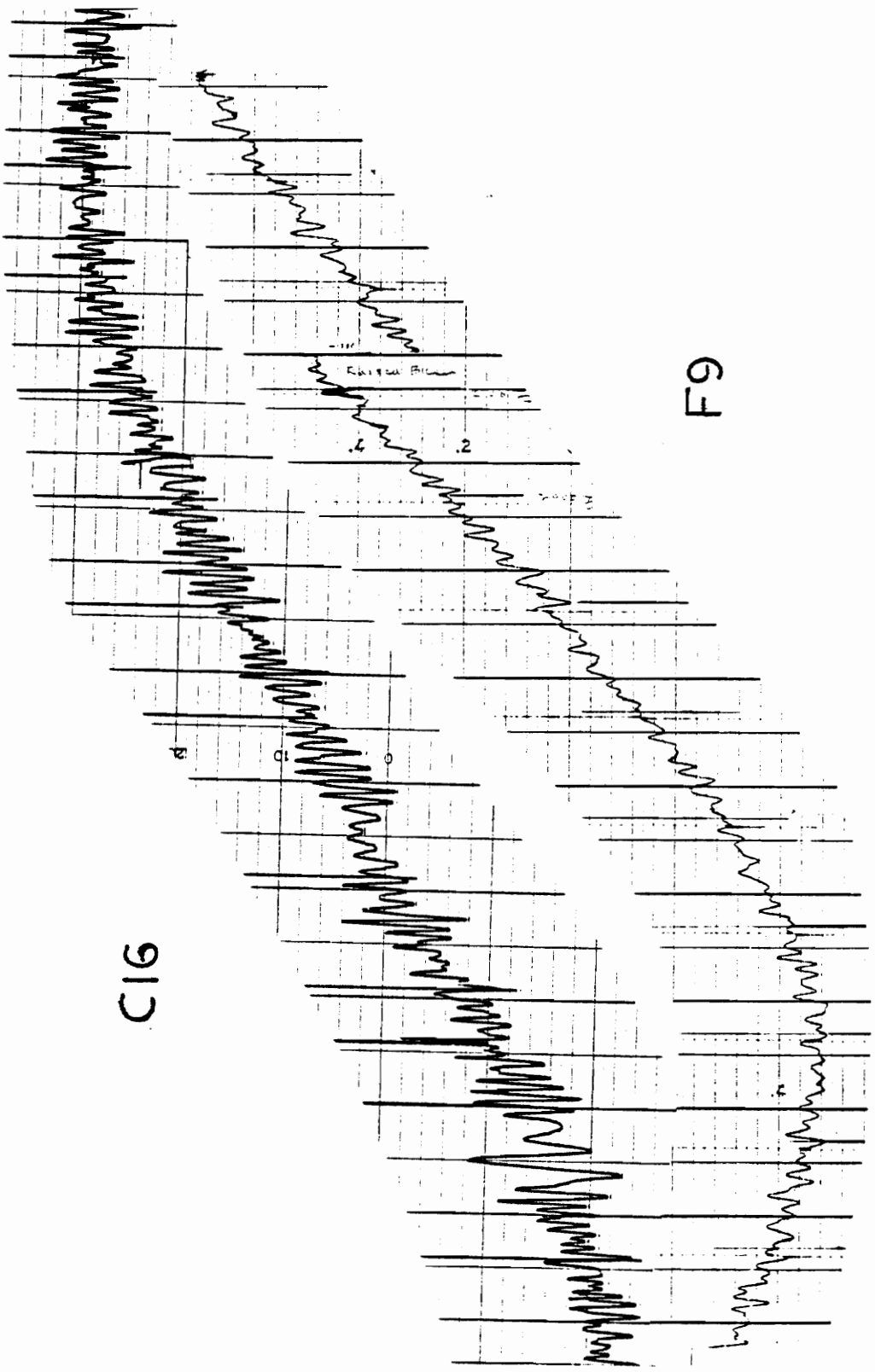

Figure 34b. Refer to Figure 34a for description.

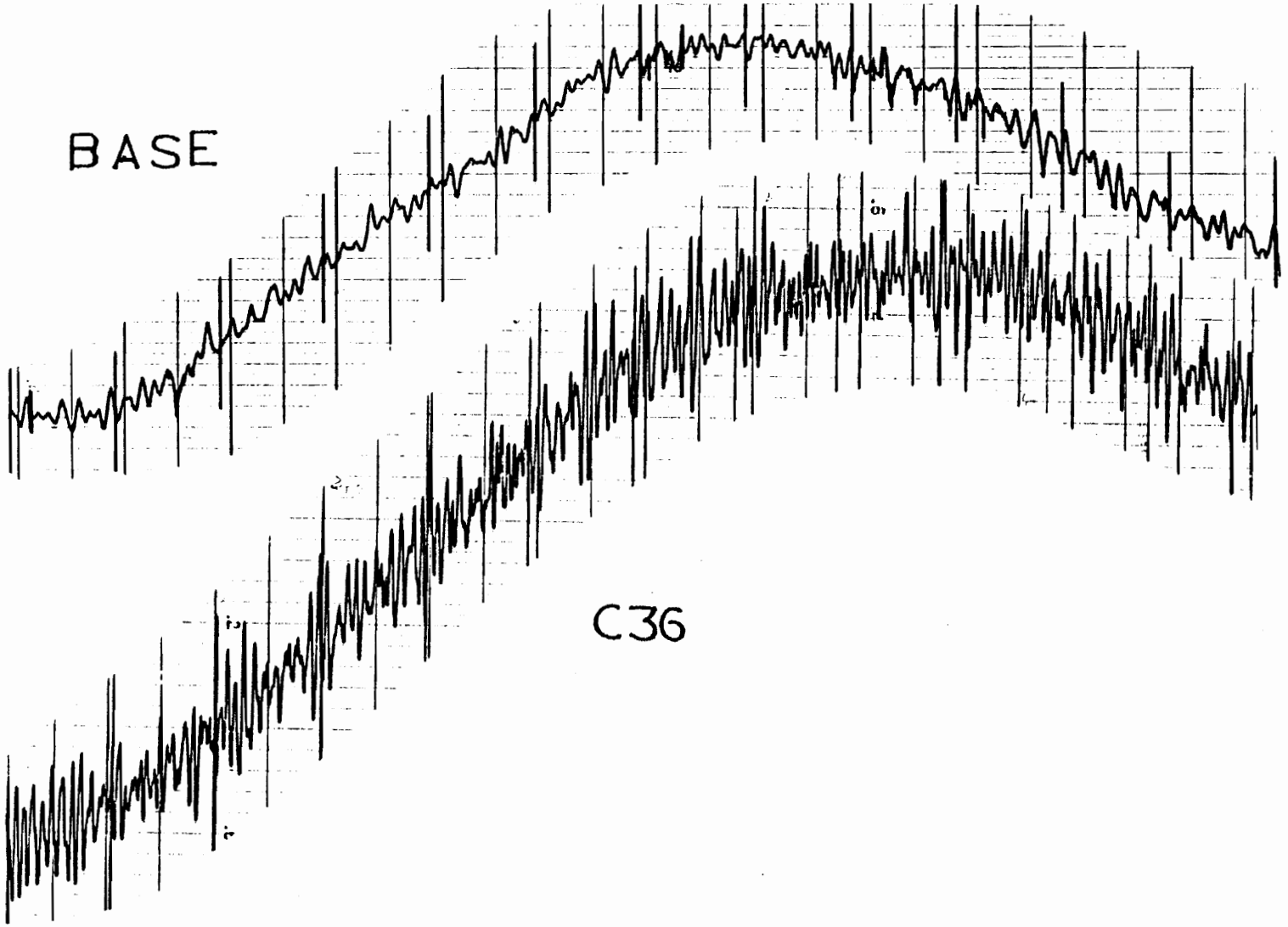

Figure 34c. Refer to Figure 34a for description.

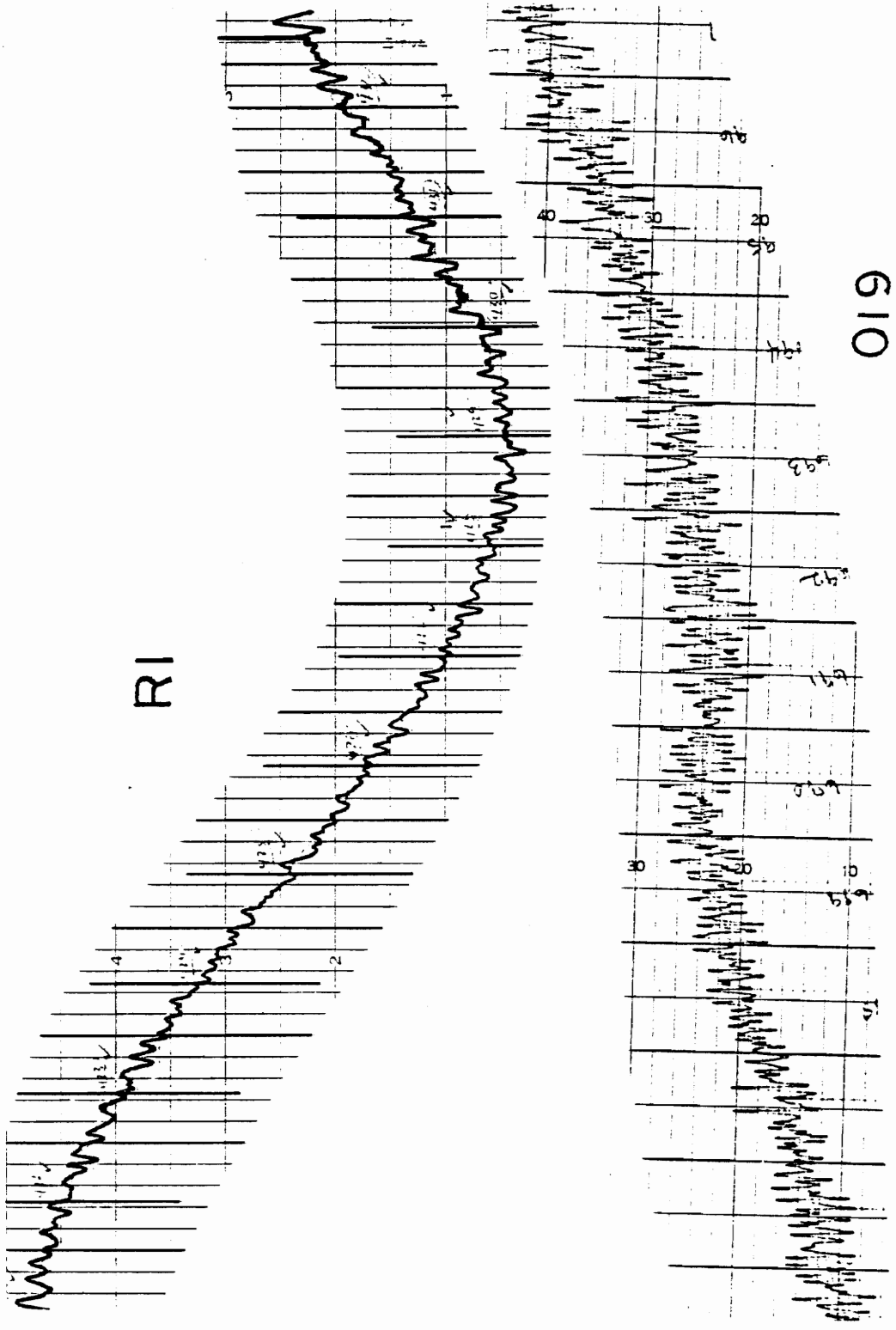

Figure 34d. Refer to Figure 34a for description.

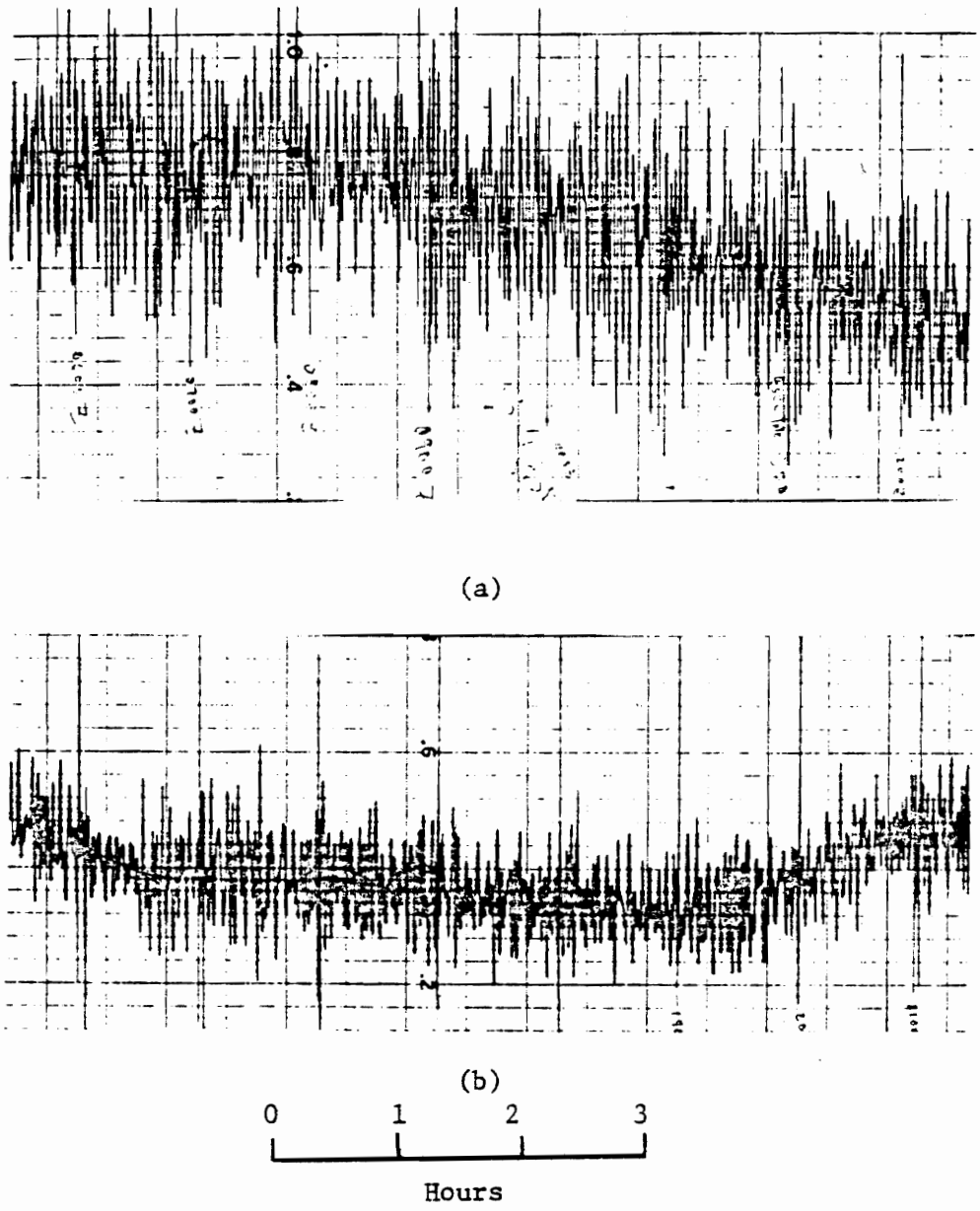

Figure 35. Short period vibrations observed at C13 during and after a storm are illustrated by (a) and (b), respectively.

The waves present on the RISP gravity records are similar to the short period motions of the gravimeter beam at Little America V, except for the period range of the motion. Thiel and others (1960) report observations of waves having periods shorter than 1 minute, and having much larger amplitudes than are present on the RISP records. According to their report, the gravimeter at LAS was unreadable, swinging from stop to stop, until midwinter when the Ross Sea north of the ice shelf was covered by sea ice. The observations at LAS are quite consistent with the RISP data. LAS was located essentially at the ice front, and, again, the motion appears to decrease in amplitude and increase in period as distance from the ice front, or open water, increases.

During the first years of the project, these nontidal waves were observed on all the RISP tidal gravity records, but no special effort was made to study them. However, some consideration was given to their nature and source, and it was hypothesized that they are elastic flexural waves, generated at the ice front by the ocean swell, and propagating in the ice and subjacent water layers. A field experiment was conducted in the last field season of the project to test this hypothesis, by measuring the speed and direction of propagation of these waves at J9. In the experiment, three gravimeters were operated simultaneously on the apicees of an equilateral triangle having 5 km long sides. The data were recorded digitally at a 4 sec digitizing interval on recorders designed and assembled for that purpose. The new recorders were necessary because the

nontidal waves were poorly recorded on the strip-chart recorders used for the tidal data (Figure 34). A short sample of the digitally recorded data from J9 is presented in Figure 36. Also shown are the positions of the recording sites relative to J9 camp. The broadening of the trace from satellite camp Beta is caused by a slightly higher level of electrical noise generated by that instrument.

Flexural Wave Theory

It is well known that the ocean swell penetrates the ice covered regions of the oceans, but that in doing so its spectrum is altered, the shorter periods being rapidly attenuated (Wadhams, 1973). Studies of this phenomenon have been done, for the most part, on floating sea ice a few meters thick. To the author's knowledge, it has not been previously studied in a body of ice as thick as the Ross Ice Shelf overlying water column of similar thickness.

The theory of elastic waves in floating ice has been well developed, although it is, perhaps, not widely known. The theory was first investigated by Greenhill (1887), whose work was extended by Ewing and Crary (1934). This result has been verified by Wilson (1958) and by Wadhams (1973). An experimental study was reported by Clements and others (1958). Flexural waves in a floating ice sheet are analogous to Rayleigh waves on a solid, and gravity waves on water. They are inversely dispersed, with the phase speed given by the following:

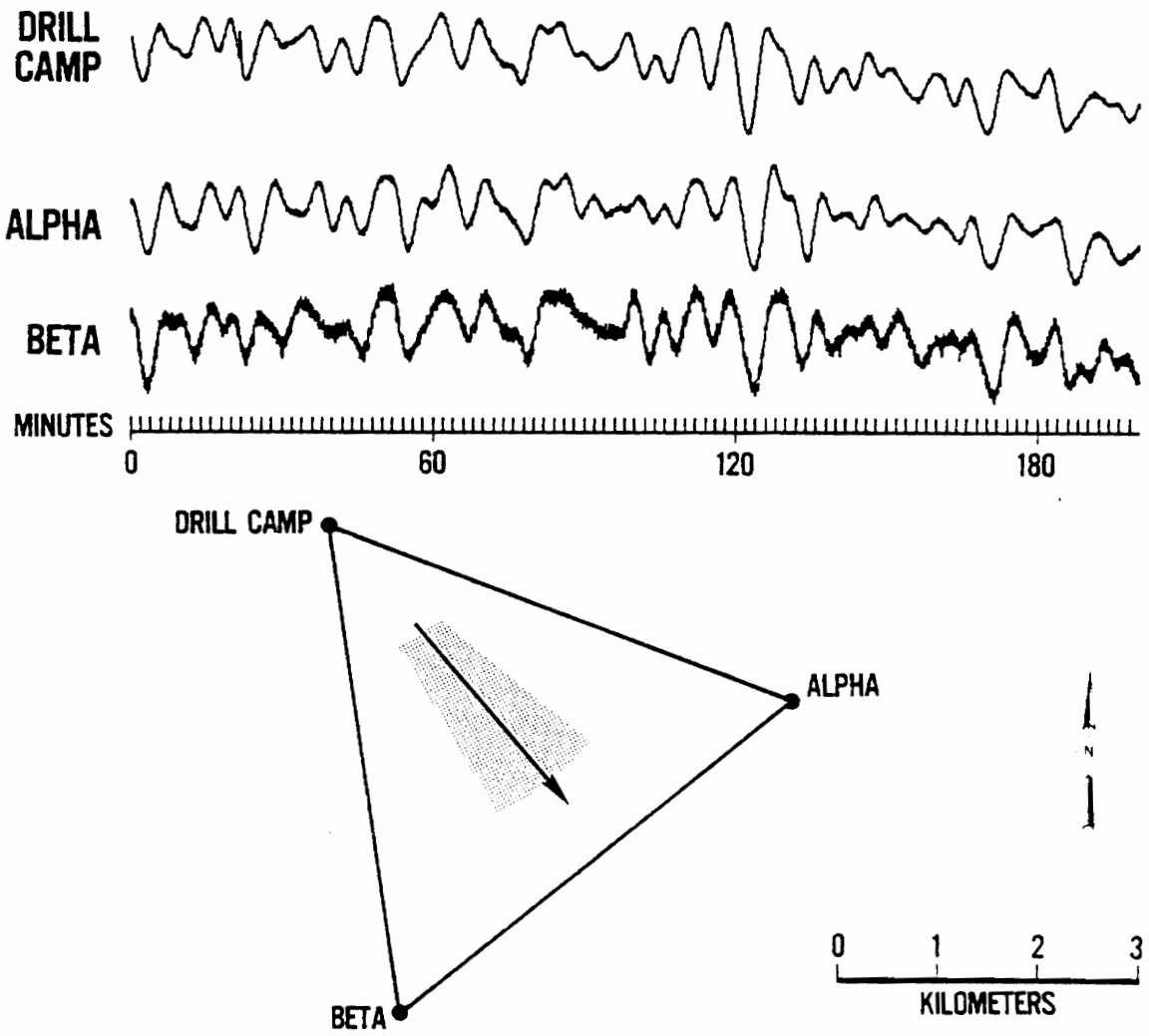

Figure 36. Waves at J9. The record segments shown were recorded beginning at 1058:52 GMT 26 Nov 1977. Also shown is a plan of the tripartitite array used to record the wave motion. The arrow and shading superposed on the array indicate the direction of propagation of the waves across the array.

$$c^2 = \frac{\frac{g}{K} + \frac{k^3 D}{\rho_w}}{\frac{\rho_i}{\rho_w} Hk + \frac{1}{\alpha} \coth(\alpha hk)} \qquad (14)$$

where D = flexural rigidity of the ice sheet,

$$D = \frac{EH^3}{12(1-\nu^2)} = c_i^2 \rho_i \frac{H^3}{12}$$

$$\alpha = \left(1 - \frac{c^2}{c_w^2}\right)^{1/2},$$

c = flexural wave phase speed

k = wave number = 2π/ wave length

c_w = speed of sound in water

c_i = speed of sound in ice

ρ_w = density of the water

ρ_i = density of the ice

h = thickness of the water layer

H = thickness of the ice

g = acceleration of gravity

ν = Poisson's ratio

E = Young's modulus

According to equation (14), the speed of the flexural wave at J9 is period dependent. A theoretical dispersion curve, based on the theory by Ewing and Crary (1934; equation 14) is presented in

Figure 37. In calculating this curve, the following physical parameters were used: c_w = 3700 m/sec and c_i = 1450 m/sec (Robertson, 1975); ρ_w = 1.03 gm/cm^3 and ρ_i = 0.86 gm/cm^3; h = 240 m and H = 240 m; g = 9.83 m/sec^2. From the figure, it is seen that in the period range of the J9 waves (apparently longer than 1 min), the flexural wave speed decreases monotonically to the shallow-water wave speed of 48 m/sec. For practical purposes, waves longer than 10 min period could be considered to travel at the shallow-water speed.

Digital Recorders for the Gravimeters

A new method of recording the gravimeter output signal was required for quantitative studies of the nontidal motion of the ice shelf. The tidal data were obtained by continuously recording the gravimeter output signal on a strip-chart recorder (Figure 34). Time was kept by an independent crystal-controlled clock that placed hourly tic marks on the record. The paper speed on the chart recorders was nominally 1 in/hr, driven by a motor synchronized to the 60 Hz power line. However, in Antarctica the line frequency was poorly controlled, and subject to short term fluctuations as great as 10%. In addition, the amplitude resolution possible with the chart recorders was poor. The sensitivity of the chart recorder was set so that the tidal cycle occupied the full width of the chart. At this setting, the nontidal waves usually had a 1/2 in to 1 in range. This was felt to be inadequate.

New microprocessor-based digital recorders were designed and constructed to supplement the strip-chart machines. These recorders

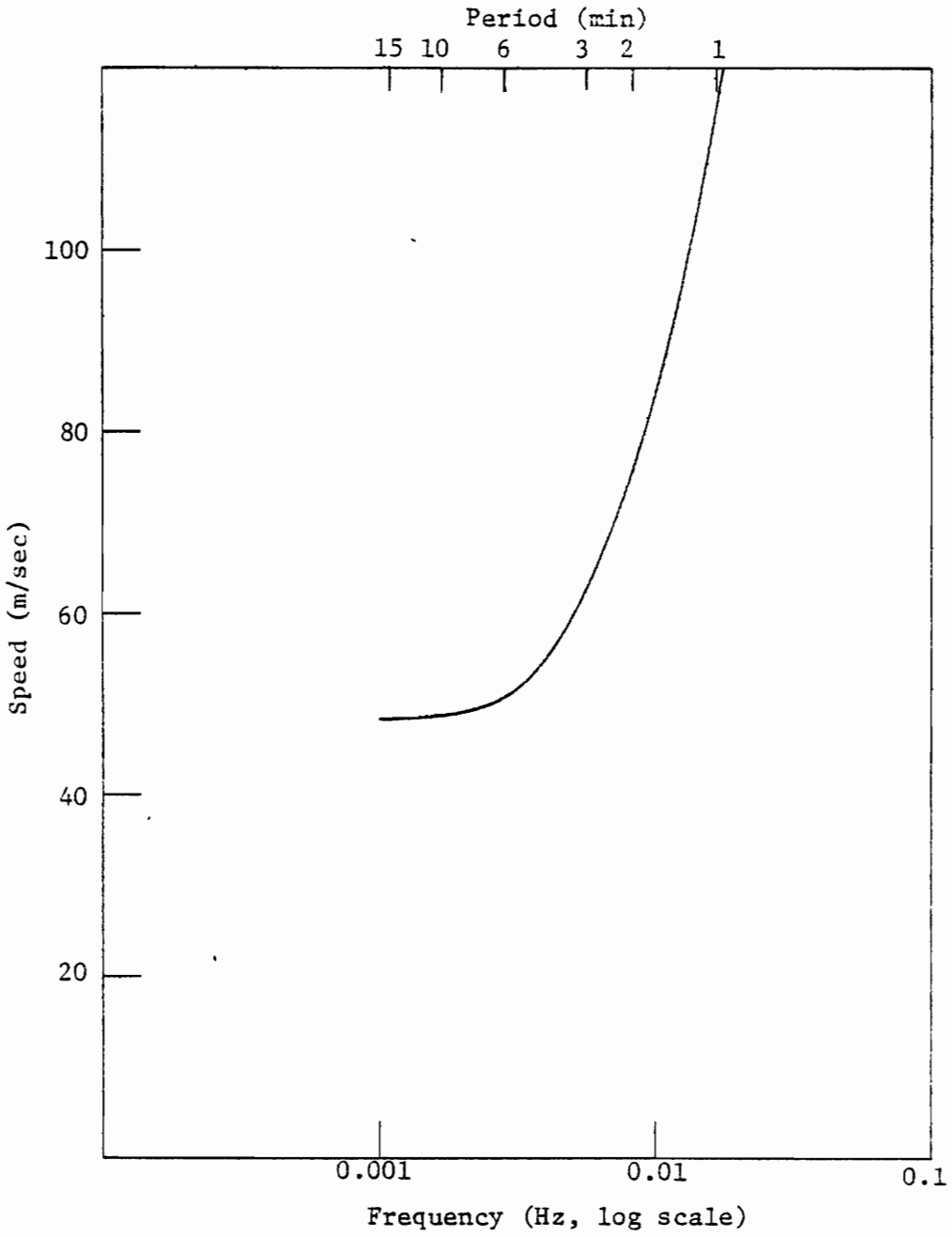

Figure 37. Flexural wave dispersion curve for J9.

are comprised of 8 basic modules. The central module is an analog-to-digital (AD) converter that samples the analog signal from the gravimeter and outputs a corresponding 12-bit binary number. A crystal-controlled clock module generates the signals that trigger the AD converter at specified intervals. There is a memory module for short-term data storage, and a cassette tape module for permanent data storage. Two modules, a typewriter-like keyboard and television monitor, allow an operator to pass instructions to the digitizer and check for proper operation. A serial interface module allows for communication between the digitizer and another machine. After the data has been recorded, it can be retrieved and transmitted to a larger computer for analysis through this interface. The last module contains the microprocessor which controls all the other modules according to a program which is stored in the memory. The manufacturers and model numbers of the component parts of this system are given in Appendix III. The controlling program, developed by the author, is also discussed.

The program under which the digitizer operates samples and records the gravimeter signal at selected intervals of 1 sec to 256 sec. The program includes a clock which, in conjunction with the clock module, keeps time in terms of the year, day of the year, and time of day. The clock drift rate is better than 1 sec per day. The data acquired by the digitizer were stored on tape cassettes, which were ultimately transmitted to the IBM machine in the Virginia Polytechnic Institute (VPI) Computing Center. A

program which causes the digitizer to read the data tapes and transmit them to the VPI main computer via the serial interface was also developed by the author.

Gravimeter Frequency Response

The tripartite measurement of the wave speed and direction requires that the time lag of the arrival of the wave along the various sides of the array be accurately measured. Since the flexural wave hypothesized here is dispersive, the time lags may be period dependent. That is, for a dispersive wave the phase changes of the Fourier component waves, at two stations relative to the third, are likely to be nonlinearly dependent on frequency. Although the three gravimeters used in this study are similarly constructed, it is certain that they are not identical (Table 2). Therefore it was necessary to measure the frequency response of each of the instruments. For measurement of the wave speed, the data must be corrected for differences in the phase response between the three gravimeters. Calculation of the amplitude spectrum of the nontidal wave requires a correction for the amplitude response of the gravimeter.

Determination of the frequency response characteristics of the gravimeters used in this study was based on the assumption that they behave linearly. Similar instruments have been modeled as underdamped harmonic oscillators, using a 17 sec natural period and 0.7 critical damping (Hunkins, 1962). Observations of the response of the instruments to an impulsive disturbance indicate that these values are approximately correct, but a more accurate determination

was desired. The frequency response was determined by comparing the known frequency content of a 10 sec long calibration pulse to the response of the instrument to the pulse. The frequency content of a 10 sec pulse is illustrated in Figure 38. As a check on this procedure, one instrument (number 735) was calibrated on the long-period shake-table at Carnegie Institute, Department of Terrestrial Magnetism, in Washington, D. C.

The results of the amplitude and phase response measurements are presented in Figures 39 and 40, respectively. It was found that the frequency response of the instruments is more complex than allowed by a simple harmonic oscillator model. In particular, meter 735, whose amplitude response is shown in Figure 39 appears to exhibit at least two resonances, one near 0.022 Hz (45 sec period) and one near 0.059 Hz (17 sec period). The principal amplitude resonance being near 0.059 Hz. The phase response of meter 735 (Figure 40) also indicates a complex behavior. Firstly, the frequency at which 90° phase lag occurs is 0.022 Hz. For an underdamped harmonic oscillator would be the natural frequency, 0.059 Hz. Secondly, the phase response at frequencies higher than 0.1 Hz is unlike that of a simple harmonic oscillator.

In order to calculate the nontidal wave speed it was necessary to know the relative phase responses of the three instruments at periods longer than 1 min. Also, knowledge of the amplitude response of only one instrument was needed to calculate the wave amplitude spectrum. This information is given in Figures 39 and 40. It is

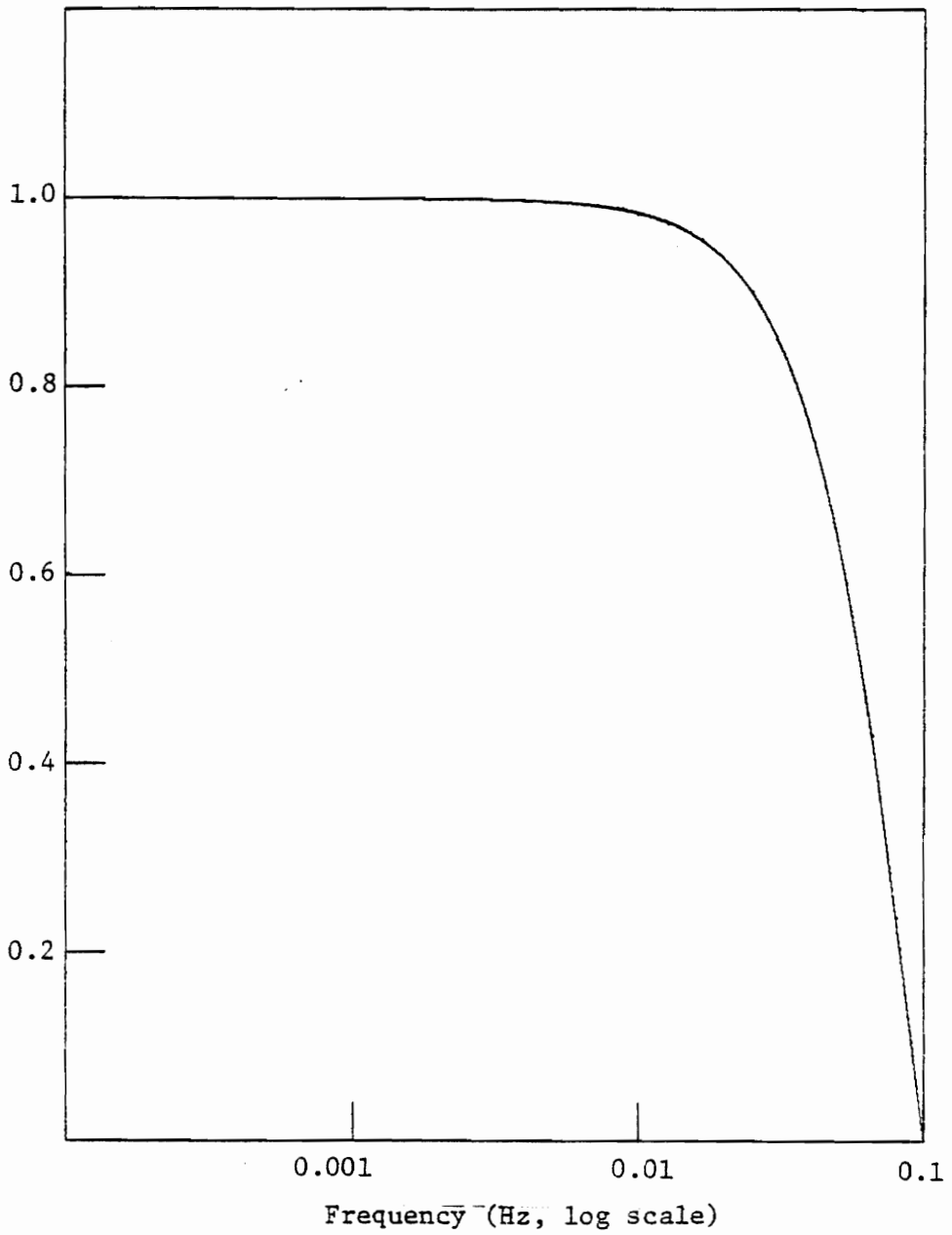

Figure 38. Amplitude spectrum of a 10 sec-long rectangular pulse.

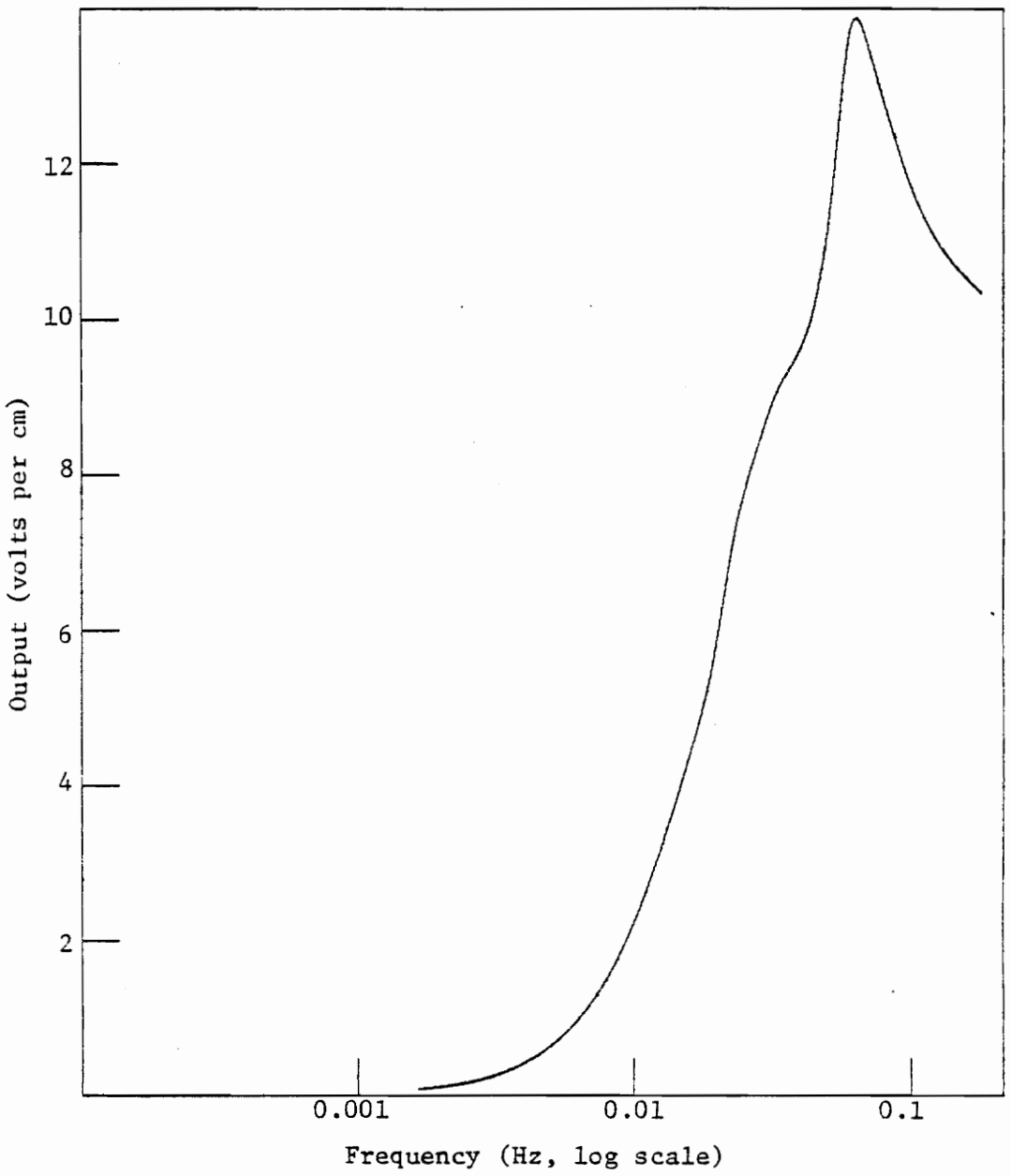

Figure 39. Meter 735 amplitude response, measured on the shake-table at Carnegie Institute.

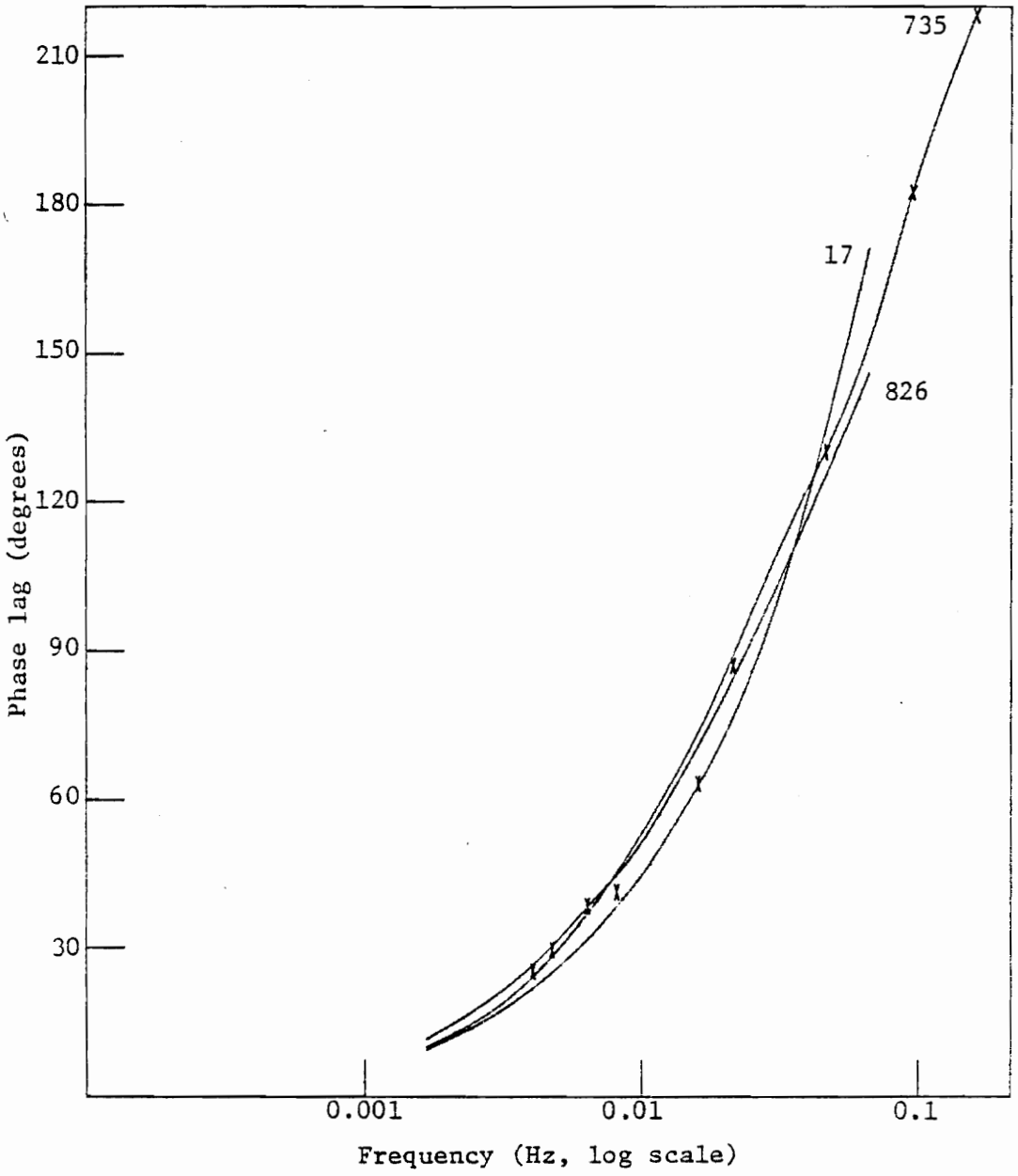

Figure 40. Gravimeter phase response curves. Solid curves were determined from the instrument response to a 10 sec-long calibration pulse. Crosses denote meter 735 phase measured on the shake-table at Carnegie Institute.

noted that for the periods of interest in this study, the phase response of meter 826, used at J9 base camp, relative to meter 735, used at Alpha, corresponds approximately to a time lag of 2 sec. Similarly, the response of 826 relative to meter 17, used at satellite camp Beta, corresponds approximately to a time lag of 3 sec.

Nontidal Wave Data

The tripartite array at J9 was operated during the period 22 to 26 November 1977. Approximately 33 hours of simultaneous data from all three instruments were obtained. Noisy record segments, due to earthquakes, camp noise, and instrument problems, were rejected. The time intervals spanned by these records are given in Table 11; the records are presented in Figure 41. The long period variation, particularly evident on the longer records, is the tidal gravity variation.

A detailed plan of the J9 tripartite array is shown in Figure 42. The dimensions of the array were determined using a surveyor's transit and chain. The angles may be regarded as accurate to 0.01 degree: The distances are accurate to $\pm$ 1 meter. From the figure it is seen that the array forms a nearly perfect equilateral triangle.

The length of a side of the array was limited by field considerations. The 5 km dimension was roughly the greatest distance at which the satellite camps could be seen from J9 base camp on a clear day.

Table 11. Times of the record segments from the J9 tripartite array.

Beginning time (GMT)		Length
12:02:20	22 Nov 77	4 hr 13 min 20 sec
18:22:20	22 Nov 77	2 hr 6 min 40 sec
22:38:04	23 Nov 77	4 hr 13 min 20 sec
4:41:04	24 Nov 77	14 hr 26 min 40 sec
14:48:24	25 Nov 77	2 hr 6 min 40 sec
8:18:52	26 Nov 77	5 hr 59 min 56 sec

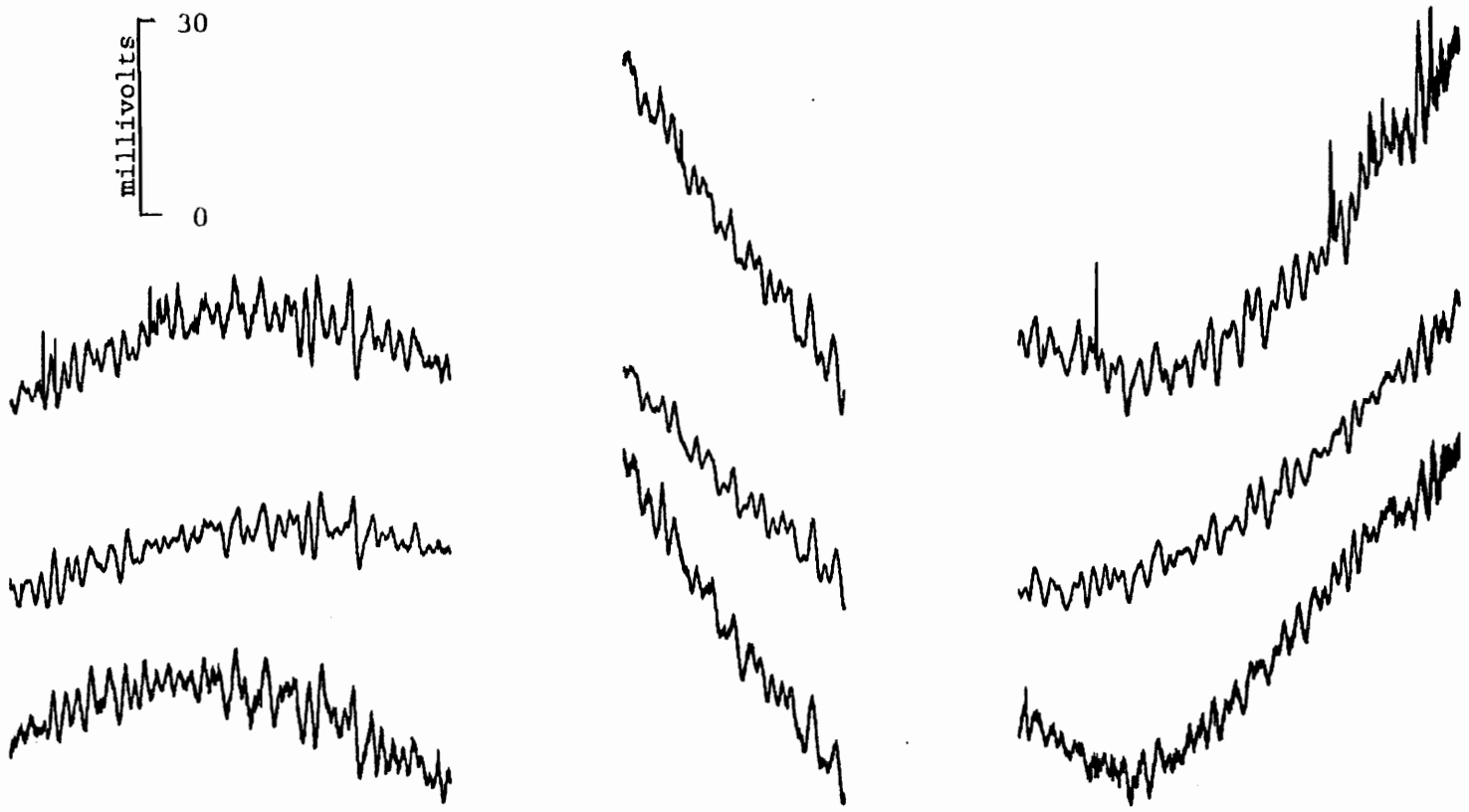

Figure 41a. Simultaneous record segments from the J9 tripartite array. Long period variations are due to the ocean tide and to instrument drift. Spikes on the records are caused by vehicle movement nearby. Small amplitude earthquake signals are also visible. The upper record is from J9 Base Camp, the center record is from satellite camp Alpha and the lower record is from satellite camp Beta. The starting time and length of each segment is given in Table 11. A short segment is shown more clearly, and with a time scale in Figure 36.

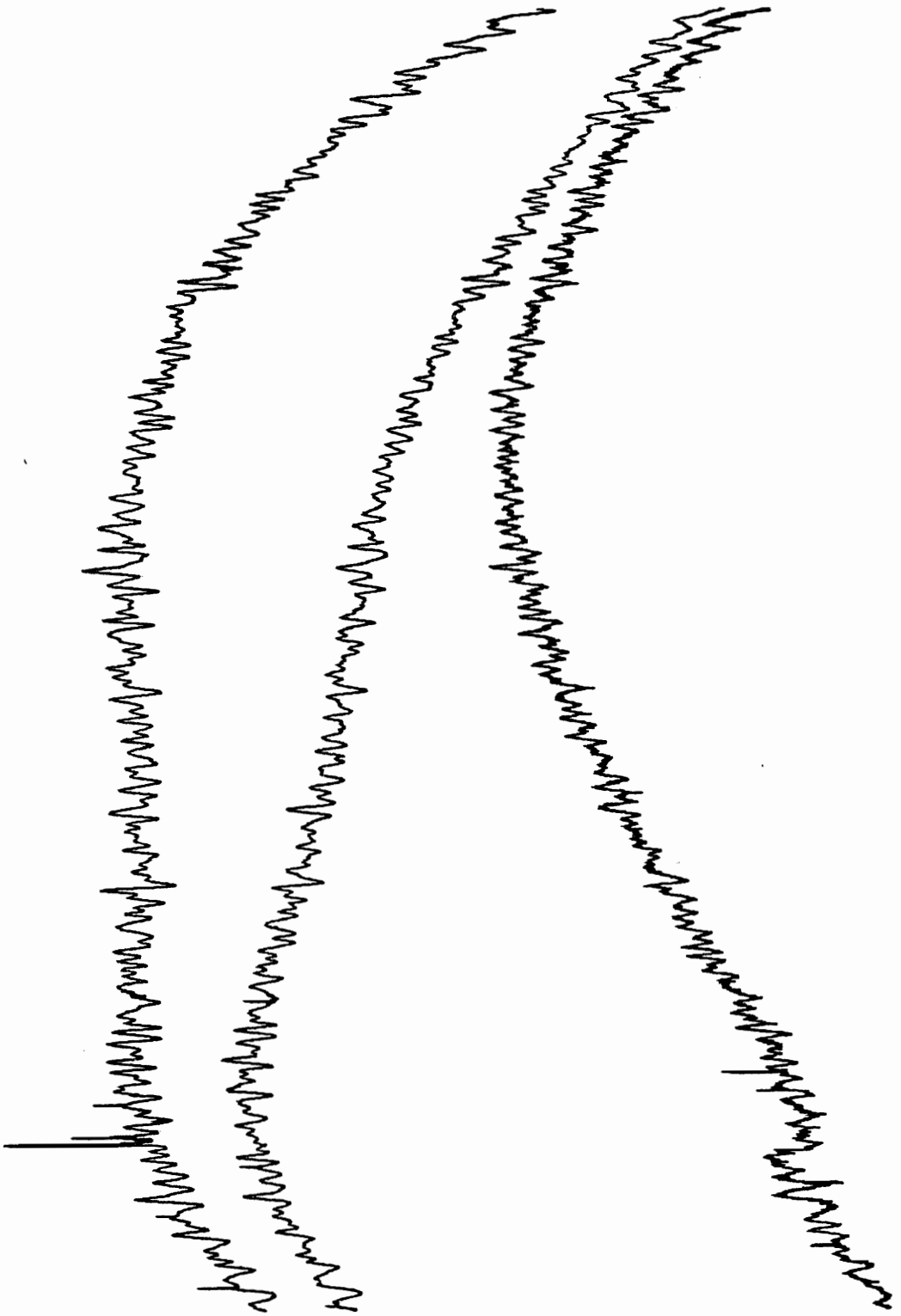

Figure 41b. Refer to Figure 41a for description.

Figure 41c. Refer to Figure 41a for description.

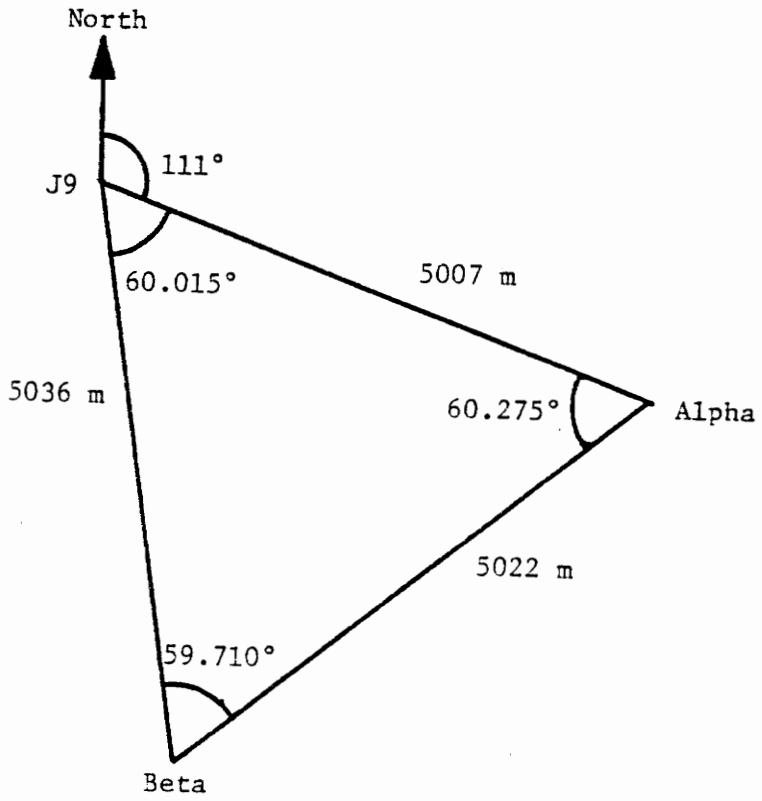

Figure 42. Dimensions and orientation of the J9 tripartite array. Distances are accurate to ± 1 m, interior angles of the array are accurate to 0.01°.

Speed and Direction of the Nontidal Waves at J9

Examination of the short record segments shown in Figure 36 reveals that the wave motion is similar, though not identical, at the three stations in the array. Further, the motion at sites Alpha and Beta occurs more or less synchronously, or with Beta slightly in the lead, while the motion at J9 clearly precedes both Alpha and Beta.

The relationship between the relative arrival times of the wave across the array, and the wave velocity is now explicitly developed. Referring to Figure 43, let s be the wave speed and ϕ be the direction of propagation, and let time be measured from the arrival of the wave front at J9. Denote the arrival times at satellite camps Alpha and Beta by Δ_α and Δ_β, respectively. Then

$$\Delta_\alpha = \frac{D_\alpha}{s}$$

$$\Delta_\beta = \frac{D_\beta}{s}$$

Referring to Figures 42 and 43, it can be seen that:

$$D_\alpha = 5007 \text{ m} \sin (201^\circ - \phi)$$

$$D_\beta = 5037 \text{ m} \sin (\phi - 81^\circ)$$

or

$$D_\alpha = -1794 \text{ m} \cos \phi + 4674 \text{ m} \sin \phi$$

$$D_\beta = -4974 \cos \phi + 786.4 \text{ m} \sin \phi$$

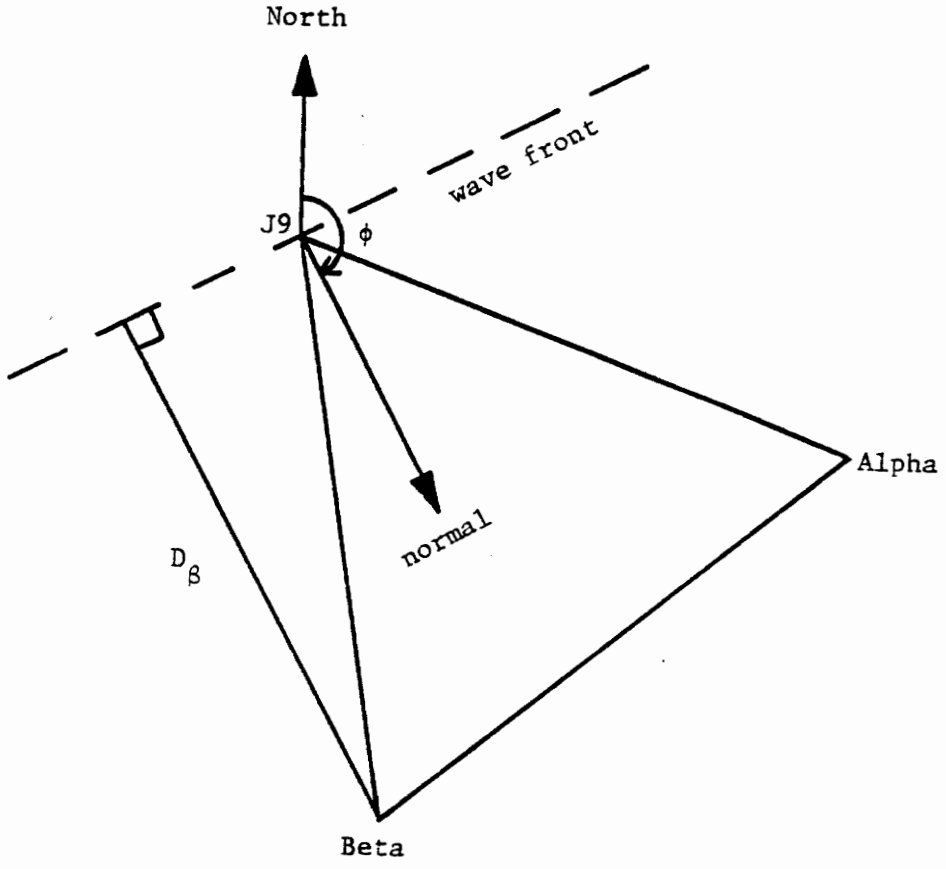

Figure 43. Schematic representation of the nontidal wave crossing the J9 tripartite array. Array dimensions are given in Figure 36.

Divide by Δ_α and Δ_β to get s, equate, and multiply by $\Delta_\alpha\Delta_\beta$ to get:

$$\sin\phi\ (\Delta_\beta\ 4674\ \text{m} - \Delta_\alpha\ 786.4\ \text{m}) = \cos\phi\ (\Delta_\beta\ 1794\ \text{m} - \Delta_\alpha\ 4974\ \text{m})$$

So that $$\phi = \tan^{-1}\ \frac{\Delta_\beta\ 1794 - \Delta_\alpha\ 4974}{\Delta_\beta\ 4674 \quad \Delta_\alpha\ 786.4}$$

Having ϕ, then D_α or D_β can be calculated, from which the wave speed s can be found from:

$$s = \frac{D_\alpha}{\Delta_\alpha} = \frac{D_\beta}{\Delta_\beta}$$

Calculations of the speed of the J9 wave from the observational data, for comparison with Figure 37, were done in two steps. Firstly, a single representative speed was calculated, neglecting the (suspected) dispersive quality of the wave. Secondly, it was attempted to measure the dispersion by bandpass filtering the data, and calculating a speed representative of each band. Calculation of the wave velocity across the J9 array requires that the time lags Δ_α and Δ_β be determined from the field observations. These values were obtained by pair-wise crosscorrelation of the data from J9, Alpha, and Beta. For the required calculations 16 nonoverlapping segments of the wave record (Table 11, Figure 41) were selected. Portions of the record containing camp noise or seismic waves were avoided, but some low-level noise on the segments was unavoidable. Most of the windows were either 120 min or 113 min 20 sec in length, depending on the available record. Results of the crosscorrelation are presented in

Table 12. It can be seen from the table that the lags Δ_α and Δ_β are roughly equal, while the crosscorrelation of the records from Alpha and Beta, $\Delta_{\alpha-\beta}$, is greatest near zero lag. Crosscorrelations of the records from Alpha and Beta were used only as a qualitative check on the values of Δ_α and Δ_β, because there is a greater possibility that this value, being near zero, will be disturbed by signals that travel across the array at high speed (a few kilometers per second). The crosscorrelation process is sensitive to coherent energy between the two time series. Because of the short dimensions of the array, energy crossing it at high speeds will result in an increased correlation near zero lag. In this study signals due to earthquakes, microseisms, and timing pulses would appear to arrive simultaneously at all stations, and thus interfere with the correlation process.

Wave velocities calculated from pairs of Δ_α and Δ_β are given in Table 12, along with the lags. There is a considerable scatter in the velocities, reflecting the scatter in the lags. To extract a single representative value for the velocity from the scatter, the concept of order statistics (Bennett and Franklin, 1954, p. 157) was applied. The application of order statistics allows a representative velocity to be determined, within error limits, without requiring an assumption that the scatter in the observations has a specific form, Gaussian for example. While this calculation implicitly assumes that the wave is not dispersive, it is recognized that dispersion could effect the scatter in the observations of the wave

Table 12. Time lags and wave velocities from the unfiltered J9 data.

Start (GMT)		Δ_α (sec)	Δ_β (sec)	s (m/sec)	ϕ (degrees)
22 Nov 77	12:02:20	98	67	50	123
22 Nov 77	14:09:00	78	83	54	144
22 Nov 77	18:22:20	114	117	38	142
23 Nov 77	22:38:04	42	75	67	167
24 Nov 77	00:44:44	94	75	50	130
24 Nov 77	04:41:04	82	95	49	148
24 Nov 77	06:41:04	82	79	54	138
24 Nov 77	08:41:04	86	71	55	131
24 Nov 77	10:41:04	66	59	69	134
24 Nov 77	12:47:44	82	71	56	133
24 Nov 77	14:54:24	66	71	63	145
24 Nov 77	17:01:04	66	67	65	141
25 Nov 77	14:18:24	94	35	53	102

Table 12 (continued)

Start (GMT)		Δ_α (sec)	Δ_β (sec)	s (m/sec)	ϕ (degrees)
26 Nov 77	08:18:52	46	59	81	153
26 Nov 77	10:18:52	86	79	53	136
26 Nov 77	12:18:52	78	79	55	141

speed. A plot of the wave speed-direction pairs from Table 12 is presented in Figure 44. From the figure, it appears that while the distribution of the wave directions may be Gaussian, the wave speeds are clustered between 50 m/sec and 58 m/sec, and only one value falls below the shallow water speed of 48 m/sec.

The median value of the wave speeds observed at J9 (Table 12) is 54.5 m/sec and the median direction is N140°E. Referring to the tables provided by Bennett and Franklin, at the 95% confidence level the median of a very large number of such observations would fall between 50 m/sec and 65 m/sec for the speed, and between 131° and 145° for the direction of propagation. Wave speeds in this range are appropriate for flexural waves having periods from 2 min to 6 min (Figure 43), and these periods are evident in the wave recordings shown in Figure 36. The range of wave directions is indicated in Figure 36 by the shaded zone surrounding an arrow superposed on the figure.

The preceding calculation shows that the nontidal waves at J9 are progressive, propagating towards the southeast at a speed in the range predicted by flexural wave theory. However, the speed calculated was averaged, in some sense, over all periods. Recognizing that the flexural wave is dispersive, an effort was made to detect dispersion in the observed waves. In this effort, the wave records were bandpass filtered, before the wave speed was determined. The frequency windows used are illustrated in Figure 45, wherein the windows are shown relative to the dispersion curve for the flexural

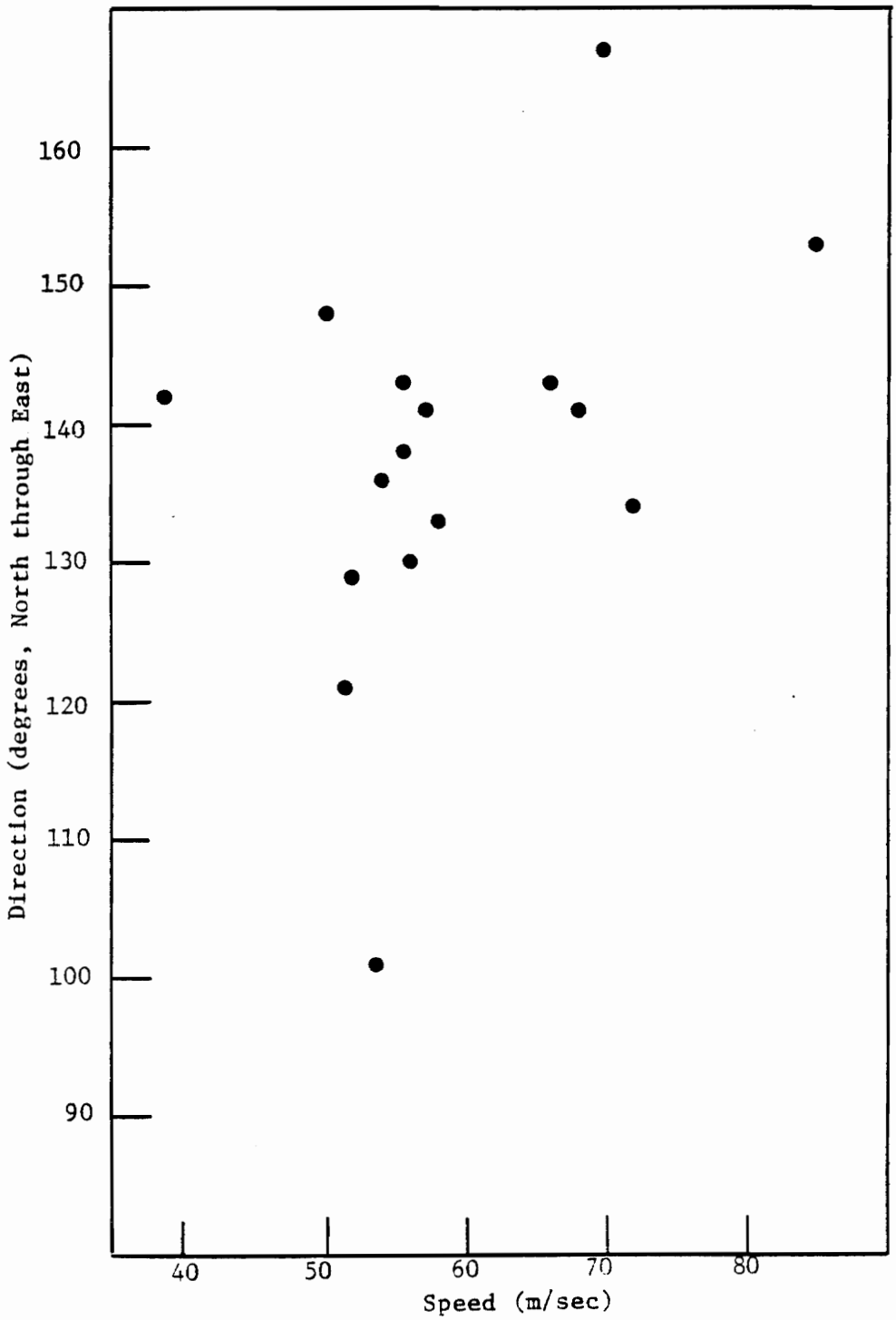

Figure 44. Nontidal wave speeds and directions determined from the unfiltered J9 data (Table 12).

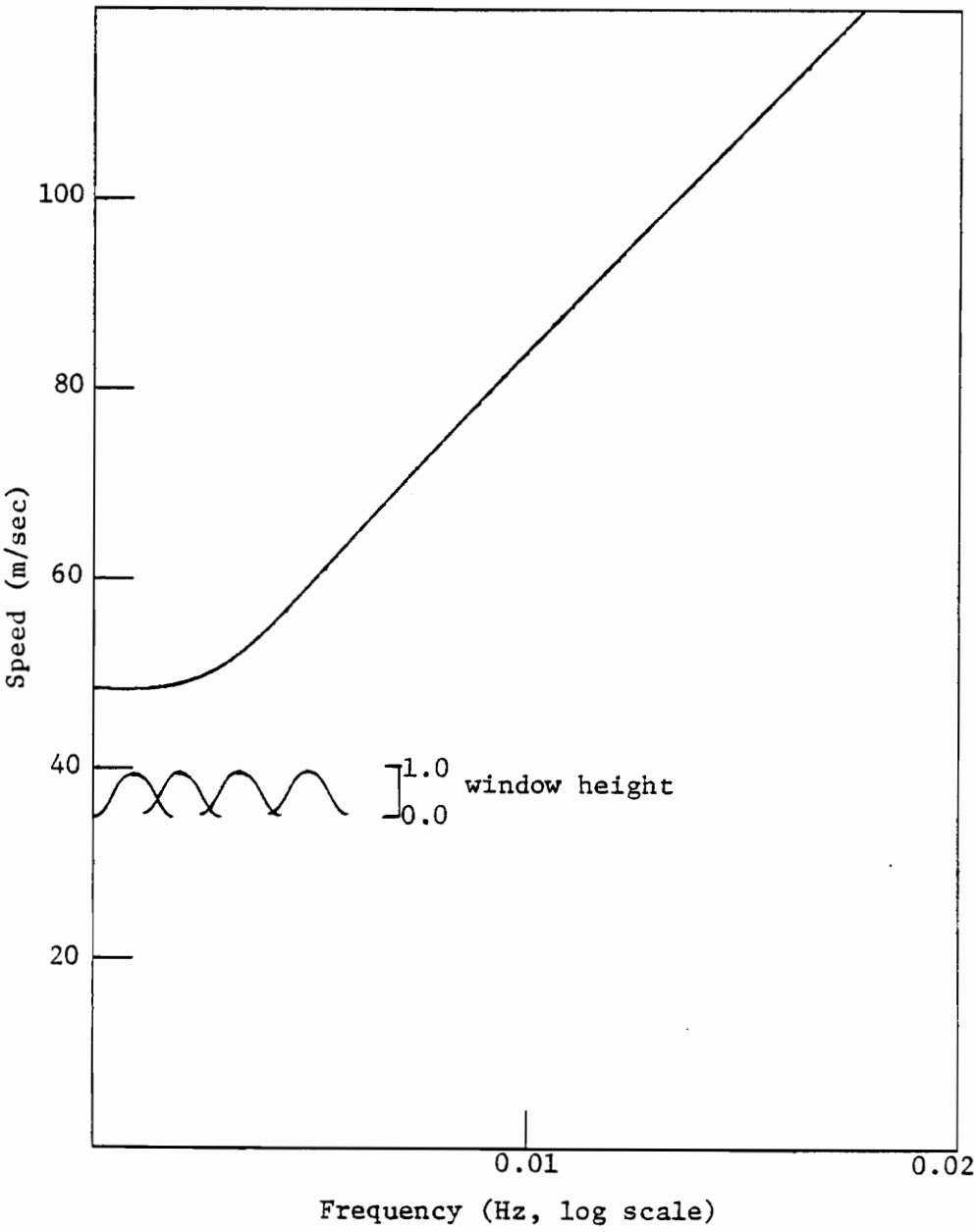

Figure 45. Flexural wave dispersion curve for J9. Also shown are cosine-tapered frequency windows used to filter the data in an attempt to measure the dispersion.

wave. In this figure the frequency scale is linear, rather than logarithmic as in Figure 43. Four cosine-tapered windows, each 0.002 Hz wide, were used, centered at 0.001 Hz, 0.002 Hz, $0.00\overline{33}$ Hz, and 0.005 Hz. The results of the speed determinations using the filtered data are presented in Table 13. Not shown are the results for the window centered at 0.005 Hz: in that case the maximum cross-correlation occurred at zero lag, for almost all record segments. For the remaining windows, the median speed and the range of the mediam at the 95% confidence level are as follows: for the window centered at 0.001 Hz, 52 m/sec and 44 m/sec to 68 m/sec; 0.002 Hz, 51 m/sec and 31 m/sec to 56 m/sec; $0.00\overline{33}$ Hz, 50 m/sec and 36 m/sec to 58 m/sec. Although the uncertainties are large, these values are quite close to the speeds predicted by flexural wave theory. Referring to Figure 45, the theory predicts that the speed increases from 48 m/sec for a 0.001 Hz wave to 52 m/sec for a $0.00\overline{33}$ Hz wave.

Flexural Wave Power Spectrum

In the preceding discussion it has been shown that the nontidal waves observed at J9 propagate at the speed and direction expected for flexural waves generated at the ice front. It will now be shown that a mechanism exists at the ice front for generating flexural waves in the observed period range. Central to this discussion is the power spectrum of the nontidal waves at J9. It is shown that the spectrum of the ocean swell at the ice front, as determined by extrapolation of the J9 spectrum, is consistent with the spectrum of the ocean swell in the Pacific Ocean.

Table 13. Time lags and wave velocities from the J9 data, bandpass filtered using a cosine tapered frequency window 0.002 Hz wide. Record starting times are the same as in Table 12.

Center Frequency 0.001 Hz				Center Frequency 0.002 Hz				Center Frequency 0.003$\overline{3}$ Hz			
Δ_α	Δ_β	s	ϕ	Δ_α	Δ_β	s	ϕ	Δ_α	Δ_β	s	ϕ
(sec)	(sec)	(m/sec)	(degrees)	(sec)	(sec)	(m/sec)	(degrees)	(sec)	(sec)	(m/sec)	(degrees)
98	99	44	141	93	66	52	123	119	76	42	120
58	97	52	164	86	105	45	150	94	77	50	130
128	139	33	145	182	194	23	140	142	174	27	150
14	69	68	191	64	90	54	157	65	53	72	130
-	-	-	-	133	155	30	148	140	123	33	134
50	67	72	155	104	162	31	162	85	51	58	115
75	71	59	137	82	73	56	135	85	93	49	145
52	86	58	164	94	86	48	135	94	65	52	122
18	70	68	188	78	37	63	108	86	71	55	130
75	75	58	140	80	84	53	143	98	70	50	124
88	79	52	135	90	77	51	132	119	122	36	141

Table 13 (continued)

Center Frequency 0.001 Hz				Center Frequency 0.002 Hz				Center Frequency $0.00\overline{33}$ Hz			
Δ_α	Δ_β	s	ϕ	Δ_α	Δ_β	s	ϕ	Δ_α	Δ_β	s	ϕ
(sec)	(sec)	(m/sec)	(degrees)	(sec)	(sec)	(m/sec)	(degrees)	(sec)	(sec)	(m/sec)	(degrees)
94	65	51	122	171	170	25	140	158	163	27	142
38	16	130	105	135	122	33	135	122	3	36	82
67	119	42	167	68	84	56	151	9	54	87	194
113	111	39	139	88	83	51	137	72	45	69	117
88	107	44	150	72	77	58	143	92	57	54	117

The power spectrum of the nontidal waves at J9 has been calculated from the wave records taken using meter 735 (Figure 40). The spectrum, corrected for the instrument response according to the measured response curve (Figure 38), is presented in Figure 46. It is seen that the wave spectrum decreases with increasing frequency from about 5×10^{-2} cm^2/Hz at 0.001 Hz to about 2×10^{-7} cm^2/Hz at 0.01 Hz.

The interchange of energy between the wave in the ocean and the wave in the ice shelf is a complex phenomenon. However, from physical arguments it can be seen that the transmission of energy into the ice covered region is biased towards the long period waves. The geometry of the ice front is illustrated in Figure 47, based on ice and water thicknesses, and elevation measurements at Little America V (Thiel and others, 1960). The phase speeds of flexural waves in the ice shelf region and gravity waves in the open sea, for this geometry, are presented in Figure 48. The flexural wave speeds were obtained from equation (14) using h equal to 400 m and H equal to 230 m. The gravity wave speeds were calculated according to the relationship (Kinsman, 1965, p. 126):

$$c^2 = \frac{g}{k} \tanh (kh) \qquad (15)$$

using h equal to 600 m. It is seen from the figure that at periods shorter than 100 sec there is an increasing contrast between the speeds of the gravity and flexural waves.

A quantative estimate of the amplitude of the flexural wave, relative to the amplitude of the ocean swell, is based on the

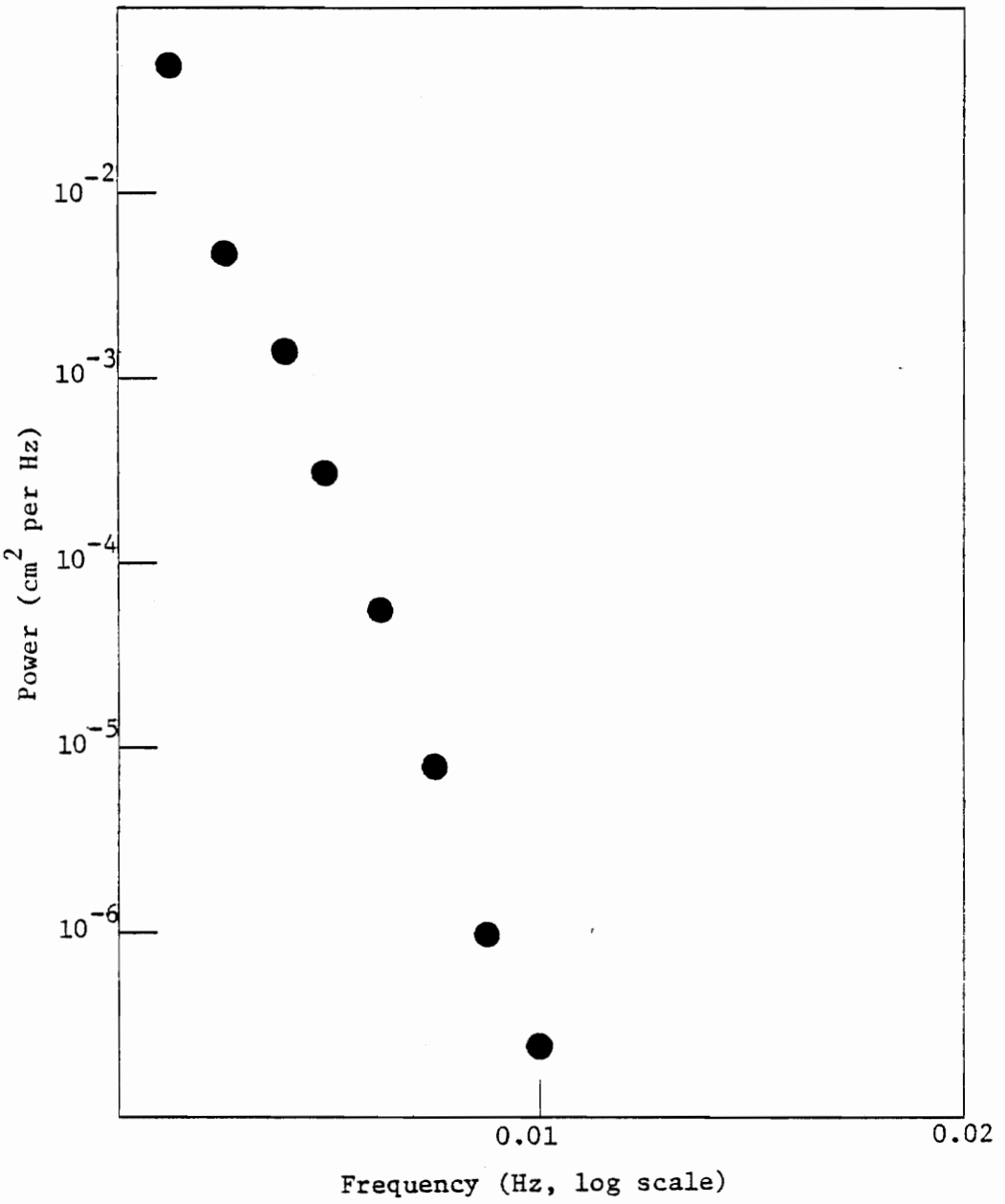

Figure 46. Power spectrum of the flexural waves observed at J9.

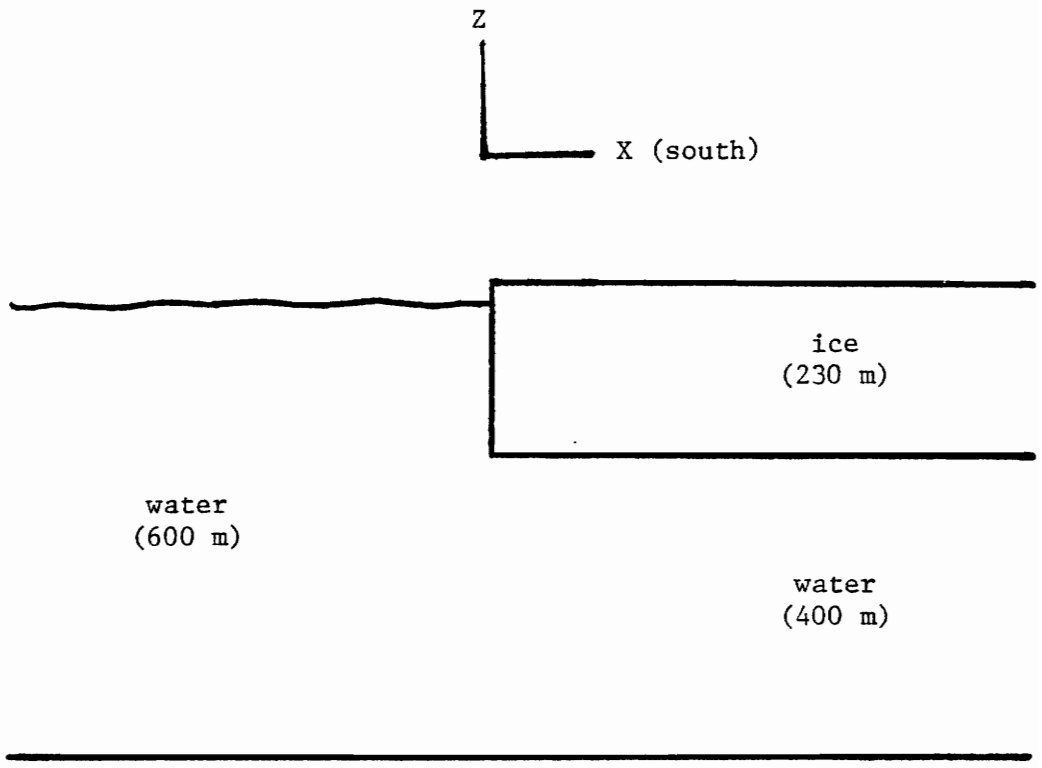

Figure 47. The geometry of the ice front based on ice and water thicknesses at Little America V (Thiel and others, 1960).

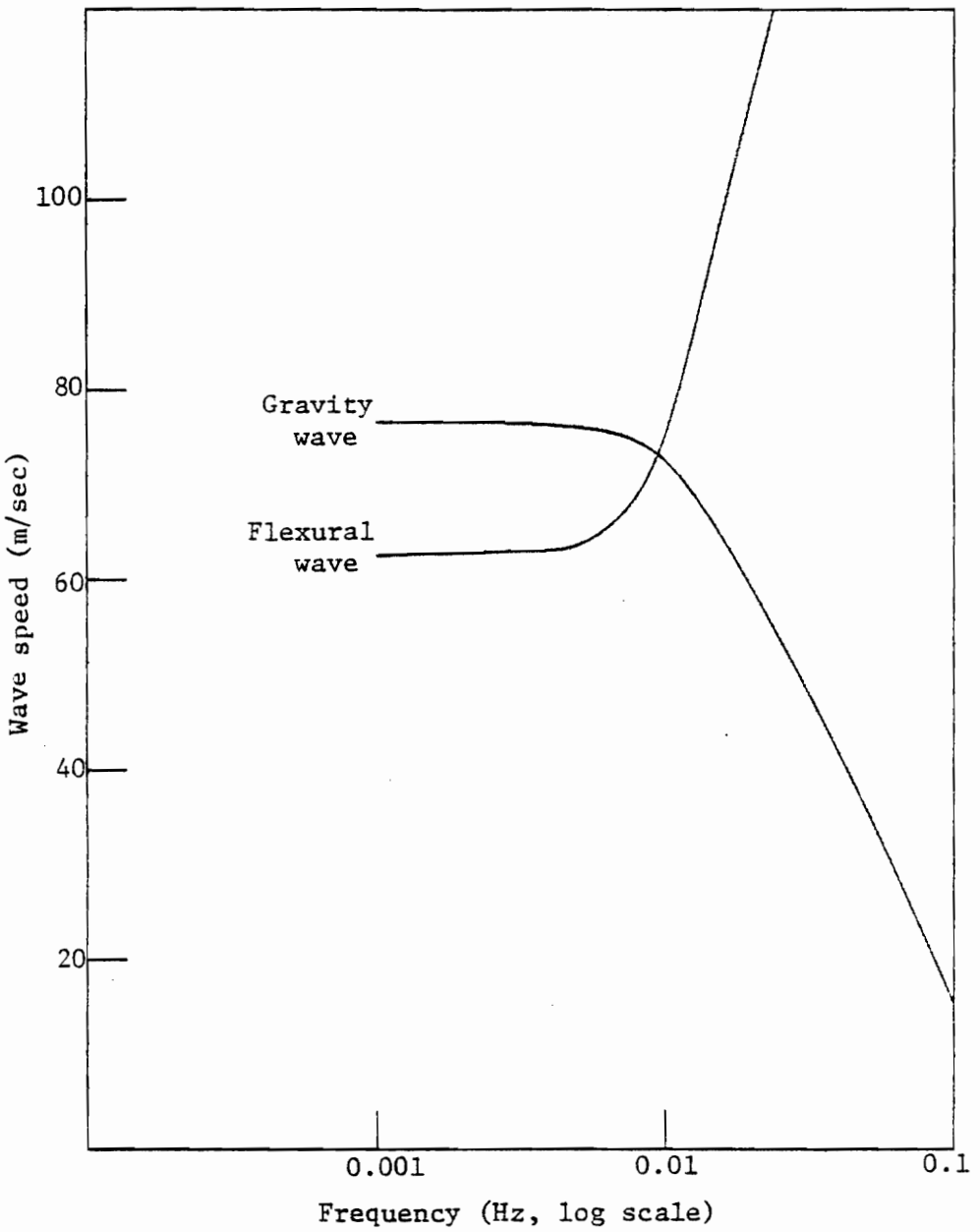

Figure 48. Speeds of flexural and gravity waves near the ice front, based on the geometry shown in Figure 47.

continuity of pressure across the ice front (the x = 0 plane in Figure 47). On either side of the ice front, the pressure in the water layer is given by the formula (Kinsman, 1965, p. 144; Ewing and Crary, 1934):

$$P = -w(z) + \frac{\rho_w \sigma^2 \cosh k(z + h)\ \eta}{k \sinh kh} \qquad (16)$$

where $\eta = a \cos (kx - \sigma t)$ represents the wave,

P = the total pressure,

z = the vertical coordinate, positive upward,

t = the weight per unit area of the mass above depth z,

h = thickness of the water layer

In the open sea, the motion is described by linear gravity wave theory (Kinsman, 1965, Chapter 3), while in the ice covered region the motion is described by the flexural wave theory of Ewing and Crary (1934). On either side of the ice front equation (16) is interpreted in a slightly different way. The quantities h, k, and η differ in the two regions, and in each case z = 0 is taken at the top of the undisturbed water column, which changes across the ice front.

The two theories do not merge across the ice front. Each assumes lateral homogeneity, and neither correctly describes the motion of the water at the ice front. To estimate the flexural wave height, it is assumed that the pressure, averaged over the thickness of the water column beneath the ice, can be calculated from either theory. Integrating equation (16) for the gravity wave side of the boundary, the average pressure is given by:

$$\overline{P} = \frac{1}{h_i} \int_{-h_w}^{-h_w + h_i} \left[-\rho_w g (\eta_w - z) + \frac{\rho_w \sigma^2 \cosh k_w (z + h_w) \eta_w}{k_w \sinh k_w h_w} \right] dz$$

where $\overline{P}$ = the average pressure

h_w = the water thickness in the open sea

k_w = the wavenumber of the wave having frequency σ according gravity wave theory

η_w = the surface disturbance by the gravity wave

Performing the integration, and applying the small amplitude assumption by neglecting terms in η compared to h, yields:

$$\overline{Ph}_i = -\rho_w g \left(h_w h_i - \frac{h_i^2}{2} \right) + \frac{\rho_w \sigma^2 \sinh k_w h_i}{k_w^2 \sinh k_w h_w} \qquad (17)$$

Equation (16) is applied to the flexural wave side of the boundary in a similar way, with h_w replaced by h_i, the water thickness beneath the ice, k_w replaced by k_i as predicted by flexural wave theory, and η_w replaced by η_i, the surface disturbance due to the flexural wave. The limits of the integral on the ice shelf side are $-h_i$ to η_i. Integrating and applying the small amplitude assumption as before yields:

$$\overline{Ph}_i = -\rho_w g \left(h_i h_w - \frac{h_i^2}{2} \right) + \frac{\rho_w \sigma^2 \eta_i}{k_i^2} \qquad (18)$$

Equating (17) and (18) and solving for η_i in terms of η_w yields:

$$\eta_i = \eta_w \frac{k_i^2 \sinh k_w h_i}{k_w^2 \sinh k_w h_w} \tag{19}$$

The amplitude ratio of the flexural wave to the ocean swell calculated according to this relationship is presented in Figure 49. The wave numbers necessary for the calculation were obtained from the phase speeds given in Figure 48.

In the preceding discussion it is shown that long period (Figure 49) waves in the ocean can generate flexural waves in the ice shelf, but that at shorter periods the transfer of energy into the ice covered region is inefficient. After the flexural wave is generated, the spectrum may change as the wave propagates away from the ice front. The attenuation of flexural waves by plastic behavior (creep) in the ice layer has been discussed by Wadhams (1973). The derivation of Wadhams' theory is lengthy, and his paper is readily available, so only his result is given here. He found that the flexural wave amplitude diminishes with distance traveled according to the relationship:

$$a^2(x) = \frac{1}{2Sx + a^{-2}(x = 0)} \tag{20}$$

where x is the distance traveled, and S is a function of wavelength, ice and water thicknesses and densities, and the speed of sound in ice and water. Critical assumptions made in the development of this theory are that the ice creep can be modeled by the flow law of Glen (1955), and that the tensile stress in the ice due to bending

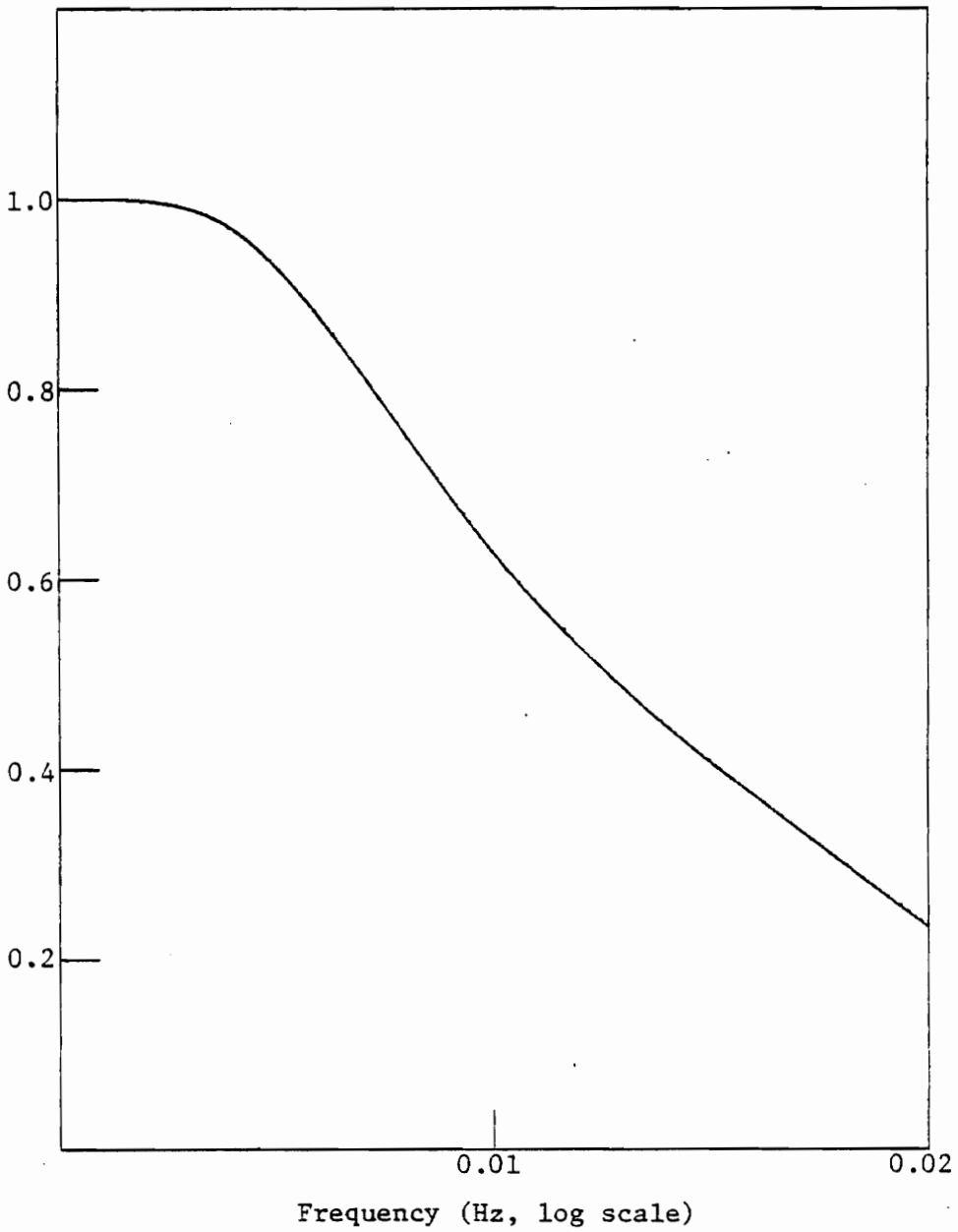

Figure 49. The ratio of the flexural wave amplitude to the ocean swell amplitude at the ice front, based on equation (9).

can be calculated using linear elastic theory. Wadhams finds that the former assumption fits his observations and those of Robin (1963) well. However, the tensile stress in the ice will be relaxed by the creep, and the value calculated from linear theory may be too large. This over estimate will ultimately cause the estimated energy loss due to creep to be too great.

Calculations of Wadhams' factor S were made using the ice parameters previously used to calculate the flexural wave speed, and the value 1.8×10^8 (mks units) for the flow law parameter for the Ross Ice Shelf (Thomas, 1971 quoted by Wadhams, 1973). The variation of S with period for three combinations of ice and water thickness representative of the Ross Ice Shelf region is shown in Figure 50. The amplitude reduction due to creep is not linear, depending on the amplitude (equation 20). However, an upper limit on the effect can be made by taking x equal to 1000 km and $a(x = 0)$ to be 1 cm. The attenuation thus predicted reduces the amplitude of the wave by less than 1% at all periods.

The estimates of the wave attenuation made by applying Wadhams' theory indicate that creep in the ice is not important for the waves observed at J9. Inspection of the field records (Figures 34 and 35) neither confirm nor contradict this conclusion. On the records from C36, Base, C16, and F9 it appears that the shorter periods are attenuated with distance from the ice front. However, the C13 record does not fit this pattern, having greater short period motion than any other record, but being intermediate to C36 and

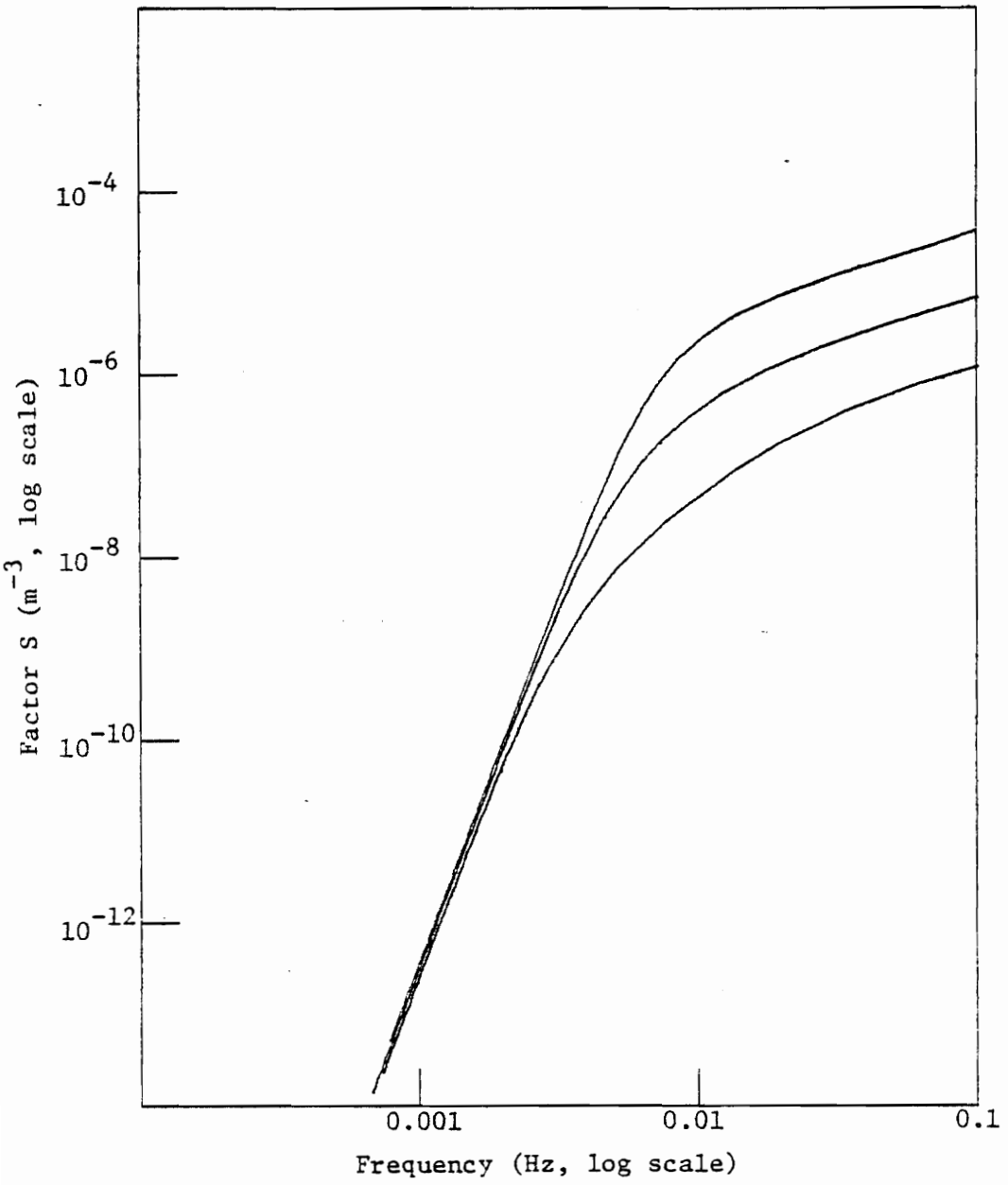

Figure 50. The factor S in equation (20) for ice and water thicknesses typical in the Ross Ice Shelf region.

Base in distance to open water. The Roosevelt Island camp and 019 records indicate that topography greatly influences the spectrum. Both stations are shielded from open water by land to the north (Figure 1), and the records contain less short period motion than the distance from open water would indicate.

The J9 spectrum can be compared to the spectrum of the ocean swell in the Pacific Ocean. Wave spectra measured by Munk (1962) in the western Pacific and at Hawaii are reproduced in Figure 51. The J9 spectrum, corrected for the effect of the ice front according to Figure 49 (equation 19) is superposed on Munk's figure. From the figure it is evident that the Pacific Ocean swell does include the waves necessary to generate the flexural waves observed at J9. It is especially noteworthy that the peak in the Pacific Ocean spectrum at frequencies higher than 40 cycles per kilosecond (periods shorter than 25 sec) is not observed on the ice shelf. The absence of this peak is consistent with the predicted response of the ice shelf to the swell (Figure 49).

Summary

The nontidal waves observed throughout the Ross Ice Shelf have been shown to be flexural waves. It has been shown that the waves are progressive, and propagate at the speed predicted by flexural wave theory. Further, the direction of propagation is away from the ice front, and it has been shown that the Pacific Ocean swell is

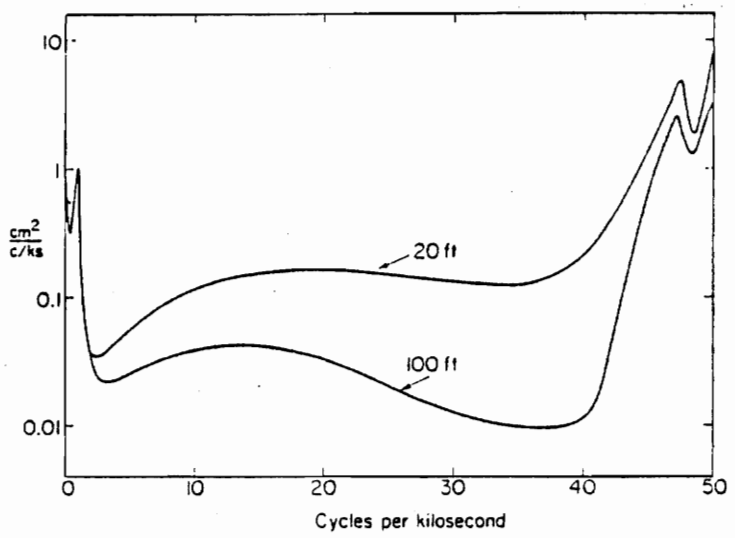

Fig. 3. A typical spectrum for Camp Pendleton, California. The two curves designate the spectra of surface elevation at distances of 8000 and 13,000 ft from the beach, respectively, and corresponding water depths of 20 and 100 ft.

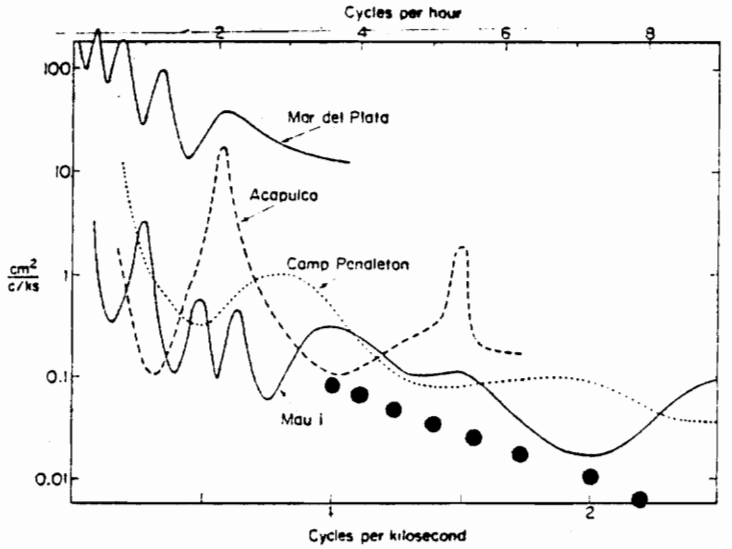

Fig. 4. Background spectra at Mar del Plata, Argentina; Acapulco, Mexico; Camp Pendleton, California; and at Lahaina Wharf, Maui, Hawaii.

Figure 51. Illustrations from Munk (1960) showing the spectrum of the Pacific Ocean swell. Circles superposed on Munk's figures show the J9 spectrum (Figure 46) corrected for the effect of the ice front (Figure 49).

capable of generating flexural waves in the ice shelf having the observed spectrum.

RESULTS

The elevation at the surface of the Ross Ice Shelf fluctuates in response to the ocean tide beneath the shelf. The motion can be described in terms of six harmonic constituents (Table 4), three diurnal and three semidiurnal. The tide is principally diurnal, the diurnal constituent amplitudes being roughly three times as large as the semidiurnal amplitudes. The range of the tropic tide is about 1 m near the ice front, and can be as great as 2 m in the southeastern part of the sea where the water is shallow. The spatial variation of the tide has been described by cotidal-coamplitude maps for these constituents. The diurnal constituents can be viewed as a relatively simple progressive wave that propagates southeastward across the region (Figures 9, 10). The diurnal tidal wave amplitudes are closely related to the thickness of the water column (Figure 15). Within the Ross Sea the diurnal constituents are larger than in the adjacent Pacific Ocean because of constructive interference between the tidal wave and its reflection from the southeastern coast of the sea. The semidiurnal constituents exhibit a more complex variation. The semidiurnal tidal waves rotate clockwise around an amphidromic region near C13 (Figures 11-13). For the diurnal constituents the cotidal contours mapped in this study are consistent with available global ocean tide maps in the southern Pacific Ocean (Figures 16-21). For the semidiurnal the situation is more complicated. Available maps showing the constituent M_2 in

the southern Pacific (Figures 22-26) are of two types: those that show the phase decreasing eastward from McMurdo, and those that show increasing phase eastward. The discovery in this study that there is an amphidromic region within the Ross Sea is an important step in reconciling the different maps of M_2 in this region.

The tidal current beneath the Ross Ice Shelf at J9 has been calculated from the cotidal-coamplitude charts (Figures 32, 33), and compared to the measured current (Figure 29). A number of important insights have been gained from these calculations. Firstly, the semidiurnal current components are relatively more important than the semidiurnal components of the tidal height, because of a resonance between the semidiurnal and inertia currents. The semidiurnal current amplitudes appear to be roughly the same as the diurnal current amplitudes (Tables 4, 9). Secondly, the calculations of this dissertation show that the tidal current is rotary, and that the sense of rotation is clockwise for the diurnal constituents and counterclockwise for the semidiurnal constituents (Figure 33). The differences between the calculated and measured currents may arise from the presence of significant nontidal currents beneath the ice shelf, and from the simplifying assumptions made in the calculations. In the theory it is assumed that the motion of the water is nearly uniform throughout the water column, and that the retarding effect of the ice and sea floor can be treated as a body force that increases with the speed of the current. Because of the resonance condition, calculations of the semidiurnal

current components are sensitive to these assumptions. In future studies it may be necessary to extend the theory to allow for variation in the current with position in the water column. More current data from beneath the shelf, and especially simultaneous measurements at different levels in the water column, would be helpful in the development of a more general method for calculating the tidal current.

The observed motion of the ice shelf at periods shorter than 20 min (Figure 34) has been identified as elastic flexural waves which are generated at the ice front by the action of the ocean swell on the ice shelf, and propagate southward. The wave speed was predicted within the uncertainty of the measurement by the classical flexural wave theory. The theory has previously been shown to apply in ice from less than 1 m to about 50 m thick. In this study that range has been extended to about 500 m.

BIBLIOGRAPHY

Bennett, C. A., and N. L. Franklin, Statistical Analysis in Chemistry and the Chemical Industry, John Wiley and Sons, New York, 1954.

Bennett, H. F., A gravity and Magnetic survey of the Ross Ice Shelf, Antarctica, Geophysical and Polar Research Center, Research Report Series 64-3, 1964.

Bernacchi, L., To the South Polar Regions, Hurst and Blackett, London, 1901.

Bogdanov, K. T., Marées de l'Océan Pacifique, Marées Terrestres Bulletin D'Informations, 67, 3727-3752, 1973.

Broucke, R. A., W. E. Zurn, and L. B. Slichter, Lunar tidal acceleration on a rigid earth, Flow and Fracture of Rocks, American Geophysical Union Geophysical Monograph 16, William Bird Press, Richmond, Va., 1972.

Bulirsch, R., and J. Stoer, Numerical treatment of ordinary differential equations by extrapolation methods, Numerische Mathematik, 8(1), 1-13, 1966.

Clements, D. H., D. E. Willis, and J. T. Wilson, Waves in lake ice from impacts, Report of Project MICHIGAN, Univ. of Michigan Willow Run Laboratories, August, 1958.

Darwin, G. D., Tidal observations of the "Discovery", National Antarctic Expedition 1901-1904. Physical Observations, Royal Society, London, 1908.

Dennis, R. E., and E. E. Long, A Users Guide to a Computer Program for Harmonic Analysis of Data at Tidal Frequencies, National Oceanic and Atmospheric Administration Technical Report NOS 41, 1971.

Doodson, A. T., Oceanic tides, Advances in Geophysics, 5, 117-152, 1958.

Doodson, A. T., Tidal observations: reduction of tide gauge records, Cape Evans, British (Terra Nova) Antarctic Expedition 1910-1913, London, 1924.

Estes, R. H., A Computer Software System for the Generation of Global Ocean Tides including Self Gravitation and Crustal Loading Effects, X-920-7782, Goddard Space Flight Center, 1-58, 1977.

Ewing, M., and A. P. Crary, Propagation of elastic waves in ice, 2, Physics, 5, 181-184, 1934.

Gilmour, A. E., Hydrological heat and mass transport across the boundary of the ice shelf in McMurdo Sound, Antarctica, New Zealand Journal of Geology and Geophysics, 6(3), 1963.

Gilmour, A. E., W. J. P. MacDonald, and F. G. van der Hoeven, Winter measurements of sea currents in McMurdo Sound, New Zealand Journal of Geology and Geophysics, 5(5), 778-789, 1962.

Glen, J. W., The creep of polycrystalline ice, Proc. Roy. Soc. London, Ser. A, 228 (1175), 519-538, 1955.

Greenhill, A. G., Wave motion in hydrodynamics, Amer. J. Math., 9, 62-112, 1887.

Greischar, L. L., and C. R. Bentley, Isostatic rebound and the configuration of the grounding line between the Ross Ice Shelf and the West Antarctic Ice Sheet, Paper presented at the 1978 Spring Meeting of the American Geophysical Union, Eos, 59, 309, 1978.

Grijalva Ortiz, N., Numerisch hydrodynamishce untersuchungen im Golf von Mexiko, Ph.D. dissertation, Univ. Hamburg, 1964.

Guldberg, C. M., and H. Mohn, Études sur les Mouvements de l'Atmosphére, Christiania, 1876. Transl. by C. Abbe, Smithsonian Inst., Misc. Collections, 3, 122-248, 1910.

Heath, R. A., Tidal constants for McMurdo Sound, Antarctica, New Zealand Journal of Marine and Fresh Water Resources, 3(2), 376-380, 1971.

Henderschott, M., and W. Munk, Tides, Ann. Rev. Fluid Mech., 2, 205-224, 1970.

Hunkins, K., Waves on the Arctic Ocean, J. Geophys. Res., 67(6), 24-7-2489, 1962.

Jachens, R. C., An experimental study of tidal gravity across the continental United States, Ph.D. dissertation, Columbia Univ., 1971.

Jacobs, S. S., E. B. Bauer, P. M. Bruchhausen, A. L. Gordon, T. F. Root, F. L. Rosselot, Eltanin Reports: Cruises 47-50, 1971; 52-55, 1972, Lamont-Doherty Geological Observatory of Columbia Univ., Palisades, New York, 1974.

Jacobs, S., P. Bruchhausen, and J. Ardai, Physical oceanography of the Ross Sea, Antarc. J. of the U.S., 5, 1978.

Kinsman, B., Wind Waves, Their Generation and Propagation on the Ocean Surface, Prentice-Hall, Englewood Cliffs, N.J., 1965.

LaCoste, J. J. B., A simplification in the conditions for the zero-length-spring seismograph, Bull. Seismol. Soc. Am., 25, 176-179, 1935.

Lamb, H., Hydrodynamics, Dover, New York, 1941.

Longman, I. M., Formulas for computing the tidal accelerations due to the moon and sun, J. Geophys. Res., 64, 2351-2355, 1959.

MacDonald, W. J. P., and A. C. Burrows, Sea-level recordings at Scott Base, Antarctica, 1957, New Zealand Journal of Geology and Geophysics, 2(2), 297-314, 1959.

Melchoir, P., The Earth Tides, Pergamon, New York, 1966.

Munk, W. H., Long ocean waves, The Sea: Ideas and observations on Progress in the Study of the Seas, v. 1, M. N. Hill ed., Interscience, 1962.

Neumann, G., Ocean Currents, Elsevier, New York, 1968.

Nihoul, J. C. J., ed., Bottom Turbulence, Elsevier, New York, 1977.

Robertson, J., Geophysical studies on the Ross Ice Shelf, Antarctica, Ph.D. dissertation, Univ. Wisconsin-Madison, 1975.

Robin, G. de Q., Wave propagation through fields of pack ice, Phil. Trans. Roy. Soc. London, Ser. A, 255(1057), 313-339, 1963.

Robinson, E. S., A reconnaissance of tidal gravity in the south-eastern United States, J. Geophys. Res., 79(29), 4418-4424, 1974.

Robinson, E. S., R. T. Williams, H. A. C. Neuburg, C. S. Rohrer, and R. L. Ayers, Interaction of the ocean tide and the solid earth gravity tide in the Ross Sea area of Antarctica. Preliminary results. Ann. Geophys., 33, 147-150, 1977.

Schureman, P., Tide and Current Glossary, U. S. Coast and Geodetic Survey Special Publication No. 228, 1949.

Schureman, P. W., Manual of Harmonic Analysis and Prediction of Tides, U. S. Coast and Geodetic Survey Special Publication No. 98, 1941.

Shackelton, E. H., The Heart of the Antarctic, v. 2, London, 1909.

Thiel, E. C., Tides on the Ross Ice Shelf, J. Geophys. Res., 64(8), 1960.

Thiel, E. C., A. P. Crary, R. A. Haubrich, and J. C. Behrendt, Gravimetric determination of the ocean tide, Weddell and Ross Seas, J. Geophys. Res., 65(2), 629-636, 1960.

Thomas, R. H., Flow law for Antarctic ice shelves, Nature, London, 232(30), 85-87, 1971.

Tiron, K. C., Y. Sorgeev, and A. Michurin, Tidal charts for the Pacific, Atlantic, and Indian Oceans, Vestn. Leningrad Univ., 24, 1967.

Wadhams, P., Attenuation of swell by sea ice, J. Geophys. Res., 78(18), 3552-3563, 1973.

Wilson, J. T., Moving Loads on Floating Ice Sheets, Univ. Michigan Research Inst., July, 1958.

Young, T., Miscellaneous Works, v. 2, 262-290, 1813.

Zahel, W., A global hydrodynamic-numerical 1°-model of the ocean-tides; the oscillation system of the M_2-tide and its distribution of energy dissipation, Ann. Geophys., 33(1-2), 31-40, 1977.

Zumberge, J. H., Ross Ice Shelf Project, Antarc. J. of the U. S., 6, 258-263, 1971.

APPENDIX I

The FORTRAN computer program developed by the author to calculate the tidal current step-wise in time from a given cotidal-coamplitude chart is presented in this appendix. This program solves equation (8) using the IMSL subroutine DREBS. The equation is specified in subroutine DFN of the program, and changes in the equation, including different treatments of the dissipation terms (equations 9 and 10) are made by changing the FORTRAN code within that subroutine.

Subroutine DREBS and UERTST are proprietary products belonging to International Mathematical and Statistical Libraries, Inc. (IMSL), in Houston, Texas. These subroutines are reproduced in this dissertation with the permission of IMSL, in order that the results can be duplicatable by others. These subroutines may not be extracted for other purposes or used as the basis for any software development.

```
      IMPLICIT REAL*8 (A-H,O-Z)
      REAL*4 NU(3000),NV(3000)
      DIMENSION COMMON(2),WK(58),ONES(2),ERRORS(2),W(2,9)
      COMMON /STAT/ FRCONS,WLONG,COLAT,DEPTH,W,GOVRA,PI,DELT,DELX,IPRIN
      COMMON /CNTS/ U,V
      COMMON /INIT/ TIMEI,UI,VI,ERRTOL,TMAX,TSTEP,STPMIN,IORDER
      COMMON /TBLE/ TOLD(58),DTOLD(58),DXOLD(58),IEND
      EQUIVALENCE (COMMON(1),U)
      EXTERNAL DFN,FCN
C
C     IN THIS PROGRAM, DISTACES ARE IN CM, TIMES ARE IN SECONDS
C
      ONES(1)=1.0
      ONES(2)=1.0
      IER=0
      INC=0
C
C     READ ALL INPUT
C
      CALL DATAIN
      TIME=TIMEI
      U=UI
      V=VI
 1001 CONTINUE
C
C     SET THE TIME STEP
C
      TINC=TSTEP
      INC=INC+1
C
C     SET THE POINTER FOR A NEW TABLE
C
```

```
      IEND=0
C
C     GET THE NEXT ESTIMATE OF THE CURRENTS USING THE IMSL SUBROUTINE
C
      IF(IPRIN.EQ.1.OR.IPRIN.EQ.2)
     : WRITE(6,1002) CURNOW,TIME,TINC,STPMIN,ERRTOL,ERRORS,ONES,IORDER
 1002 FORMAT(/10G12.5,2I6)
      CALL DREBS1(DFN,CURNOW,TIME,2,IORDER,3,0,TINC,STPMIN,ERRTOL,ERRORS
     :           ,ONES,WK,IER)
      IF(IPRIN.EQ.1.OR.IPRIN.EQ.2)
     : WRITE(6,1003) CURNOW,TIME,TINC,ERRORS,IER,IEND
 1003 FORMAT(10G12.5,2I6)
C
C     CHECK THE ERROR INDICATOR
C
      IF(IER.NE.0)  STOP
C
C     SAVE VALUES OF CURRENT IN CM/SEC TO OUTPUT LATER
C
      NU(INC)=U
      NV(INC)=V
C
C     CHECK FOR END OF SERIES
C
      IF(TIME.GE.TMAX)  GO TO 1000
C
C     CHECK RECOMMENDED TIME STEP
C
      IF(TSTEP.LE.TINC)  GO TO 1001
      WRITE(6,1004) TSTEP,TINC,TIME
 1004 FORMAT('WARNING - THE SPECIFIED TIME STEP ',G12.5,
     :' MAY BE TOO LARGE.  ',G12.5,' IS RECOMMENDED.  TIME= ',
```

```
     :G12.5)
      GO TO 1001
 1000 CONTINUE
      WRITE(2,1005) TIME1,INC,TSTEP,TIME
 1005 FORMAT(4G14.6)
      DTOR=3.14159265400/180.D0
      AMPI=DSQRT(UI*UI+VI*VI)
      AZII=DATAN2(VI,-UI)/DTOR
      IF(AZII.LT.0.)  AZII=AZII+360.DO
      DO 2001 I=1,INC
      TAMP=SQRT(NU(I)**2+NV(I)**2)
      TAZI=ATAN2(NV(I),-NU(I))/DTOR
      IF(TAZI.LT.0.)  TAZI=TAZI+360.DO
      NU(I)=TAMP
      NV(I)=TAZI
 2001 CONTINUE
      WRITE(2,2002) AMPI,AZII,(NU(I),NV(I),I=1,INC)
 2002 FORMAT(12F6.1/12F6.1/12F6.1/12F6.1/)
      STOP
      END
      SUBROUTINE DFN(CURNOW,TIME,NEQ,SLOPES)
      IMPLICIT REAL*8 (A-H,O-Z)
      DIMENSION CURNOW(NEQ),SLOPES(NEQ)
      COMMON /STAT/ FRCONS,WLONG,CORLAT,DEPTH,W,CORKA,PI,DELT,DELX,IPRIN
      ENTRY FCN(NEQ,TIME,CURNOW,SLOPES)
      U=CURNOW(1)
      V=CURNOW(2)
C
C     CALCULATE FRICTIONAL TERMS
C
      TEMP=FRCONS*DSQRT(U*U+V*V)
      FRICTU=-TEMP*U
```

```
      FRICTV=-TEMP*V
C
C     CALCULATE CORICLIS TERMS
C
      CORU=W*V
      CORV=-W*U
C
C     CALCULATE THE SURFACE GRADIENT TERMS
C        GET THE SURFACE GRADIENTS
C
      CALL GRADS(TIME,DZSDT,DZSDX)
      FGRADU=-GOVRA*DZSDT
      FGRADV=-GOVRA*DZSDX/DSIN(COLAT)
C
C     SUM THE TERMS TO GET THE TIME DERIVATIVE
C
      SLOPES(1)=FRICTU+CORU+FGRADU
      SLOPES(2)=FRICTV+CORV+FGRADV
      IF(IPRIN.EQ.1.OR.IPRIN.EQ.3)
     : WRITE(6,1) TEMP,FRICTU,FRICTV,CORU,CORV,FGRADU,FGRADV,SLOPES
    1 FORMAT(' DFN      ',10G12.5)
      RETURN
      END
      SUBROUTINE GRADS(TIME,DZSDT,DZSDX)
      IMPLICIT REAL*8 (A-H,O-Z)
      COMMON /STAT/ ERCONS,WEIGHG,COLAT,DEPTH,W,GOVRA,PI,DELT,DELX,IPRIN
      COMMON /TBLE/ TOLD(58),DTOLD(58),DXOLD(58),IEND
C
C     KEEP A TABLE OF UP TO 58 VALUES
C
      IF(IEND.EQ.0)  GO TO 10
      DO 2  I=1,IEND
```

```
      IF(TIME.NE.TOLD(I))  GO TO 2
      GO TO 11
    2 CONTINUE
   10 IEND=IEND+1
C
C     DELT IS THE THETA GRID SPACING IN RADIANS, DELX IS THE CHI
C     DIRECTION SPACING.
C
C     GET THE HEIGHT OF THE DRIVING FORCE NEARBY
C
      CALL HEIGHT(HNORTH,HSOUTH,HEAST,HWEST,TIME)
C
C     DIVIDE BY THE GRID SPACING TO ESTIMATE THE DERIVATIVE
C
      DZSDT=(HSOUTH-HNORTH)/(2.*DELT)
      DZSDX=(HEAST-HWEST)/(2.*DELX)
      TOLD(IEND)=TIME
      DTOLD(IEND)=DZSDT
      DXOLD(IEND)=DZSDX
      IF(IPRIN.EQ.1.OR.IPRIN.EQ.3)
     : WRITE(6,1) TIME,HNORTH,HSOUTH,HEAST,HWEST,DZSDT,DZSDX
    1 FORMAT(' GRADS     ',10G12.5)
      RETURN
   11 DZSDT=DTOLD(I)
      DZSDX=DXOLD(I)
      IF(IPRIN.EQ.1.OR.IPRIN.EQ.3)
     : WRITE(6,1) TIME,DZSDT,DZSDX
      RETURN
      END
      SUBROUTINE HEIGHT(HNOR,HSOU,HEAS,HWES,TIME)
C
C     CALCULATE THE HEIGHT OF THE TIDE - EQUILIBRIUM HEIGHT.
```

```
C
      IMPLICIT REAL*8 (A-H,O-Z)
      COMMON /STAT/ FRCONS,MLONG,COLAT,DEPTH,W,CONVRA,PI,DELT,DELX,IPRIN
      COMMON /CONS/ FN(7),HN(7),HS(7),HE(7),HW(7),SP(7),PO(7),PNK(7),PSK
     :(7),PEK(7),PWK(7),DN(7),DS(7),DE(7),DW(7)
C
C     THE TIDE IS ASSUMED TO BE THE SUM OF SEVEN CONSTITUENTS
C     P1,K1,O1,Q1,M2,N2,S2
C
      HNOR=0.D0
      HSOO=0.D0
      HEAS=0.D0
      HWES=0.D0
C
C     FN IS THE NODE FACTOR; HN IS THE AMPLITUDE
C     SP IS CONSTITUENT SPEED IN DEGREES PER HOUR
C     TIME IS IN SECONDS
C     PO IS THE GREENWICH EQUILIBRIUM ARGUMENT AT TIME ZERO
C     PNK IS THE CONSTITUENT PHASE LAG
C     DN IS THE EQUILIBRIUM TIDE AMPLITUDE
C
      DO 1  I=1,7
      TEMP=SP(I)*TIME+PO(I)
      HNOR=HNOR+FN(I)*(HN(I)*DCOS(TEMP-PNK(I))-DN(I)*DCOS(TEMP))
      HSOO=HSOO+FN(I)*(HS(I)*DCOS(TEMP-PSK(I))-DS(I)*DCOS(TEMP))
      HEAS=HEAS+FN(I)*(HE(I)*DCOS(TEMP-PEK(I))-DE(I)*DCOS(TEMP))
    1 HWES=HWES+FN(I)*(HW(I)*DCOS(TEMP-PWK(I))-DW(I)*DCOS(TEMP))
      RETURN
      END
      SUBROUTINE DATAIN
C
C     READ ALL INPUT AND INITIALIZE SOME ARRAYS
```

```
C
      IMPLICIT REAL*8 (A-H,O-Z)
      DIMENSION ID(7),SPDEG(7),DMAX(7)
      COMMON /STAT/ FRCONS,WLONG,COLAT,DEPTH,W,GOVRA,PI,DELT,DELX,IPRIN
      COMMON /CONS/ TN(7),HN(7),HS(7),HE(7),HW(7),SP(7),PO(7),PNK(7),PSK
     :(7),PEK(7),PWK(7),DN(7),DS(7),DE(7),DW(7)
      COMMON /INIT/ TIMEI,UI,VI,ERRTOL,TMAX,TSTEP,STPMIN,IORDER
      DATA ID/'P1','K1','O1','Q1','M2','N2','S2'/
      DATA SPDEG/14.95893140D0,15.04106860D0,13.94303560D0,
     :13.39866090D0,28.98410420D0,28.43972950D0,30.0D0/
      DATA DMAX/4.58,14.16,10.06,1.95,24.24,4.69,11.23/
C
C     LATITUDE DEPENDENCE OF THE EQUILIBRIUM TIDE
C
      DFACT(X)=DSIN(2.*DABS(X-PI/2.))
      SFACT(X)=(DCOS(DABS(X-PI/2.)))**2
      PI=3.141592654
      DTOR=2.*PI/360.
C
C     GET DATA FOR THE SOLUTION AT A SINGLE POINT
C
      READ(1,*) WLONG,COLAT,DEPTH,TIMEI,UI,VI,TSTEP,STPMIN,TMAX,ERRTOL,
     :FRCONS,DELT,DELX,IORDER,IPRIN
    1 FORMAT(8F10.0/5F10.0,2I5)
      WRITE(2,6) WLONG,COLAT,DEPTH,TIMEI,UI,VI,TSTEP,STPMIN,TMAX,ERRTOL,
     :FRCONS,DELT,DELX,IORDER,IPRIN
    6 FORMAT(' INPUT DATA'/
     :1X,2F8.3,F8.0,5F8.3/
     :1X,2F10.3,E10.2,2F10.2,2I10)
      WLONG=WLONG*DTOR
      COLAT=COLAT*DTOR
      DELT=DELT*DTOR
```

```
      DELX=DELX*DTOR
      DEPTH=DEPTH*100.
C
C     CONVERT TIMES TO SECONDS
C
      TIMEI=TIMEI*3600.
      TSTEP=TSTEP*3600.
      STPMIN=STPMIN*3600.
      TMAX=TMAX*3600.
C
C     GRAVITY DIVIDED BY EARTH RADIUS
C
      GOVRA=(980./6.374E8)
      ESPEED=2.*PI/(24.*3600.)
      W=2.*ESPEED*DCOS(COLAT)
C
C     GET  SPEEDS, EQUILIBRIUM AMPLITUDES, AND INITIALIZE NODE FACTORS
C
      DO 2 I=1,7
      SP(I)=SPDEG(I)*DTOR/3600.
      PU(I)=0.0
      HN(I)=0.
      HS(I)=0.
      HE(I)=0.
      HW(I)=0.
      PNK(I)=0.
      PSK(I)=0.
      PEK(I)=0.
      PWK(I)=0.
      FN(I)=0.0
C
C     FIRST FOUR CONSTITUENTS ARE DIURNAL
```

```
C
      IF(I.GE.5)  GO TO 3
      DN(I)=DMAX(I)*DFACT(COLAT-DELT)
      DS(I)=DMAX(I)*DFACT(COLAT+DELT)
      DE(I)=DMAX(I)*DFACT(COLAT)
      DW(I)=DE(I)
      GO TO 2
    3 DN(I)=DMAX(I)*SFACT(COLAT-DELT)
      DS(I)=DMAX(I)*SFACT(COLAT+DELT)
      DE(I)=DMAX(I)*SFACT(COLAT)
      DW(I)=DE(I)
    2 CONTINUE
C
C     READ CONSTITUENT LABEL, MEAN NODE FACTOR FOR THE SERIES,
C     GREENWICH EQUILIBRIUM ARGUMENT AT TIME=0, AND AMPLITUDE
C     AND GREENWICH PHASE OF THE CONSTITUENT AT POINTS NORTH,
C     SOUTH, EAST, AND WEST, RESPECTIVELY.
C
  998 READ(1,4,END=999) LBL,A1,A2,A3,A4,A5,A6,A7,A8,A9,A10
    4 FORMAT(A2,3X,10F5.0)
      WRITE(2,7) LBL,A1,A2,A3,A4,A5,A6,A7,A8,A9,A10
    7 FORMAT(1X,A2,3X,F7.3,9F7.1)
      I=0
      DO 5  J=1,7
    5 IF(LBL.EQ.ID(J)) I=J
      IF(I.EQ.0)  CALL EXIT
      FN(I)=A1
      PO(I)=A2*DTOR
      HN(I)=A3
      PNK(I)=A4*DTOR
      HS(I)=A5
      PSK(I)=A6*DTOR
```

```
      HE(I)=A7
      PEK(I)=A8*DTOR
      HW(I)=A9
      PWK(I)=A10*DTOR
      GO TO 998
  999 CONTINUE
      IF(IPRIN.NE.1.AND.IPRIN.NE.4)  RETURN
      WRITE(6,997) WLONG,COLAT,DEPTH,W,DELT,DELX,
     :             UI,VI,TIME1,TMAX,ISTEP,STPMIN,
     :             ERCONS,ERRTOL,IORDER,IPRIN
      DO 996 I=1,7
  996 WRITE(6,997) I,SP(I),PN(I),PO(I),DN(I),DS(I),DE(I),DW(I),
     :             HN(I),PNK(I),HS(I),PSK(I),HE(I),PEK(I),HW(I),PWK(I)
  997 FORMAT(' DATAIN    ',10G12.5/10X,6G12.5/)
      RETURN
      END
C     SUBROUTINE DREBS  (DFN,Y,T,N,JM,IND,JSTART,H,HMIN,EPS,R,S,WK,IER) DTRB0010
C                                                                       DTRB0020
C-DREBS---------S/D-----LIBRARY 1---------------------------------------DTRB0030
C                                                                       DTRB0040
C   FUNCTION              - FIRST ORDER DIFFERENTIAL EQUATION SOLVER -    DTRB0050
C                             THE METHOD OF BULIRSCH - STOER FOR        DTRB0060
C                             DY/DT = F(Y,T)                            DTRB0070
C   USAGE                 - CALL DREBS(DFN,Y,T,N,JM,IND,JSTART,H,HMIN,    DTRB0080
C                             EPS,R,S,WK,IER)                           DTRB0090
C   PARAMETERS   DFN      - USER SUPPLIED EXTERNAL SUBROUTINE,            DTRB0100
C                             DFN(Y,T,N,DY). DFN MUST CALCULATE DY(I) =   DTRB0110
C                             F(Y(1),Y(2),...,Y(N),T) FOR I=1,2,...,N.    DTRB0120
C                Y        - ON INPUT Y(1),Y(2),...,Y(N) ARE INITIAL VALUESDTRB0130
C                             ON OUTPUT Y(1),Y(2),...,Y(N) CONTAIN AN       DTRB0140
C                             APPROXIMATE SOLUTION TO Y AT T (AS SET ON   DTRB0150
C                             OUTPUT).                                  DTRB0160
```

```
C                T       - T IS THE INDEPENDENT VARIABLE.  ON INPUT, T    DTRB0170
C                  SHOULD CONTAIN THE INITIAL VALUE OF THE                DTRB0180
C                  INDEPENDENT VARIABLE. ON OUTPUT, T                     DTRB0190
C                  CONTAINS THE UPDATED VALUE OF THE INDEPEN-             DTRB0200
C                  DENT VARIABLE.                                         DTRB0210
C                N       - THE NUMBER OF EQUATIONS IN THE SYSTEM          DTRB0220
C                JM      - THE MAXIMUM ORDER OF THE RATIONAL APPROX-      DTRB0230
C                  IMATION. JM MUST BE LESS THAN 7.                       DTRB0240
C                IND     - CONVERGENCE TYPE INDICATOR (INPUT)             DTRB0250
C                  IND = 1 SPECIFIES THE STANDARD ERROR TEST              DTRB0260
C                  IND = 2 SPECIFIES THE RELATIVE ERROR TEST              DTRB0270
C                  IND = 3 SPECIFIES THE ABSOLUTE ERROR TEST              DTRB0280
C                JSTART  - AN INPUT INDICATOR WITH THE FOLLOWING MEANINGSDTRB0290
C                  0 - PERFORM A STEP. THE FIRST STEP                     DTRB0300
C                    MUST BE DONE WITH THIS VALUE OF JSTART SO            DTRB0310
C                    THAT THE SUBROUTINE CAN INITIALIZE ITSELF.           DTRB0320
C                  -1 - REPEAT THE LAST STEP WITH A NEW VALUE             DTRB0330
C                    OF H OR JM. THE INITIAL VALUES OF Y, S,              DTRB0340
C                    AND T ARE SET TO THE INITIAL VALUES OF Y,            DTRB0350
C                    S, AND T FROM THE MOST RECENT CALL TO                DTRB0360
C                    DREBS WITH JSTART = 0.                               DTRB0370
C                H       - ON INPUT, H IS AN INITIAL GUESS FOR THE STEP   DTRB0380
C                  SIZE.                                                  DTRB0390
C                  ON OUTPUT, H CONTAINS A SUGGESTED STEP SIZE            DTRB0400
C                  FOR THE NEXT STEP. THE SUGGESTED VALUE MAY             DTRB0410
C                  BE LARGER OR SMALLER THAN THE ORIGINAL                 DTRB0420
C                  STEP SIZE.                                             DTRB0430
C                HMIN    - HMIN IS THE SMALLEST PERMISSIBLE STEP SIZE.    DTRB0440
C                  DREBS WILL DECREASE THE STEP SIZE                      DTRB0450
C                  UNTIL CONVERGENCE CAN BE OBTAINED.                     DTRB0460
C                EPS     - ERROR TOLERANCE                                DTRB0470
C                F       - ON OUTPUT, THE N-VECTOR F CONTAINS THE         DTRB0480
```

```
C                                ABSOLUTE ERRORS IN EACH COMPONENT FOR        DTRB0490
C                                THE CURRENT STEP.                            DTRB0500
C                     S       - AN N-VECTOR CONTAINING EITHER (1) THE LARGEST DTRB0510
C                                VALUE OF EACH Y COMPUTED SINCE THE START OF DTRB0520
C                                THE INTEGRATION FOR THE STANDARD ERROR TEST,DTRB0530
C                                (2) THE LARGEST VALUE OF EACH Y COMPUTED     DTRB0540
C                                DURING THE CURRENT STEP BEING TAKEN FOR      DTRB0550
C                                RELATIVE ERROR TEST, OR (3) THE VALUE 1.0    DTRB0560
C                                FOR THE ABSOLUTE ERROR TEST.                 DTRB0570
C                                S MUST BE INITIALIZED IN ACCORDANCE WITH     DTRB0580
C                                THE ERROR TEST SELECTED BEFORE THE FIRST     DTRB0590
C                                CALL TO DREBS. IF IND = 1 OR 2, S(I) SHOULD  DTRB0600
C                                EQUAL Y(I) ON THE FIRST CALL. IF IND = 3,    DTRB0610
C                                S(I) SHOULD EQUAL I.                         DTRB0620
C                     WK      - WORKING STORAGE OF DIMENSION 29*N             DTRB0630
C                     IER     - ERROR INDICATOR                               DTRB0640
C                               TERMINAL ERROR = 128 + N                      DTRB0650
C                                 N = 1 INDICATES CONVERGENCE COULD NOT BE    DTRB0660
C                                   OBTAINED WITH CURRENT VALUES OF H AND     DTRB0670
C                                   HMIN. Y,T, AND H HAVE BEEN UPDATED.       DTRB0680
C                               WARNING ERROR (WITH FIX) = 64 + N             DTRB0690
C                                 N = 2 INDICATES JM IS LESS THAN 1 OR GREATERDTRB0700
C                                   THAN 6. SET JM = 6.                       DTRB0710
C   PRECISION             - SINGLE/DOUBLE                                     DTRB0720
C   REQD. IMSL ROUTINES   - UERTST                                            DTRB0730
C   LANGUAGE              - FORTRAN                                           DTRB0740
C-----------------------------------------------------------------------------DTRB0750
C   LATEST REVISION       - APRIL 5, 1977                                     DTRB0760
C                                                                             DTRB0770
      SUBROUTINE DREBS(DFN,Y,T,N,JM,IND,JSTART,H,HMIN,EPS,R,S,WK,IER)         DTRB0780
C                                                                             DTRB0790
      DIMENSION          Y(N),S(N),R(N),D(7),WK(1)                          DTRB0800
```

```
C*    DOUBLE PRECISION   Y,T,H,HMIN,EPS,R,S,RK,D,ZOTUP,A,G,                DTRB0810
C*   1                   B,XU,U,C,TA,B1,V,UST,TOLD,HALF                    DTRB0820
C1    DATA               ZOTUP/Z4040000000000000/,HALF/.500/               DTRB0830
      DATA               ZOTUP/Z40400000/,HALF/.5/                         DTRB0840
      LOGICAL            KONVF,KONV,SC,BH                                  DTRB0850
      IER=0                                                                DTRB0860
      N2=N+N                                                               DTRB0870
      N3=N2+N                                                              DTRB0880
      N4=N3+N                                                              DTRB0890
      N5=N4+N                                                              DTRB0900
      N6=N5+N5+N2                                                          DTRB0910
      N7=N6+N5+N3                                                          DTRB0920
      N8=N7+N5+N3                                                          DTRB0930
      N2P1=N2+1                                                            DTRB0940
      N3P1=N3+1                                                            DTRB0950
      N8P1=N8+1                                                            DTRB0960
      IF(JM.GT.0.AND.JM.LE.6) GO TO 5                                      DTRB0970
      IER = 66                                                             DTRB0980
      JM=6                                                                 DTRB0990
C                                  FOR AN EXTRAPOLATION OF ORDER JM,       DTRB1000
C                                  JM+1 APPROXIMATIONS ARE REQUIRED.       DTRB1010
C                                  THREE MORE ARE ALLOWED IN ATTEMPTING    DTRB1020
C                                  TO ACHIEVE CONVERGENCE.                 DTRB1030
    5 JMAX = JM+4                                                          DTRB1040
      IF(JSTART.NE.0) GO TO 135                                            DTRB1050
C                                  INITIALIZATION                          DTRB1060
C                                  SAVE THE INITIAL VALUES FOR THE DEP-    DTRB1070
C                                  ENDENT VARIABLES AND THE ERROR TEST     DTRB1080
C                                  VECTOR FOR THE STEP                     DTRB1090
      TOLD = T                                                             DTRB1100
      IJK4=N4                                                              DTRB1110
      DO 10 I = 1,N                                                        DTRB1120
```

```
          WK(I) = Y(I)                                                    DTRB1130
          IJK4=IJK4+1                                                     DTRB1140
          WK(IJK4) = S(I)                                                 DTRB1150
       10 CONTINUE                                                        DTRB1160
C                                     USE THE FUNCTION ROUTINE TO OBTAIN  DTRB1170
C                                     THE INITIAL SLOPES                  DTRB1180
C                                     DZ = DY/DX                          DTRB1190
          CALL DFN(Y,T,N,WK(N3P1))                                        DTRB1200
C                                     THE LOGICAL VARIABLE,BH, DETERMINES DTRB1210
C                                     WHETHER THE STEPSIZE HAS BEEN       DTRB1220
C                                     HALVED. INITIALLY FALSE.            DTRB1230
C                                     LATER BH IS FALSE IF THE STEPSIZE IS DTRB1240
C                                     CUT BY A FACTOR NOT 2               DTRB1250
       15 BH = .FALSE.                                                    DTRB1260
C                                     PRESET THE CONVERGENCE SUCCESS FLAG DTRB1270
C                                        TRUE                             DTRB1280
          KONVF = .TRUE.                                                  DTRB1290
C                                     ADVANCE THE INDEPENDENT VARIABLE BY DTRB1300
C                                     THE STEPSIZE, H                     DTRB1310
       20 A = H+T                                                         DTRB1320
C                                     SET THE SWITCH BD FOR THE FIRST SET DTRB1330
C                                     OF COEFFICIENTS, D                  DTRB1340
          BD = .FALSE.                                                    DTRB1350
C                                     INITIALIZE THE H SEQUENCE...        DTRB1360
C                                        H/M,H/JR,H/JS                    DTRB1370
          M = 1                                                           DTRB1380
          JR = 2                                                          DTRB1390
          JS = 3                                                          DTRB1400
C                                     JJ IS THE INDEX FOR THE ARRAY OF    DTRB1410
C                                     VALUES SAVED IN CASE THE INTERVAL   DTRB1420
C                                     MUST BE HALVED                      DTRB1430
          JJ = 0                                                          DTRB1440
```

```
C                                       INTEGRATION STEP                        DTRB1450
C                                       MIDPOINT + EXTRAPOLATION                DTRB1460
      IJ6=N6-N                                                                  DTRB1470
      IJ7=N7-N                                                                  DTRB1480
      I6=IJ6                                                                    DTRB1490
      I7=IJ7                                                                    DTRB1500
      DO 125 J = 1,JMAX                                                         DTRB1510
C                                       SET THE VALUES OF THE EXTRAPOLATION     DTRB1520
C                                       COEFFICIENTS TO THEIR CORRECT VALUES    DTRB1530
C                                       FOR THIS EXTRAPOLATION STEP             DTRB1540
        IJ6=IJ6+N                                                               DTRB1550
        IJ7=IJ7+N                                                               DTRB1560
        IF (.NOT. GO) GO TO 25                                                  DTRB1570
C*      D(2)=1.7777777777778D0                                                  DTRB1580
C*      D(4)=7.1111111111111D0                                                  DTRB1590
C3      D(6)=28.444444444444D0                                                  DTRB1600
        D(2)=1.77778                                                            DTRB1610
        D(4)=7.11111                                                            DTRB1620
        D(6)=28.44444                                                           DTRB1630
        GO TO 30                                                                DTRB1640
C* 25    D(2)=2.25D0                                                             DTRB1650
C*      D(4)=9.D0                                                               DTRB1660
C3      D(6)=36.D0                                                              DTRB1670
   25   D(2)=2.25                                                               DTRB1680
        D(4) = 9.                                                               DTRB1690
        D(6) = 36.                                                              DTRB1700
C                                       IF THE ORDER OF THE EXTRAPOLATION       DTRB1710
C                                       STEP BEING COMPUTED IS LESS THAN JM/2   DTRB1720
C                                       SET KONV FALSE                          DTRB1730
   30   KONV = .TRUE.                                                           DTRB1740
        IF (J .LE. (JM/2)) KONV = .FALSE.                                       DTRB1750
        IF (J .LE. (JM+1)) GO TO 35                                             DTRB1760
```

```
C                                       RESTRICT THE ORDER OF THE EXTRAPOL-  DTRB1770
C                                       ATION TO JM                          DTRB1780
C                                       ADJUST THE EXTRAPOLATION COEFFICIENT DTRB1790
      L = JM+1                                                               DTRB1800
C1    D(L) = 4.D0*D(L-2)                                                     DTRB1810
      D(L) = 4.*D(L-2)                                                       DTRB1820
C                                       DISCOURAGE THE STEP-INCREASING FACTORDTRB1830
C                                       FC, BY A FACTOR OF SQRT(2) SINCE     DTRB1840
C                                       CONVERGENCE WAS NOT OBTAINED         DTRB1850
C                                       IN JM EXTRAPOLATIONS                 DTRB1860
      FC = .7071068*FC                                                       DTRB1870
      GO TO 40                                                               DTRB1880
C                                       THE NUMBER, J, OF EXTRAPOLATIONS HAS DTRB1890
C                                       NOT EXCEEDED JM                      DTRB1900
C                                       FIND D(J) = ((H DIVIDED BY H/M)**2   DTRB1910
C                                       ADJUST THE FACTOR,FC, USED TO ADJUST DTRB1920
C                                       THE STEPSIZE FOR THE NEXT STEP TO BE DTRB1930
C                                       TAKEN                                DTRB1940
   35 L = J                                                                  DTRB1950
C1    D(L) = DFLOAT(M*M)                                                     DTRB1960
      D(L) = FLOAT(M*M)                                                      DTRB1970
      FC = 1.0+FLOAT(JM+1-J)*.1666667                                        DTRB1980
C                                       MODIFIED MIDPOINT RULE USED TO FIND  DTRB1990
C                                       FIRST VALUE FOR THIS EXTRAPOLATION   DTRB2000
C                                       STEP                                 DTRB2010
   40 M = M+M                                                                DTRB2020
      G = H/FLOAT(M)                                                         DTRB2030
      Y = G+G                                                                DTRB2040
C                                       IF THE STEPSIZE HAS NOT BEEN HALVED  DTRB2050
C                                       OR IF THE ORDER OF THE EXTRAPOLATION DTRB2060
C                                       STEP EXCEEDS THAT FOR WHICH PREVIOUS-DTRB2070
C                                       LY COMPUTED VALUES WERE SAVED, THEY  DTRB2080
```

```
C                                       MUST BE COMPUTED                        DTRB2090
      IF ((.NOT. BIG) .OR. (J .GE. (JMAX-1))) GO TO 50                          DTRB2100
C                                       OTHERWISE THE VALUES HAVE BEEN SAVED    DTRB2110
C                                       AND CAN BE RESTORED                     DTRB2120
      IJK1=N                                                                    DTRB2130
      IJK2=N2                                                                   DTRB2140
      IJK6=IJ6                                                                  DTRB2150
      IJK7=IJ7                                                                  DTRB2160
      DO 45 I = 1,N                                                             DTRB2170
         IJK2=IJK2+1                                                            DTRB2180
         IJK7=IJK7+1                                                            DTRB2190
         WK(IJK2) = WK(IJK7)                                                    DTRB2200
         IJK1=IJK1+1                                                            DTRB2210
         IJK6=IJK6+1                                                            DTRB2220
         WK(IJK1) = WK(IJK6)                                                    DTRB2230
   45 CONTINUE                                                                  DTRB2240
      GO TO 75                                                                  DTRB2250
C                                       COMPUTE STARTING VALUES FOR THE MODI-   DTRB2260
C                                       FIED MIDPOINT RULE                      DTRB2270
   50 IJK1=N                                                                    DTRB2280
      IJK2=N2                                                                   DTRB2290
      IJK3=N3                                                                   DTRB2300
      DO 55 I = 1,N                                                             DTRB2310
         IJK1=IJK1+1                                                            DTRB2320
         WK(IJK1) = WK(I)                                                       DTRB2330
         IJK2=IJK2+1                                                            DTRB2340
         IJK3=IJK3+1                                                            DTRB2350
         WK(IJK2) = WK(I)+G*WK(IJK3)                                            DTRB2360
   55 CONTINUE                                                                  DTRB2370
      KH = M/2                                                                  DTRB2380
      XU=T                                                                      DTRB2390
C                                       THE MEMBER OF THE H SEQUENCE            DTRB2400
```

```
C                                       BEING USED BY THE MIDPOINT INTEGRA-  DTRB2410
C                                       TION RULE IS H/M. COMPUTE THE END    DTRB2420
C                                       OF THE STEP  FOR EACH DEPENDENT VARI-DTRB2430
C                                       ABLE                                 DTRB2440
      DO 70 K = 2,M                                                          DTRB2450
         XU = XU + G                                                         DTRB2460
         CALL DFN(WK(N2P1),XU,N,WK(N8P1))                                    DTRB2470
         IJK1=N                                                              DTRB2480
         IJK2=N2                                                             DTRB2490
         IJK8=N8                                                             DTRB2500
         DO  60 I = 1,N                                                      DTRB2510
            IJK1=IJK1+1                                                      DTRB2520
            IJK8=IJK8+1                                                      DTRB2530
            U = WK(IJK1) + B*WK(IJK8)                                        DTRB2540
            IJK2=IJK2+1                                                      DTRB2550
            WK(IJK1) = WK(IJK2)                                              DTRB2560
            WK(IJK2) = U                                                     DTRB2570
   60       CONTINUE                                                         DTRB2580
C                                       IN CASE THE INTERVAL MUST BE HALVED  DTRB2590
C                                       NEXT TIME, SAVE THE VALUES AT HALFWAYDTRB2600
C                                       ALONG (KH=M/2) THE STEP UNLESS K=3   DTRB2610
         IF ((K .NE. KH) .OR. (K .EQ. 3)) GO TO 70                           DTRB2620
         JJ = 1+JJ                                                           DTRB2630
         I6=I6+N                                                             DTRB2640
         I7=I7+N                                                             DTRB2650
         IJK1=N                                                              DTRB2660
         IJK2=N2                                                             DTRB2670
         IJK6=I6                                                             DTRB2680
         IJK7=I7                                                             DTRB2690
         DO 65 I = 1,N                                                       DTRB2700
            IJK2=IJK2+1                                                      DTRB2710
            IJK7=IJK7+1                                                      DTRB2720
```

```
                WK(IJK7) = WK(IJK2)                                          DTRB2730
                IJK6=IJK6+1                                                  DTRB2740
                IJK1=IJK1+1                                                  DTRB2750
                WK(IJK6) = WK(IJK1)                                          DTRB2760
   65         CONTINUE                                                       DTRB2770
   70       CONTINUE                                                       DTRB2780
   75       CALL DFN(WK(N2P1),A,N,WK(N8P1))                                DTRB2790
            IJK1=N                                                         DTRB2800
            IJK2=N2                                                        DTRB2810
            IJK5=N5                                                        DTRB2820
            IK5=N5                                                         DTRB2830
            IJK8=N8                                                        DTRB2840
            DO 115 I = 1,N                                                 DTRB2850
C                                   V IS USED TO SAVE THE VALUE OBTAINED   DTRB2860
C                                   BY THE MIDPOINT RULE USING THE PREVI-DTRB2870
C                                   OUS MEMBER OF THE H SEQUENCE           DTRB2880
C                                   (THE FIRST TIME THROUGH THIS VALUE ISDTRB2890
C                                   MEANINGLESS, BUT IT IS NOT USED SINCEDTRB2900
C                                   L IS LESS THAN 2)                      DTRB2910
               IJK1=IJK1+1                                                 DTRB2920
               IJK2=IJK2+1                                                 DTRB2930
               IJK5=IJK5+1                                                 DTRB2940
               IK5=IK5+1                                                   DTRB2950
               IF (L .GE. 2) V = WK(IJK5)                                  DTRB2960
C                                   COMPUTE THE FINAL VALUE OBTAINED FOR   DTRB2970
C                                   THIS MEMBER OF THE H SEQUENCE BY THE   DTRB2980
C                                   MODIFIED MIDPOINT RULE                 DTRB2990
               IJK8=IJK8+1                                                 DTRB3000
               WK(IJK5) = (WK(IJK2) + WK(IJK1) + C * WK(IJK8))*HALF        DTRB3010
               C = WK(IJK5)                                                DTRB3020
               TA = C                                                      DTRB3030
C                                   AT LEAST TWO VALUES ARE NEEDED TO      DTRB3040
```

```
C                                       START EXTRAPOLATION                     DTRB3050
            IF (L .LT. 2) GO TO 90                                              DTRB3060
C                                       IF THE VALUE JUST COMPUTED BY THE       DTRB3070
C                                       MIDPOINT RULE SHOWS A LARGE JUMP FROMDTRB3080
C                                       THE PREVIOUS, HALVE THE INTERVAL        DTRB3090
C1          IF((DABS(V)*ZOTUP .LT. DABS(C)) .AND. (H .NE. HMIN) .AND.           DTRB3100
            IF ((ABS(V)*ZOTUP .LT. ABS(C)) .AND. (H .NE. HMIN) .AND.            DTRB3110
     1           (J.GT.JM/2+1)) GO TO 130                                       DTRB3120
C                                       PERFORM THE L STEPS FOR THE CURRENT     DTRB3130
C                                       LTH GROUP EXTRAPOLATION STEP. IF THE    DTRB3140
C                                       DENOMINATOR OF THE RATIONAL FUNCTION    DTRB3150
C                                       GOES TO ZERO AT ANY STEP, SET DT AT     DTRB3160
C                                       THAT STEP TO ITS VALUE JUST BEFORE      DTRB3170
            IP5=IK5                                                             DTRB3180
            DO 85 K = 2,L                                                       DTRB3190
               IP5=IP5+N                                                        DTRB3200
               B1 = D(K) * V                                                    DTRB3210
               B = B1-C                                                         DTRB3220
               U = V                                                            DTRB3230
               IF (B .EQ. 0.) GO TO 80                                          DTRB3240
               B = (C-V)/B                                                      DTRB3250
               U = C*B                                                          DTRB3260
               C = B1*B                                                         DTRB3270
   80          IF(K.LT.L) V=WK(IP5)                                             DTRB3280
               WK(IP5) = U                                                      DTRB3290
               TA = U + TA                                                      DTRB3300
   85       CONTINUE                                                           DTRB3310
C                                       USE THE ERROR ROUTINE FOR EACH          DTRB3320
C                                       DEPENDENT VARIABLE TO CHECK WHETHER     DTRB3330
C                                       CONVERGENCE HAS BEEN ACHIEVED           DTRB3340
   90       GO TO (95,100,105),IND                                             DTRB3350
C1 95       UST=DABS(TA)                                                       DTRB3360
```

```
   95       UST=ABS(TA)                                                    DTRB3370
            IF(UST.GT.S(I)) S(I)=UST                                       DTRB3380
            GO TO 110                                                      DTRB3390
C1100       S(I)=DABS(Y(I))                                                DTRB3400
  100       S(I)=ABS(Y(I))                                                 DTRB3410
            GO TO 110                                                      DTRB3420
  105       S(I)=1.                                                        DTRB3430
C1110       R(I)=DABS(Y(I)-TA)                                             DTRB3440
  110       R(I)=ABS(Y(I)-TA)                                              DTRB3450
            Y(I)=TA                                                        DTRB3460
            IF(S(I).LT.EPS) S(I)=EPS                                       DTRB3470
            IF(R(I).GT.EPS*S(I)) KONV=.FALSE.                              DTRB3480
  115   CONTINUE                                                           DTRB3490
        IF(KONV) GO TO 155                                                 DTRB3500
C                                   RESET THE EXTRAPOLATION COEFFICIENTS   DTRB3510
        D(3) = 4.                                                          DTRB3520
        D(5) = 16.                                                         DTRB3530
C                                   FLIP THE BD SWITCH FOR THE NEXT SET    DTRB3540
C                                   OF COEFFICIENTS                        DTRB3550
        BD = (.NOT.BD)                                                     DTRB3560
C                                   RESET S                                DTRB3570
        IJK4=N4                                                            DTRB3580
        DO 120 I=1,N                                                       DTRB3590
           IJK4=IJK4+1                                                     DTRB3600
           S(I)=WK(IJK4)                                                   DTRB3610
  120   CONTINUE                                                           DTRB3620
C                                   TAKE THE NEXT MEMBER                   DTRB3630
C                                   OF THE H SEQUENCE                      DTRB3640
        M = JR                                                             DTRB3650
        JR = JS                                                            DTRB3660
        JS = M+4                                                           DTRB3670
C                                   AND GO BACK FOR THE                    DTRB3680
```

```
C                                       NEXT EXTRAPOLATION                      DTRB3690
  125 CONTINUE                                                                  DTRB3700
C                                       IF, AFTER ALL THE EXTRAPOLATIONS        DTRB3710
C                                       ALLOWED, CONVERGENCE HAS NOT BEEN       DTRB3720
C                                       ACHIEVED, ATTEMPT TO HALVE H SO THAT    DTRB3730
C                                       THE SAVED VALUES CAN BE USED (SET BH    DTRB3740
C                                       TRUE FOR THIS PURPOSE)                  DTRB3750
C                                       IF HALVING H MAKES IT LESS THAN HMIN,   DTRB3760
C                                       SET H = HMIN                            DTRB3770
C                                       IN THIS CASE THE SAVED VALUES CANNOT    DTRB3780
C                                       BE USED                                 DTRB3790
C                                       IF H HAD ALREADY BEEN AT HMIN,          DTRB3800
C                                       CONVERGENCE CANNOT BE ACHIEVED FOR      DTRB3810
C                                       THIS HMIN AND THIS EPS CRITERION.       DTRB3820
C                                       SET KONV FALSE                          DTRB3830
      BH = (.NOT. BH)                                                           DTRB3840
C1130 IF (DABS(H) .LE. DABS(HMIN)) GO TO 150                                    DTRB3850
  130 IF (ABS(H) .LE. ABS(HMIN)) GO TO 150                                      DTRB3860
      H = H * HALF                                                              DTRB3870
C1    IF (DABS(H) .GE. DABS(HMIN)) GO TO 20                                     DTRB3880
      IF (ABS(H) .GE. ABS(HMIN)) GO TO 20                                       DTRB3890
C1    H = DSIGN(HMIN,H)                                                         DTRB3900
      H = SIGN(HMIN,H)                                                          DTRB3910
      GO TO 15                                                                  DTRB3920
  135 DO 140 I = 1,N                                                            DTRB3930
          Y(I) = AK(I)                                                          DTRB3940
  140 CONTINUE                                                                  DTRB3950
      IJK4=N4                                                                   DTRB3960
      DO  145 I=1,N                                                             DTRB3970
          IJK4=IJK4+1                                                           DTRB3980
          S(I)=WK(IJK4)                                                         DTRB3990
  145 CONTINUE                                                                  DTRB4000
```

```
      T = TOLD                                                          DTRB4010
      GO TO 15                                                          DTRB4020
  150 KONVF = .FALSE.                                                   DTRB4030
C                                   WHETHER OR NOT CONVERGENCE HAS BEEN DTRB4040
C                                   ACHIEVED SET A NEW SUGGESTED STEPSIZEDTRB4050
C                                   FOR THE NEXT STEP                   DTRB4060
C                                   ASSIGN THE END OF STEP VALUE TO THE DTRB4070
C                                   INDEPENDENT VARIABLE                DTRB4080
  155 H = FC*H                                                          DTRB4090
      T=A                                                               DTRB4100
      IF(KONVF) GO TO 160                                               DTRB4110
      IER=129                                                           DTRB4120
  160 IF(IER.EQ.0) GO TO 9005                                           DTRB4130
 9000 CONTINUE                                                          DTRB4140
      CALL UERTST (IER,6HDREBS )                                        DTRB4150
 9005 RETURN                                                            DTRB4160
      END                                                               DTRB4170
C     SUBROUTINE UERTST (IER,NAME)                                      UERT0010
C                                                                       UERT0020
C-UERTST----------------LIBRARY 1-------------------------------------UERT0030
C                                                                       UERT0040
C   FUNCTION              - ERROR MESSAGE GENERATION                    UERT0050
C   USAGE                 - CALL UERTST(IER,NAME)                       UERT0060
C   PARAMETERS   IER      - ERROR PARAMETER. TYPE + N  WHERE            UERT0070
C                             TYPE= 128 IMPLIES TERMINAL ERROR          UERT0080
C                                   64 IMPLIES WARNING WITH FIX         UERT0090
C                                   32 IMPLIES WARNING                  UERT0100
C                             N    = ERROR CODE RELEVANT TO CALLING ROUTINEUERT0110
C                NAME     - INPUT VECTOR CONTAINING THE NAME OF THE    UERT0120
C                             CALLING ROUTINE AS A SIX CHARACTER LITERAL UERT0130
C                             STRING.                                   UERT0140
C   LANGUAGE              - FORTRAN                                     UERT0150
```

```
C-------------------------------------------------------------------------UERT0160
C   LATEST REVISION      - JANUARY 18, 1974                                 UERT0170
C                                                                           UERT0180
      SUBROUTINE UERTST(IER,NAME)                                           UERT0190
C                                                                           UERT0200
      DIMENSION           ITYP(5,4),IBIT(4)                                 UERT0210
      INTEGER*2           NAME(3)                                           UERT0220
      INTEGER             WARN,WARF,TERM,PRINTR                             UERT0230
      EQUIVALENCE         (IBIT(1),WARN),(IBIT(2),WARF),(IBIT(3),TERM)      UERT0240
      DATA      ITYP      /'WARN','ING ',',    ',',    ',',    ',          UERT0250
     *                     'WARN','ING(',',WITH',' FIX',')   ',          UERT0260
     *                     'TERM','INAL',',    ',',    ',',    ',          UERT0270
     *                     'NON-','DEFI','NED ',',    ',',    '/,         UERT0280
     *          IBIT      / 32,64,128,0/                                    UERT0290
      DATA      PRINTR    / 6/                                              UERT0300
      IER2=IER                                                              UERT0310
      IF (IER2 .GE. WARN) GO TO 5                                           UERT0320
C                                       NON-DEFINED                         UERT0330
      IER1=4                                                                UERT0340
      GO TO 20                                                              UERT0350
    5 IF (IER2 .LT. TERM) GO TO 10                                          UERT0360
C                                       TERMINAL                            UERT0370
      IER1=3                                                                UERT0380
      GO TO 20                                                              UERT0390
   10 IF (IER2 .LT. WARF) GO TO 15                                          UERT0400
C                                       WARNING(WITH FIX)                   UERT0410
      IER1=2                                                                UERT0420
      GO TO 20                                                              UERT0430
C                                       WARNING                             UERT0440
   15 IER1=1                                                                UERT0450
C                                       EXTRACT 'N'                         UERT0460
   20 IER2=IER2-IBIT(IER1)                                                  UERT0470
```

```
C                                       PRINT ERROR MESSAGE                    UERT0480
      WRITE (PRINTR,25) (ITYP(I,IER1),I=1,5),NAME,IER2,IER                     UERT0490
   25 FORMAT(' *** I M S L(UERTST) ***  ',5A4,4X,3A2,4X,I2,                    UERT0500
     *    ' (IER = ',I3,')')                                                  UERT0510
      RETURN                                                                   UERT0520
      END                                                                      UERT0530
```

APPENDIX II

Two FORTRAN computer programs developed by the author to calculate the harmonic constants fo the tidal current directly from the harmonic constants of the tidal elevation (equation 12), and to generate a time series from the harmonic constants (equation 5), are presented in this appendix. If it is assumed that each harmonic constituent of the tide can be treated separately, these programs can be used to provide the same results as the program of Appendix I, but at significant savings in computation time.

```
C
C       PROGRAM TO INFER TIDAL CURRENTS FROM GIVEN SURFACE
C       ELEVATIONS.  CGS UNITS ARE USED UNLESS OTHERWISE
C       NOTED.  ALL INPUT IS THROUGH SUBROUTINE DATAIN.
C
        IMPLICIT REAL*8 (A-H,O-Z)
        REAL*8 IFIRST,JFIRST,KFIRST,IFST,JFST,KFST
        DIMENSION A(16),R(4)
        COMMON /BLOCK1/U1(200),U2(200),V1(200),V2(200)
        COMMON /BLOCK2/ZS1(200),ZS2(200)
        COMMON /BLOCK3/COLAT(200),ELONG(200),DEPTH(200),SIGMA
        COMMON /BLOCK4/Z1(200),Z2(200),ZB1(200),ZB2(200)
        COMMON /BLOCK5/FRCONS,CSYS,MPTS,MAXITR,IORDER
        COMMON /BLOCK6/NUMPNT(20,20),MLONG,MCOLAT
        COMMON /BLCK12/TIDE,AMPMAX
        IER=0
        PI=3.141592654
        ESPEED=2.*PI/(24.*3600.)
        ACCEL=980.
        ERAD=6.374E8
        DTOR=2.*PI/360.
C
C       READ ALL INPUT AND IDENTIFY TIDAL CONSTITUENT
C
        CALL DATAIN(IER)
        CALL PHASE(IER)
        IF(IER.EQ.-1)  STOP
C
C       SUBTRACT EQUILIBRIUM ELEVATIONS FROM GIVEN SURFACE
C
        CALL ZBAR
        DO 1  I=1,MPTS
```

```
      ZS1(I)=Z1(I)-ZB1(I)
    1 ZS2(I)=Z2(I)-ZB2(I)
C
C     SOLUTION IS PERFORMED 'MAXITR' TIMES TO ALLOW
C     SUCCESSIVE CORRECTION FOR THE EFFECT OF FRICTION.
C     INITALIZE CURRENTS.  MAGNITUDE OF THE GUESS DETER-
C     MINES THE MAGNITUDE OF THE FRICTIONAL TERM ON THE
C     FIRST ITERATION.
C
      DO 2  I=1,MPTS
      U1(I)=1.
      U2(I)=0.
      V1(I)=1.
    2 V2(I)=0.
C
C     LOOP OVER THE CURRENT CALCULATIONS 'MAXITR' TIMES
C
      DO 3  INDX=1,MAXITR
C
C     LOOP OVER ALL POINTS OF THE GRID
C
      DO 4  I=1,MPTS
C
C     SET UP COEFFICIENTS MATRIX
C
C      FB=FRCONS*DSQRT(U1(I)**2+U2(I)**2+V1(I)**2+V2(I)**2)/DEPTH(I)
      FB=FRCONS
      GB=FB
      W=2.*ESPEED*DCOS(COLAT(I))
      A(1)  =SIGMA
      A(5)  =-GB
      A(9)  =0.
```

```
      A(13) =W
      A(2)=A(5)
      A(6)=-SIGMA
      A(10)=W
      A(14)=0.
      A(3)=0.
      A(7)=-W
      A(11)=SIGMA
      A(15)=-F3
      A(4)=-W
      A(8)=0.
      A(12)=A(15)
      A(16)=-SIGMA
C
C     SET UP RIGHT-HAND-SIDE VECTOR
C     APPROXIMATE DERIVATIVES
C
      CALL PARTAL(I,DZ1DT,DZ2DT,DZ1DX,DZ2DX,IER)
      IF(IER.EQ.-1)  STOP
      R(1)  =DZ2DT*ACCEL/ERAD
      R(2)  =DZ1DT*ACCEL/ERAD
      R(3)  =DZ2DX*ACCEL/(ERAD*DSIN(COLAT(I)))
      R(4)  =DZ1DX*ACCEL/(ERAD*DSIN(COLAT(I)))
C
C     SOLVE FOR THE CURRENTS
C
      CALL SOLVER(4,A,R,GDET)
      IF(GDET.EQ.0.D0)  STOP
      U1(I)=R(1)
      U2(I)=R(2)
      V1(I)=R(3)
      V2(I)=R(4)
```

```
    4 CONTINUE
    3 CONTINUE
C
C     PRINT THE RESULTS OF THE CURRENT CALCULATIONS
C      IN POLAR COORDINATES
C
      DO 9  I=1,MPTS
      AMPU=DSQRT(U1(I)**2+U2(I)**2)
      PHSU=DATAN2(U2(I),U1(I))/DTOR
      IF(PHSU.LT.0.)  PHSU=PHSU+360.
      AMPV=DSQRT(V1(I)**2+V2(I)**2)
      PHSV=DATAN2(V2(I),V1(I))/DTOR
      IF(PHSV.LT.0.)  PHSV=PHSV+360.
      WRITE(2,5) I,AMPU,PHSU,AMPV,PHSV
    5 FORMAT(I5,F10.2,F10.3,F10.2,F10.0)
    9 CONTINUE
      STOP
      END
      SUBROUTINE  AROUND(INDEX,LNORTH,LSOUTH,LEAST,LWEST,IER)
C
C     FIND THE NUMBERS OF THE POINTS AROUND POINT NUMBER
C     'INDEX' THAT WILL BE INVOLVED IN THE APPROXIMATION
C     OF THE DERIVATIVES.  AT ANY POINT OF THE GRID THERE
C     MUST BE AT LEAST THREE CONSECUTIVE POINTS ALONG A LINE
C     THROUGH THAT POINT, INCLUDING THAT POINT.  LNORTH AND
C     LSOUTH ARE THE CLOSEST POINTS ALONG A LONGITUDE LINE.
C
      COMMON /BLOCK6/NUMPNT(20,20),MLONG,MCOLAT
      DO 1  J=1,MLONG
      DO 1  I=1,MCOLAT
      IF(NUMPNT(I,J).NE.INDEX)  GO TO 1
      LN=I-1
```

```
      IF(LN.LT.1)  LN=I+2
      LS=I+1
      IF(LS.GT.NCOLAT)  LS=I-2
      LE=J+1
      IF(LE.GT.MLONG)  LE=J-2
      LW=J-1
      IF(LW.LT.1)  LW=J+2
      LNORTH=NUMPNT(LN,J)
      IF(LNORTH.GT.0)  GO TO 2
      LN=I+2
      LNORTH=NUMPNT(LN,J)
    2 LSOUTH=NUMPNT(LS,J)
      IF(LSOUTH.GT.0)  GO TO 3
      LS=I-2
      LSOUTH=NUMPNT(LS,J)
    3 LEAST=NUMPNT(I,LE)
      IF(LEAST.GT.0)  GO TO 4
      LE=J-2
      LEAST=NUMPNT(I,LE)
    4 LWEST=NUMPNT(I,LW)
      IF(LWEST.GT.0)  GO TO 5
      LW=J+2
      LWEST=NUMPNT(I,LW)
    5 CONTINUE
      RETURN
    1 CONTINUE
      IER=-1
      RETURN
      END
      SUBROUTINE DATAIN(IER)
      IMPLICIT REAL*8 (A-H,O-Z)
      DIMENSION CMT(30),FMT(18),NCHECK(200)
```

```
      COMMON /BLOCK1/U1(200),U2(200),V1(200),V2(200)
      COMMON /BLOCK3/COLAT(200),ELONG(200),H(200),SIGMA
      COMMON /BLOCK4/Z1(200),Z2(200),ZB1(200),ZB2(200)
      COMMON /BLOCK5/FRCONS,CSYS,MPTS,MAXITR,IORDER
      COMMON /BLOCK6/NUMPNT(20,20),MLONG,MCOLAT
      COMMON /BLOCK7/X(200),Y(200)
      COMMON/BLCK12/TIDE,AMPMAX
      DATA SPHE/'SPHE'/
      PI=3.141592654
      DTOR=2.*PI/360.
      ERAD=6.374E8
      ATOL=2.*PI*ERAD/360.
      WRITE(6,46)
   46 FORMAT(' CONTROL INPUT IS ON UNIT 1, GRID INPUT IS'/
     :' ON UNIT 1, RESULTS ARE OUTPUT ON UNIT 2')
C
C     TWO TITLE CARDS ARE REQUIRED
C
      WRITE(6,32)
   32 FORMAT(' INPUT TWO LINES AS COMMENT')
      READ(1,30) CMT
   30 FORMAT(15A4)
      WRITE(2,31) CMT
   31 FORMAT(1X,15A4)
C
C     'TIDE' IS THE TIDAL CONSTITUENT.  SEE SUBROUTINE PHASE.
C     'MAXITR' IS THE NUMBER OF PASSES MADE TO CORRECT
C     FOR FRICTION.
C
   39 WRITE(6,47)
   47 FORMAT(' ENTER TIDE CONSTITUENT')
      READ(1,30) TIDE
```

```
      WRITE(2,31) TIDE
      WRITE(6,48)
   48 FORMAT(' ENTER NO. OF PASSES TO CORRECT FOR FRICTION, 2 DIGITS')
      READ(1,5) MAXITR
    5 FORMAT(I2)
      WRITE(2,1) MAXITR
      WRITE(6,481)
  481 FORMAT(' ENTER COEFFICIENT OF FRICTION TERM')
      READ(1,*) FRCONS
      WRITE(2,482) FRCONS
  482 FORMAT(E20.5)
C
C     EITHER A POLAR STEREOGRAPHIC, OR SPHERICAL COORDINATE SYSTEM
C     CAN BE USED.
C
      WRITE(6,49)
   49 FORMAT(' SPHERICAL COORDINATES OR NAVAGATION GRID?')
      READ(1,30) CSYS
      WRITE(2,31) CSYS
      IF(CSYS.EQ.SPHE) GOTO 50
      WRITE(6,51)
   51 FORMAT(' ON THE NAVIGATION GRID, ONE DEGREE IS EQUIVALENT TO 111.3
     :17 KM'/' GRID DIRECTIONS NORTH AND EAST ARE NEGATIVE VALUED')
   50 CONTINUE
C
C     'MCOLAT' IS THE NUMBER OF LATITUDE LINES IN THE GRID.
C     'MLONG' IS THE NUMBER OF LONGITUDE LINES IN THE GRID.
C     'MPTS' IS THE NUMBER OF POINTS ON THE SEA.
C
      READ(1,1) MCOLAT,MLONG
    1 FORMAT(5I5)
C
```

```
C     READ IN GRID POINT NUMBERS BY ROWS.  GRID INTERSECTIONS
C     OUTSIDE THE AREA OF INTEREST MUST BE NUMBERED 0.
C
      READ(1,2) ((NUMPNT(I,J),J=1,MLONG),I=1,MCOLAT)
    2 FORMAT(16I5)
      NMAX=0
      MPTS=0
      DO 37  I=1,MCOLAT
      DO 37  J=1,MLONG
      NMAX=MAXO(NMAX,NUMPNT(I,J))
      IF(NUMPNT(I,J).GT.0)  MPTS=MPTS+1
   37 CONTINUE
      WRITE(2,14)
   14 FORMAT(' THE FOLLOWING GRID WAS GIVEN (NORTH IS AT THE TOP)')
      DO 15  K=1,MCOLAT
   15 WRITE(2,16) (NUMPNT(K,J),J=1,MLONG)
   16 FORMAT(25I5)
C
C     READ IN PHYSICAL PARAMETERS AT EACH GRID POINT BY FORMAT
C     'FMT'
C     'COLAT' IS THE COLATITUDE OF THE POINT.  'ELONG' IS
C     THE EAST LONGITUDE OF THE POINT.  'H' IS THE WATER DEPTH
C     IN METERS.
C
      WRITE(2,10)
   10 FORMAT(' THE FOLLOWING PHYSICAL PARAMETERS WERE READ',
     :/,1X,'GRID POINT',7X,'LATITUDE',6X,'LONGITUDE',9X,
     :'DEPTH',11X,'TIDE',9X,'PHASE',/,3X,'NUMBER',7X,
     :'(CO- OR GRID)',3X,'( WEST  )',8X,'(METERS)',8X,'(CM)',
     :8X,'(DEGREES)')
      READ(1,4) FMT
    4 FORMAT(20A4)
```

```
      DO 34  I=1,MPTS
   34 NCHECK(I)=0
    3 READ(1,FMT,END=999) I,A,B,C,D,E
      IF(I.EQ.0.OR.I.GT.MPTS)  GO TO 7
      IF(NCHECK(I).EQ.1)  GO TO 7
      NCHECK(I)=1
      WRITE(2,11) I,A,B,C,D,E
   11 FORMAT(I10,2F15.3,F15.0,4F15.2)
C
C     CHANGE FROM POLAR TO RECTANGULAR FORM
C
      Z1(I)=D*DCOS(E*DTOR)
      Z2(I)=D*DSIN(E*DTOR)
C
C     CHANGE DEPTH TO CENTIMETERS
C
      H(I)=C*100.
C
C    THE NAVAGATION GRID
C
      IF(CSYS.EQ.SPHE)  GO TO 52
      Y(I)=A*ATOL
      X(I)=B*ATOL
      GO TO 3
C
C     SPHERICAL WAS RIGHT, RADIANS AND EAST LONGITUDE ARE REQUIRED
C
   52 COLAT(I)=A*DTOR
      ELONG(I)=2.*PI-B*DTOR
      GO TO 3
  999 DO 36  I=1,MPTS
      IF(NCHECK(I).NE.1)  GO TO 7
```

```
   36 CONTINUE
C
C      IN CASE WE ARE USING THE NAVAGATION GRID, CALCULATE THE
C      COLATITUDES AND EAST LONGITUDES
C
       IF(CSYS.EQ.SPHE)  RETURN
       DO 53  I=1,MPTS
       CFACT=4.*ERAD**2/(X(I)**2+Y(I)**2)
       CFACT2=1.D0-CFACT
       COLAT(I)=DARCOS(CFACT2/(2.D0-CFACT2))
       ELONG(I)=DATAN2(-X(I),-Y(I))
       ELONG(I)=DMOD(ELONG(I)+2.*PI,2.*PI)
   53 CONTINUE
      RETURN
    7 WRITE(2,9) I
    9 FORMAT('1EXECUTION TERMINATED BY SUBROUTINE DATAIN',
     :/,' ERROR IN INPUT DATA',/,' SOMETHING STRANGE ABOUT GRID POINT ',
     :'NUMBERED',I5,' WAS FOUND.')
      IER=-1
      RETURN
      END
      SUBROUTINE PHASE(IER)
C
C      FIND THE SPEED 'SIGMA' AND THE AMPLITUDE OF THE RIGID
C      EARTH GRAVITY TIDE FROM THE VARIABLE 'TIDE'
C      RIGID EARTH TIDE AMPLITUDES IN MICROGALS (MELCHOIR)
C      O1-31, P1-15, K1-44, M2-74, S2-34, N2-15
C
      IMPLICIT REAL*8 (A-H,O-Z)
      COMMON/BLOCK3/COLAT(200),ELONG(200),DEPTH(200),SIGMA
      COMMON/BLCK12/TIDE,AMPMAX
      DATA O1,P1,AK1,AM2,S2,AN2/'O1  ','P1  ','K1  ','M2  ','S2  ',
```

```
     :'N2  '/
      ACCEL=980.
      DTOR=2.*3.14159/360.
      ERAD=6.374E8
      IF(TIDE.EQ.O1)  GO TO 1
      IF(TIDE.EQ.P1)  GO TO 21
      IF(TIDE.EQ.AK1)  GO TO 22
      IF(TIDE.EQ.AM2)  GO TO 3
      IF(TIDE.EQ.S2)  GO TO 4
      IF(TIDE.EQ.MN2)  GO TO 5
      WRITE(6,10) TIDE
   10 FORMAT(' SPECIFIED TIDE (',A4,') WAS NOT FOUND.')
      IER=-1
      RETURN
    1 SIGMA=13.9430356
      AMPMAX=10.06
      GO TO 6
   21 SIGMA=14.9589314
      AMPMAX=4.68
      GO TO 6
   22 SIGMA=15.0410686
      AMPMAX=14.16
      GO TO 6
    3 SIGMA=28.9841042
      AMPMAX=24.24
      GO TO 6
    4 SIGMA=30.
      AMPMAX=11.28
      GO TO 6
    5 SIGMA=28.4397295
      AMPMAX=4.69
    6 CONTINUE
```

```
C
C       CONVERT SIGMA TO RADIANS PER SECOND
C
        SIGMA=SIGMA*DTOR/3600.
        RETURN
        END
        SUBROUTINE ZBAR
C
C       COMPUTE AMPLITUDE AND GREENWICH PHASE OF EQUILIBRIUM TIDE
C
        IMPLICIT REAL*8 (A-H,O-Z)
        COMMON/BLOCK3/COLAT(200),ELONG(200),DEPTH(200),SIGMA
        COMMON /BLOCK4/Z1(200),Z2(200),ZB1(200),ZB2(200)
        COMMON /BLOCK5/FRCONS,CSYS,MPTS,MAXITR,IORDER
        COMMON/BLCK12/TIDE,AMPMAX
        PI=3.141593
        DTOR=2.*PI/360.
        DO 1  K=1,MPTS
C
C       FIND THE LATITUDE
C
        TLAT=DABS(COLAT(K)-PI/2.)
C
C       COMPUTE THE AMPLITUDE AND PHASE OF THE EQUILIBRIUM TIDE
C
C         MUST CHOSE BETWEEN DIURNAL AND SEMIDIURNAL CONSTITUENT
C
        XX=22.5*DTOR/3600.
        IF(SIGMA.GT.XX)  GO TO 2
C
C         DIURNAL
C
```

```
      AMPEQ=AMPMAX*DSIN(2.*TLAT)
      PHSEQ=0.D0
      GO TO 3
C
C        SEMIDIURNAL
C
    2 AMPEQ=AMPMAX*(DCOS(TLAT))**2
      PHSEQ=0.D0
    3 CONTINUE
C
C     CONVERT FROM POLAR TO RECTANGULAR REPRESENTATION
C
      ZB1(K)=AMPEQ*DCOS(PHSEQ)
      ZB2(K)=AMPEQ*DSIN(PHSEQ)
    1 CONTINUE
      RETURN
      END
      SUBROUTINE PARTAL(I,A,B,C,D,IER)
C
C     COMPUTE DERIVATIVES AT POINT 'I'
C
      IMPLICIT REAL*8 (A-H,O-Z)
      REAL*8 IFIRST,JFIRST,KFIRST,IFST,JFST,KFST
      COMMON /BLOCK1/U1(200),U2(200),V1(200),V2(200)
      COMMON /BLOCK2/ZS1(200),ZS2(200)
      COMMON /BLOCK3/COLAT(200),ELONG(200),DEPTH(200),SIGMA
      COMMON /BLOCK5/FRCONS,CSYS,MPTS,MAXITR,ICRDER
      COMMON /BLOCK7/X(200),Y(200)
      DATA SPHE/'SPHE'/
      ERAD=6.374E8
C
C     FIND POINTS TO BE USED IN DERIVATIVES
```

```
C
      CALL AROUND(I,J,K,KK,JJ,IER)
      IF(CSYS.EQ.SPHE)  GO TO 3
C
C     NAVAGATION GRID
C
      AA=Y(K)-Y(I)
      BB=Y(J)-Y(I)
      CC=X(KK)-X(I)
      DD=X(JJ)-X(I)
      GO TO 2
C
C     SPHERICAL GRID
C
    3 AA=COLAT(K)-COLAT(I)
      BB=COLAT(J)-COLAT(I)
      CC=ELONG(KK)-ELONG(I)
      DD=ELONG(JJ)-ELONG(I)
    2 CONTINUE
      FIRST=(AA*AA-BB*BB)/(AA*BB*BB-AA*AA*BB)
      JFIRST=AA/(AA*BB-BB*BB)
      KFIRST=BB/(AA*BB-AA*AA)
      IFST=(CC*CC-DD*DD)/(CC*DD*DD-CC*CC*DD)
      JFST=CC/(CC*DD-DD*DD)
      KFST=DD/(CC*DD-CC*CC)
      A=IFIRST*ZS1(I)+JFIRST*ZS1(J)+KFIRST*ZS1(K)
      B=IFIRST*ZS2(I)+JFIRST*ZS2(J)+KFIRST*ZS2(K)
      C=IFST*ZS1(I)+JFST*ZS1(JJ)+KFST*ZS1(KK)
      D=IFST*ZS2(I)+JFST*ZS2(JJ)+KFST*ZS2(KK)
      IF(CSYS.EQ.SPHE)  RETURN
C
C     CONVERT DERIVATIVES FROM STEREOGRAPHIC SYSTEM TO SPHERICAL SYSTEM
```

```
C
      STHETA=DSIN(COLAT(I))
      DZS1DY=A
      DZS2DY=B
      DZS1DX=C
      DZS2DX=D
      A=(-X(I)*DZS1DX-Y(I)*DZS1DY)/STHETA
      B=(-X(I)*DZS2DX-Y(I)*DZS2DY)/STHETA
      C=(Y(I)*DZS1DX-X(I)*DZS1DY)
      D=(Y(I)*DZS2DX-X(I)*DZS2DY)
      RETURN
      END
```

```
      SUBROUTINE SOLVER(N,A,R,G)
C
C     SUBROUTINE TO SOLVE SIMULTANEOUS EQUATIONS BY METHOD
C     OF ELIMINATION (GAUSS-JORDAN).  'N' IS THE NUMBER OF
C     EQUATIONS.  'G' IS THE DETERMINANT OF THE OF THE
C     COEFFICIENTS MATRIX 'A'.  'R' IS THE RIGHT-HAND-SIDE
C     VECTOR.
C
      IMPLICIT REAL*8 (A-H,O-Z)
      DIMENSION A(N,N),R(N)
      G=1.DO
      DO 1  I=1,N
      G=G*A(I,I)
      IF(G.EQ.0.DO)  RETURN
      TEMP=1.DO/A(I,I)
      DO 2  J=I,N
    2 A(I,J)=A(I,J)*TEMP
      R(I)=R(I)*TEMP
      DO 1  K=1,N
      IF(K.EQ.I)  GO TO 1
      D=A(K,I)
      DO 3  J=I,N
    3 A(K,J)=A(K,J)-D*A(I,J)
      R(K)=R(K)-D*A(I,J)
    1 CONTINUE
      RETURN
      END
```

```
      IMPLICIT REAL*8 (A-H,O-Z)
      DIMENSION AMP(744),AZI(744)
C
C     PROGRAM TO CALCULATE CURRENT AMPLITUDES AND DIRECTIONS
C     DURING THE MONTH OF DECEMBER, 1977 FROM THE STEADY-
C     STATE SOLUTIONS TO THE LTE.
C
C     U=CURRENT SOUTH
C     V=CURRENT EAST
C     AZIMUTH MEASURED NORTH THRU EAST
C
      U(T)=FP1*AP1U*DCOS((SP1*T+PHIP1-PHSP1U)*DTOR)
     :    +FK1*AK1U*DCOS((SK1*T+PHIK1-PHSK1U)*DTOR)
     :    +FO1*AO1U*DCOS((SO1*T+PHIO1-PHSO1U)*DTOR)
     :    +FM2*AM2U*DCOS((SM2*T+PHIM2-PHSM2U)*DTOR)
     :    +FN2*AN2U*DCOS((SN2*T+PHIN2-PHSN2U)*DTOR)
     :    +FS2*AS2U*DCOS((SS2*T+PHIS2-PHSS2U)*DTOR)
      V(T)=FP1*AP1V*DCOS((SP1*T+PHIP1-PHSP1V)*DTOR)
     :    +FK1*AK1V*DCOS((SK1*T+PHIK1-PHSK1V)*DTOR)
     :    +FO1*AO1V*DCOS((SO1*T+PHIO1-PHSO1V)*DTOR)
     :    +FM2*AM2V*DCOS((SM2*T+PHIM2-PHSM2V)*DTOR)
     :    +FN2*AN2V*DCOS((SN2*T+PHIN2-PHSN2V)*DTOR)
     :    +FS2*AS2V*DCOS((SS2*T+PHIS2-PHSS2V)*DTOR)
C
C     JD CURRENT AMPLITUDES
C
      AP1U=1.14
      AP1V=0.64
      AK1U=3.39
      AK1V=1.92
      AO1U=3.01
      AO1V=2.15
```

```
      AM2U=4.43
      AM2V=2.68
      AN2U=4.83
      AN2V=2.54
      AS2U=3.91
      AS2V=1.86
C
C     J9 CURRENT PHASES
C
      PHSP1U=149.
      PHSP1V=82.
      PHSK1U=148.
      PHSK1V=83.
      PHSO1U=126.
      PHSO1V=65.
      PHSM2U=148.
      PHSM2V=220.
      PHSN2U=52.
      PHSN2V=146.
      PHSS2U=56.
      PHSS2V=128.
C
C     NODE FACTORS
C
      FP1=1.0
      FK1=0.887
      FO1=0.814
      FM2=1.036
      FN2=1.036
      FS2=1.0
C
C     EQUILIBRIUM ARGUMENTS
```

```
C
      PHIP1=20.3
      PHIK1=343.3
      PHIO1=253.1
      PHIM2=238.4
      PHIN2=12.2
      PHIS2=0.0
C
C     CONSTITUENT SPEEDS
C
      SP1=14.958931400
      SK1=15.041068600
      SO1=13.943035600
      SM2=28.984104200
      SN2=28.439729500
      SS2=30.000000000
C
      DTOR=3.141592654D0/180.00
      DO 1   I=1,744
      T=DFLOAT(I-1)
      CO=U(I)
      CV=V(I)
      AMP(I)=DSQRT(CO*CO+CV*CV)
      AZI(I)=DATAN2(CV,-CO)/DTOR
    1 IF(AZI(I).LT.0.)  AZI(I)=AZI(I)+360.
      WRITE(6,2) (AMP(I),AZI(I),I=1,744)
    2 FORMAT(1X,12F6.1/1X,12F6.1/1X,12F6.1/1X,12F6.1/)
      STOP
      END
```

APPENDIX III

The digital recorders used on the gravimeters to record the flexural waves in the ice shelf are the subject of this appendix. The recorders were based on the Sol-20 computer manufactured by Processor Technology Corporation of Pleasanton, California, with 16K memory, audio cassette tape recorder, and video monitor. This micro-computer was adapted for use as a digitizer by the installation of the following modules, which plug into the card cage of the computer: 88-ADC analog-to-digital converter by MITS Corporation of Albuquerque, New Mexico; 88-SPM clock module by International Data Systems, Incorporated of Falls Church, Virginia; and PIC-8 priority interrupt controller by IMSAI Manufacturing Corporation of San Leandro, California. The digitizing functions were controlled on an interrupt basis, hence the need for the PIC-8 module.

System software was based on machine language programs provided by the manufacturer with each of the system components although extensive modifications were made to the software provided. This software is distributed on a proprietary basis to the purchaser of the hardware. Because the system is both modular and programmable it is readily adaptable to a variety of functions, including processing of the acquired data. In service in Antarctica, the system proved to be rugged and reliable.

VITA

Richard Turl Williams II was born December 23, 1950 in Richmond, Kentucky. He obtained his elementary and high school education in the Madison County, Kentucky, school system. He graduated from high school in the spring of 1968 and entered Eastern Kentucky University, in the fall of that year. He majored in mathematics and physics and received his Bachelor of Science degree in June 1973. The following September he enrolled in the Graduate School at Virginia Polytechnic Institute and State University, in Blacksburg, Virginia as a geophysics major in the Department of Geological Sciences, and completed his Master of Science degree in July 1976. He is a member of the Society of Exploration Geophysicists.

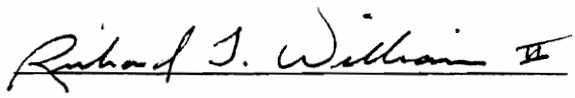

THE OCEAN TIDE AND WAVES BENEATH THE ROSS ICE SHELF, ANTARCTICA

by

Richard T. Williams II

(ABSTRACT)

Widely spaced tidal gravity records have been used to determine the spatial and temporal variation of the ocean tide beneath the Ross Ice Shelf. Cotidal-coamplitude maps have been drawn for the six greatest harmonic constituents of the tide. These are K_1, P_1, O_1, M_2, S_2, and N_2. The tide is principally diurnal, the diurnal amplitudes being roughly 3 times longer than the semidiurnals. The range of the tropic tide is about 1 m at the northern extremity of the ice shelf, and can be as great as 2 m in the southeastern part of the region. The diurnal constituents can each be viewed as a wave that propagates towards the southwest across the sea, having an amplitude that is closely related to the thickness of the water-layer beneath the ice. For each of the semidiurnal constituents there is an amphidromic region located within the Ross Sea near 80° S latitude, 190° W longitude, and having a clockwise sense of rotation.

Theoretical calculations of the tidal current indicate that the semidiurnal and diurnal current constituents have roughly the

same amplitude. The semidiurnal current is magnified by near resonance with the inertia current due to the high latitude of the sea. Because of the resonance, calculations of the semidiurnal components of the tidal current are sensitive to the treatment of the retarding effects of the ice shelf and sea floor.

Waves having periods shorter than 20 min were observed in the ice shelf. These have been identified as flexural waves that are generated by the action of the ocean swell on the northern edge of the shelf. The observed speed of these waves was predicted within the uncertainty of the measurement by the classical flexural wave theory.